Coupled-channel dynamics in mesonic systems

Gekoppelte Kanal-Dynamik in mesonischen Systemen
Zur Erlangung des Grades eines Doktors der Naturwissenschaften (Dr. rer. nat.)
genehmigte Dissertation von Igor Danilkin, M.Sc. aus Moskau (Russland)
2013 — Darmstadt — D 17

TECHNISCHE UNIVERSITÄT DARMSTADT

Fachbereich Physik
GSI Theorie

Coupled-channel dynamics in mesonic systems
Gekoppelte Kanal-Dynamik in mesonischen Systemen

Genehmigte Dissertation von Igor Danilkin, M.Sc. aus Moskau (Russland)

1. Gutachten: Priv. Doz. Dr. Matthias F. M. Lutz
2. Gutachten: Prof. Dr. Achim Schwenk

Tag der Einreichung: November 27, 2012
Tag der Prüfung: Dezember 19, 2012

Darmstadt — D 17

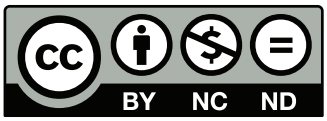

Erklärung zur Dissertation

Hiermit versichere ich, die vorliegende Dissertation ohne Hilfe Dritter nur mit den angegebenen Quellen und Hilfsmitteln angefertigt zu haben. Alle Stellen, die aus Quellen entnommen wurden, sind als solche kenntlich gemacht. Diese Arbeit hat in gleicher oder ähnlicher Form noch keiner Prüfungsbehörde vorgelegen.

Darmstadt, den February 15, 2013

(I. Danilkin)

Zusammenfassung

Die starke Wechselwirkung wird durch die Quantenchromodynamik (QCD) beschrieben, die eine $SU(3)$-Eichtheorie in den drei Farbfreiheitsgraden von Quarks und Gluonen ist. Bei hohen Energien zeigt die QCD die Eigenschaft der *asymptotischen Freiheit*, welche es erlaubt, störungstheoretische Berechnungen in diesem Bereich durchzuführen. Bei niedrigen Energien wird die laufende Kopplungskonstante allerdings groß was (*Confinement*), und die Anwendung der Störungstheorie unmöglich macht. Aufgrund dieses Problems ist die Anwendung nichtperturbativer Methoden der QCD nötig, wie z.B. QCD-Summenregeln oder numerische Simulationen auf einem Gitter. Einen weiteren theoretischen Ansatz stellt die *chirale Störungstheorie* dar, die mit dem Phänomen der chiralen Symmetriebrechung in der QCD verbunden ist. Letzteres sagt nach dem Goldstone-Theorem die Existenz eines Oktetts von Goldstone-Bosonen voraus, die man als die pseudoskalaren Mesonen (π, K, η) identifizieren kann. Die chirale Störungstheorie beschreibt starke Wechselwirkungen bei niedrigen Energien direkt mit diesen experimentell messbaren Hadronen, statt in expliziten Quark- und Gluon-Freiheitsgraden. Die auftretenden Matrixelemente können dabei als Potenzreihe in den leichten Quarkmassen und kleinen Impulsen entwickelt werden.

Die chirale Störungstheorie führt jedoch nur in ausreichender Nähe der Produktionsschwelle eines Prozesses zu verlässlichen Resultaten. Um auch Berechnungen in der Resonanzregion anstellen zu können, ist daher eine Erweiterung des Gültigkeitsbereichs wünschenswert. Hier geschieht das durch die Einbeziehung der leichten Vektormesonen als Freiheitsgrade in die Lagrangedichte der chiralen Störungstheorie (nach der sogenannten *hadrogenesis conjecture*), sowie durch Betrachtung nichtperturbativer Effekte mittels einer neuartigen Unitarisierungsmethode. Letztere basiert auf den Forderungen der Mikro-Kausalität und der gekoppelten Kanal-Unitarität und bewahrt zusätzlich auch die elektromagnetische Eichinvarianz.

In dieser Arbeit wird zuerst die eben erwähnte Methode anhand von nichtrelativistischer Streuung an einem Yukawa-Potential verschiedener Stärken und Reichweiten untersucht. Dies ist sehr nützlich, um die Anwendbarkeit und den Gültigkeitsbereich des neuen Ansatzes zu verstehen. Dabei wird der typische Fall der Überlagerung von schwachen, langreichweitigen und starken, kurzreichweitigen Kräften betrachtet. Im nächsten Schritt wird die Streuung von Goldstone-Bosonen mit diesem Ansatz analysiert, basierend auf der oben erwähnten chiralen $SU(3)$-Lagrangedichte mit leichten Vektormesonen. Die Ergebnisse dieser gekoppelten Kanal-Rechnung werden mit den experimentell bekannten s- und p-Wellen-Streuphasen bis zu einer Energie von 1.2 GeV verglichen. In den isoskalaren und isovektoriellen-Sektoren erkennt man die dynamische Generierung der Resonanzen $f_0(980)$ und $a_0(980)$. In der p-Wellen-Streuung werden die Vektormesonen dabei als Castillejo-Dalitz-Dyson Pole beschrieben. Schließlich erfolgt eine Ausdehnung der Analyse auf die Photon-Fusions-Reaktionen $\gamma\gamma \to \pi^0\pi^0$, $\pi^+\pi^-$, $K^0\bar{K}^0$, K^+K^-, $\eta\eta$ und $\pi^0\eta$, die sehr sensitiv auf hadronische Endzustands-Wechselwirkungen sind. Hier enthält die Lagrangedichte einige unbekannte Kopplungskonstanten, die die Wechselwirkungsterme mit zwei Vektormeson-Feldern parametrisieren. Diese werden durch einen Fit der Ergebnisse an Daten für die Prozesse $\gamma\gamma \to \pi^0\pi^0, \pi^+\pi^-$ und den Zerfall $\eta \to \pi^0\gamma\gamma$ bestimmt. Unter Verwendung der erhaltenen Parameterbereiche werden dann Vorhersagen für die Wirkungsquerschnitte der Prozesse $\gamma\gamma \to K^0\bar{K}^0$, K^+K^- und $\eta\eta$ gemacht.

Contents

Introduction

Quantum chromodynamics (QCD) is the $SU(3)$ colour gauge theory, which describes strong interactions. Together with the spontaneously broken $SU(2) \times U(1)$ electroweak theory, QCD forms the Standard Model of elementary particle physics. At high energies QCD possesses a remarkable property of *asymptotic freedom* which allows the use of the standard perturbation theory (pQCD).

At low energies, however, the running coupling becomes strong and the associated confinement makes perturbative calculations impossible. To overcome this problem one has to apply nonperturbative methods like QCD sum rules [SVZ79, CK00, Kle11] or lattice simulations [Kog83, A$^+$09]. Another powerful theoretical framework is chiral perturbation theory (χPT) [Wei67, GL84]. The origin of χPT is connected with another main property of QCD - spontaneous chiral symmetry breaking. According to the Goldstone theorem, this breakdown leads to the appearance of an octet of Goldstone bosons which are identified with pseudo-scalar mesons (π, K, η). An analysis of the low energy region is conducted in terms of experimentally detected hadrons rather than explicit quark-gluon degrees of freedom. A systematic expansion of matrix elements is performed in terms of masses of the light quarks and small momenta. The χPT was successfully applied to numerous physical processes in recent years. In [Sch03] one can find an introduction to χPT and a comprehensive overview of the basic results. However, χPT leads to controlled results in the close-to-threshold region only and a generalization to higher energies is desirable.

An important progress has been made by including additional degrees of freedom and taking into account nonperturbative effects. In particular the so-called *hadrogenesis conjecture* [LK01, LK04, LKK04, LK05, LS08, LL08, TLL12] relies on the relevance of a few "quasi-fundamental" hadronic degrees of freedom. Interactions between them, namely between pseudo-scalar and vector mesons, together with the baryon octet and decuplet are expected to generate the low energy spectrum of QCD. For instance in [LK04] it was demonstrated that the leading chiral interaction of Goldstone bosons with the light vector mesons generates an axial-vector meson spectrum. In [KL04] a set of $\frac{3}{2}^-$ resonances was dynamically generated, based on the interaction of Goldstone bosons with baryon decuplet fields. These results are in qualitative agreement with empirical data. The summation of an infinite number of terms was performed by solving the Bethe-Salpeter-Equation (BSE). This is one of the possible coupled-channel unitary techniques that allow to extend the applicability domain of χPT to higher energies where meson resonances play a crucial role.

In practice, however, use of the BSE has different limitations. If the interaction kernel is truncated in perturbation theory, where the electromagnetic gauge invariance is guaranteed order by order, the resulting scattering amplitude would generally depend on the gauge and choice of field.

Both difficulties of the BSE are removed in a novel scheme introduced in [GL10, GLP11]. The main objective of that work is a controlled realization of the causality and unitarity condition in a perturbative application of the chiral Lagrangian. The starting point are partial-wave dispersion relations. A generalized potential is constructed from the chiral Lagrangian in the

subthreshold region and analytically extrapolated to higher energies in terms of suitably constructed conformal variables. The partial-wave scattering amplitudes are defined as solutions of non-linear integral equations that are solved by means of the N/D ansatz.

In this work, first we apply the novel scheme to non-relativistic Yukawa interactions of various couplings and ranges. There are few essential features kept in Yukawa ansatz. First, the exact solution is easily accessible from the Lippmann-Schwinger equation. Second, the analytic structure of the Yukawa partial-wave amplitude is similar to a realistic case. Therefore this analysis helps us to realize the usefulness of the new approach and to what extent it is valid. The typical case of a superposition of strong short-range and weak long-range forces is investigated. Then we study Goldstone boson scattering based on the flavour $SU(3)$ chiral Lagrangian with dynamical light vector mesons as formulated within the hadrogenesis conjecture. A coupled-channel computation is confronted with the empirical s- and p-wave phase shifts up to 1.2 GeV. The system is characterized by two relevant and known parameters only, the chiral limit value of the pion decay constant and the coupling constant characterizing the decay of the rho meson into a pair of pions. Finally, we extend our analysis to the photon-fusion reactions $\gamma\gamma \to \pi^0\pi^0$, $\pi^+\pi^-$, $K^0\bar{K}^0$, K^+K^-, $\eta\eta$ and $\pi^0\eta$ which are very sensitive to hadronic final-state interactions. In this case the Lagrangian contains five unknown coupling constants parameterizing the interaction terms with two vector meson fields. These parameters are fitted to photon fusion data $\gamma\gamma \to \pi^0\pi^0$, $\pi^+\pi^-$ and to the decay $\eta \to \pi^0\gamma\gamma$. Based on our parameter sets we predict the $\gamma\gamma \to K^0\bar{K}^0$, K^+K^- and $\eta\eta$ cross sections.

The thesis is organized in the following way. In the first chapter we summarize the basic aspects of QCD and give a short introduction to χPT supplemented with light vector mesons. Chapter 2 is divided into three parts. First, in Section 2.1 the novel technique [GL10] is illustrated by means of a Yukawa interaction, where the exact solution is known. After the Yukawa toy model, we consider the scattering of Goldstone bosons in Section 2.2. Section 2.3 shows the study of photon-fusion processes. We conclude in Chapter 3, where a summary and outlook of our results are given. Appendices A, B, C and D collect some calculational details.

Sections 2.1, 2.2 and 2.3 are based on Refs. [DGL11a, DGL11b, DL12, DLLT12] with more detailed explanations.

1 QCD at low energy

1.1 QCD and chiral Symmetry

QCD is a non-Abelian gauge theory of interacting quarks and gluons. Quark fields are fermions, which come in six different flavours, in addition to their three possible colours. Gluons come in eight colour combinations and hadrons are colour-singlet combinations of quarks, anti-quarks and gluons.

1.1.1 The QCD Lagrangian and the coupling α_s

The gauge invariant QCD Lagrangian is given by (up to gauge-fixing terms) [Ynd06]

$$\begin{aligned}
\mathcal{L}_{\text{QCD}} &= \sum_{f=\substack{u,d,s,\\c,b,t}} \bar{q}_f \left(i\gamma^\mu D_\mu - m_f\right) q_f - \frac{1}{4} G^{(a)}_{\mu\nu} G^{(a)\mu\nu}, \\
D_\mu &= \partial_\mu - i g_s \frac{\lambda^{(a)}}{2} A^{(a)}_\mu, \\
G^{(a)}_{\mu\nu} &= \partial_\mu A^{(a)}_\nu - \partial_\nu A^{(a)}_\mu + g_s f^{abc} A^{(b)}_\mu A^{(c)}_\nu,
\end{aligned} \tag{1.1}$$

where g_s is the QCD coupling constant and f^{abc} are the standard totally antisymmetric $SU(3)$ structure constants[1]. For each flavour f and colour, the quark fields q_f are the four component Dirac spinors and the $A^{(a)}_\mu(x)$ are the eight $(a = 1, ..., (N_c^2 - 1) = 8)$ Yang-Mills gluon fields. The non-Abelian nature of QCD introduces an additional term in the field strength tensor $G^{(a)}_{\mu\nu}$, giving rise to triplet and quadruple gluon self-interactions and eventually to the asymptotic freedom property.

The gauge principle imposes the local $SU(3)$ transformation

$$q_f \mapsto q'_f = \exp\left(-i \sum_{a=1}^{8} \Theta_a(x) \frac{\lambda^{(a)}}{2}\right) q_f = U q_f, \tag{1.2}$$

described by the set of parameters $\Theta_a(x) = [\Theta_1(x), ..., \Theta_8(x)]$ and $\lambda^{(a)}$ are the eight Gell-Mann matrices (see Appendix A). The quark field q_f ($\bar{q}_f$) belongs to the fundamental (complex conjugate) representation of the $SU(3)$ gauge group, while the gluon belongs to the adjoint representation and all hadrons belong to the trivial representation. Formally, one can write $3 \otimes \bar{3} = 8 \oplus 1$. The interaction between quarks and gluons rotates the quark's colour.

The effective QCD coupling $\alpha_s = g_s^2/4\pi$ is defined by

$$\alpha_s(Q) = \frac{4\pi}{\beta_0 \ln(Q^2/\Lambda^2)} \left[1 - \frac{2\beta_1}{\beta_0^2} \frac{\ln[\ln(Q^2/\Lambda^2)]}{\ln(Q^2/\Lambda^2)} + ...\right] \tag{1.3}$$

[1] $f_{abc} = \frac{1}{4i}\text{Tr}([\lambda_a, \lambda_b]\lambda_c)$

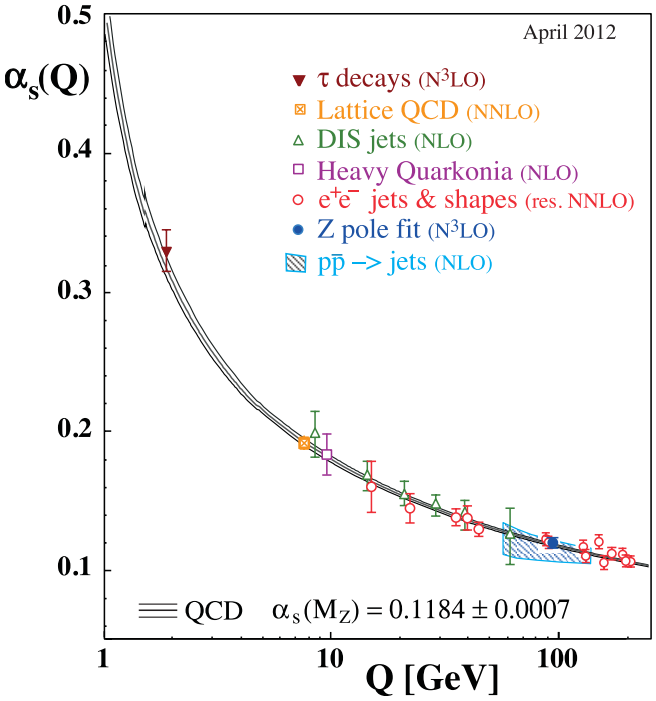

Figure 1.1.: The QCD coupling constant α_s as a function of the respective energy scale Q. The figure is taken from [N⁺10].

where $\beta_0 = 11 - 2/3\,n_f$, $\beta_1 = 51 - 19/3\,n_f$ and n_f is the number of flavours of quarks with mass less than the characteristic energy scale Q. Λ is the fundamental parameter of QCD (it sets the scale of the running coupling).

From Eq.(1.3), one can see that the "running coupling" is small if the renormalization scale is chosen high enough ($\alpha_s \to 0$ as $Q \to \infty$). This property is called "asymptotic freedom" [GW73, Pol73], and leads to a perturbative treatment of QCD for high energy processes. On the other hand, QCD becomes strongly coupled at the energy scale $Q \sim \Lambda$, giving rise to confinement of quarks and gluons. As a consequence, we are not able to work perturbatively at low energies. A nonperturbative approach is needed.

Table 1.1.: Current quark masses according to PDG [N⁺10]. The result is given for the $\overline{\text{MS}}$ running mass at a scale $\mu \approx 2$ GeV.

$m_u = 1.7 - 3.3$ MeV	$m_c = 1.27^{+0.07}_{-0.09}$ GeV
$m_d = 4.1 - 5.8$ MeV	$m_b = 4.19^{+0.18}_{-0.06}$ GeV
$m_s = 101^{+29}_{-21}$ MeV	$m_t = 172.0 \pm 0.9 \pm 1.3$ GeV

In Eq.(1.1) m_f are the quark masses. Quarks have not been observed as isolated states and therefore are not directly measurable quantities. This experimental finding is called color confinement. The numerical values of quark masses generally depend on the renormalization scale and scheme. In Table 1.1 the current $\overline{\text{MS}}$ quark masses according to PDG [N⁺10] are presented. By inspecting this table one finds that the masses of the u, d and, to a lesser extent, s quarks are small compared to the masses of hadrons[2], or to the typical hadronic mass scale of ∼1 GeV. This implies that besides the discrete C, P, and T symmetries, QCD exhibits an additional symmetry, which we will discuss in the next subsection. In the following we are keeping only the three lightest quarks (up, down and strange) in the Lagrangian (1.1).

[2] like e.g. the ρ meson mass

1.1.2 Chiral symmetry

As a starting point in the discussion of low energy QCD, let us consider the so-called chiral limit $m_u, m_d, m_s \to 0$. In this case the QCD Lagrangian is given by

$$\mathcal{L}^0_{\rm QCD} = \sum_{f=u,d,s} \left(\bar{q}_{f,R}\, i\gamma^\mu D_\mu\, q_{f,R} + \bar{q}_{f,L}\, i\gamma^\mu D_\mu\, q_{f,L} \right) - \frac{1}{4}\, G^{(a)}_{\mu\nu} G^{(a)\,\mu\nu}, \tag{1.4}$$

where the right-handed (R) and left-handed (L) quark fields[3]

$$q_R = \frac{1}{2}\,(1+\gamma_5)\,q, \quad q_L = \frac{1}{2}\,(1-\gamma_5)\,q, \tag{1.5}$$

do not interact with each other.

Due to the flavour blindness of the covariant derivative, $\mathcal{L}^0_{\rm QCD}$ is invariant under the global $U(1)_V \times U(1)_A \times SU(3)_V \times SU(3)_A$ (formally $SU_V(3) \times SU_A(3) = SU_L(R) \times SU_R(3)$) transformations of the quark fields

$$q \to \exp\left(i\theta_V + i\theta^a_V \frac{\lambda_a}{2} \right) q, \qquad q \to \exp\left(i\gamma_5\theta_A + i\gamma_5\theta^a_A \frac{\lambda_a}{2} \right) q\,. \tag{1.6}$$

According to Noether's theorem, each symmetry of the Lagrangian is associated with the conserved currents. Under the global $U(1)_V \times SU(3)_V \times U(1)_A \times SU(3)_A$ symmetry we obtain the following vector and axial vector current densities

$$\begin{aligned} V^\mu_a &= \bar{q}\,\gamma^\mu \frac{\lambda_a}{2}\, q, & V^\mu &= \bar{q}\,\gamma^\mu\, q, & \partial_\mu V^\mu_a &= 0, \quad \partial_\mu V^\mu = 0\,, \\ A^\mu_a &= \bar{q}\,\gamma^\mu\gamma_5 \frac{\lambda_a}{2}\, q, & A^\mu &= \bar{q}\,\gamma^\mu\gamma_5\, q, & \partial_\mu A^\mu_a &= 0, \quad \partial_\mu A^\mu \neq 0\,. \end{aligned} \tag{1.7}$$

The vector $U(1)_V$ symmetry is related to baryon number conservation, while the axial $U(1)_A$ is broken by quantum fluctuations (Abelian anomaly) [tH76, CDG76], resulting in

$$\partial_\mu A^\mu = \frac{3\, g_s^2}{32\,\pi^2}\, \epsilon_{\mu\nu\rho\sigma}\, G^{(a)\,\mu\nu}\, G^{(a)\,\rho\sigma}\,. \tag{1.8}$$

Note that in (1.8), the factor of three corresponds to the number of flavours and $g_s^2 \sim 1/N_c$ in the large N_c (number of colours) limit. The remaining $SU(3)_V \times SU(3)_A = SU(3)_R \times SU(3)_L$ symmetry is called *chiral symmetry*.

From $SU(3)_V \times SU(3)_A$ symmetry one can naively expect that the hadron spectrum should consist of degenerate multiplets with opposite parity. In fact, this is not realized in nature and the chiral symmetry is spontaneously broken down to the vector subgroup $SU(3)_V$,

$$SU(3)_V \times SU(3)_A \to SU(3)_V\,. \tag{1.9}$$

[3] The terminology right-handed and left-handed fields can easily be seen in terms of helicity eigenstates. In the zeros mass limit the chiral operators $P_{R/L} = \frac{1}{2}(1 \pm \gamma_5)$ also project onto the positive/negative helicity eigenstates.

It turns out that the ground state of the theory is not symmetric under the chiral rotations and according to the Goldstone theorem [Gol61, GSW62], QCD must contain $N_F^2 - 1 = 8$ massless bosons with spin 0. The quantum numbers of these Goldstone bosons are $J^P = 0^-$ and associated with the broken axial generators. From the analysis of the hadron spectrum one can easily see that the eight lightest hadrons (π^+, π^-, π^0, K^+, K^-, K^0, $\bar{K}^0$ and η) are pseudo-scalar mesons. We identify them with Goldstone bosons. Their masses are nonzero but small[4]. This is a consequence of the fact that the physical quark masses are not exactly zero.

If we include the quark mass term $\mathcal{M} = \mathrm{diag}\{m_u, m_d, m_s\}$ in the Lagrangian (1.4) we obtain the mixing between left- and right-handed quark fields,

$$\mathcal{L}_{\mathcal{M}} = -\bar{q}\,\mathcal{M}\,q = -\left(\bar{q}_R\,\mathcal{M}\,q_L + \bar{q}_L\,\mathcal{M}\,q_R\right), \tag{1.10}$$

and therefore explicit breaking of the chiral symmetry. The divergences of the currents are modified to

$$\begin{aligned}
\partial_\mu V^{\mu,a} &= i\,\bar{q}\left[\mathcal{M}, \frac{\lambda_a}{2}\right]_- q, \\
\partial_\mu A^{\mu,a} &= i\,\bar{q}\left[\mathcal{M}, \frac{\lambda_a}{2}\right]_+ \gamma_5\, q, \\
\partial_\mu V^{\mu} &= 0, \\
\partial_\mu A^{\mu} &= 2i\,\bar{q}\,\mathcal{M}\,\gamma_5\, q + \frac{3\,g_s}{32\,\pi^2}\,\epsilon_{\mu\nu\rho\sigma}\,G^{(a)\mu\nu}\,G^{(a)\rho\sigma}.
\end{aligned} \tag{1.11}$$

From Eq.(1.11) one can see that $U(1)_V$ symmetry is always conserved. In the case of equal quark masses $m_u = m_d = m_s$, QCD is invariant under vector transformations[5], while the divergences of the axial-vector currents $A^{\mu,a}$ are proportional to the quark masses. Hence the masses of light quarks are small compared to the typical hadronic scale, the axial current is approximately conserved. This is the so called Partially Conserved Axial Current (PCAC) effect, and as we will see later, chiral perturbation theory is an appropriate framework to treat this effect perturbatively.

1.2 Effective field theory

Effective field theories (EFTs) have become a powerful theoretical approach widely used in particle, nuclear and condensed-matter physics [Kap05, Man96]. An important feature of EFT is the application of a systematic approximation in a certain energy domain only, defined with respect to some energy scale Λ. Within the given scale, relevant (effective) degrees of freedom might be different from the underlying ones. As a consequence, EFTs can substantially simplify the calculation (or sometimes even make them possible) if it is not clear how to work with the underlying theory. In case of QCD we know that at low energies the interactions between quarks and gluons become strong and standard perturbation theory (pQCD) cannot be applied. Therefore, it turns out very difficult to perform the calculations in terms of fundamental degrees of freedom, such as quarks and gluons. On the other hand, due to confinement, hadronic states are assumed to be appropriate degrees of freedom. Combination of the concept of EFT together with the chiral symmetry properties of QCD is the base of chiral perturbation theory.

[4] Therefore the light pseudo-scalar mesons are sometimes called pseudo-Goldstone bosons.

[5] Note $[\lambda^a, 1]_- = 0$

1.2.1 χPT

The most powerful way to construct the effective chiral Lagrangian is to use the external field technique. The extended QCD Lagrangian [GL84, GL85]

$$\begin{aligned} \mathcal{L} &= \mathcal{L}^0_{QCD} + \mathcal{L}_{ext} \\ &= \mathcal{L}^0_{QCD} + \bar{q}\left(\gamma^\mu\left(v_\mu(x) + \gamma_5\, a_\mu(x)\right) - \left(s(x) - i\gamma_5\, p(x)\right)\right)q \end{aligned} \tag{1.12}$$

includes the quark couplings to external scalar (s), pseudo-scalar (p), vector (v_μ) and axial-vector (a_μ) fields. These fields are colour-neutral, hermitian (3×3) matrices in flavour space (for instance, $v_\mu = \sum_{a=1,..,8} v^a_\mu \frac{\lambda^a}{2}$). The Lagrangian density $\mathcal{L}^0_{QCD}$ corresponds to massless QCD, while the quark mass term from Eq.(1.10) is included in the scalar field $s(x) = \mathcal{M} + \ldots$. The external fields allow us to calculate the Green's functions by taking functional derivatives of the generating functional $Z[v,a,s,p]$,

$$\exp\left(iZ[v,a,s,p]\right) = \int [DA_\mu]\,[Dq]\,[D\bar{q}]\,\exp\left(i\int d^4x\,\mathcal{L}_{QCD}(q,\bar{q},G_{\mu\nu};v,a,s,p)\right) \tag{1.13}$$

around $v_\mu = 0$, $a_\mu = 0$, $p = 0$ and $s = \mathcal{M}$. If the generating functional is invariant under *local* $SU(3)_L \times SU(3)_R$ transformations of the external fields, then all Green's functions obtained from Eq.(1.13) satisfy the chiral Ward identities. In addition, the external sources can be used to include the electromagnetic and semi-leptonic weak interactions

$$\begin{aligned} r_\mu &= v_\mu + a_\mu = -e\,\mathcal{Q}A_\mu + \ldots \\ l_\mu &= v_\mu - a_\mu = -e\,\mathcal{Q}A_\mu + \text{weak int.}\ldots \end{aligned} \tag{1.14}$$

where $\mathcal{Q}$ is the quark charge matrix,

$$\mathcal{Q} = \begin{pmatrix} \frac{2}{3} & 0 & 0 \\ 0 & -\frac{1}{3} & 0 \\ 0 & 0 & -\frac{1}{3} \end{pmatrix} \tag{1.15}$$

and $e \simeq 0.303$ is the positron charge.

Since we are interested in the low energy realization of QCD, where hadrons are dynamical degrees of freedom, the path integral representation will take the following form

$$\exp\left(iZ[v,a,s,p]\right) = \int [DU]\,\exp\left(i\int d^4x\,\mathcal{L}_{\text{eff}}(U;v,a,s,p)\right), \tag{1.16}$$

where the matrix U contains the Goldstone boson fields. The most convenient parametrization is exponential,

$$U(x) = \exp\left(i\,\frac{\Phi(x)}{f}\right) \tag{1.17}$$

with

$$\Phi \;=\; \sum_{a=1}^{8} \phi_a \lambda_a = \begin{pmatrix} \pi^0 + \frac{1}{\sqrt{3}}\eta & \sqrt{2}\,\pi^+ & \sqrt{2}K^+ \\ \sqrt{2}\,\pi^- & -\pi^0 + \frac{1}{\sqrt{3}}\eta & \sqrt{2}K^0 \\ \sqrt{2}K^- & \sqrt{2}\bar{K}^0 & -\frac{2}{\sqrt{3}}\eta \end{pmatrix} . \tag{1.18}$$

Each element of the Φ matrix is identified with real particles by comparing the isospin and hypercharge quantum numbers. The normalization of Φ is such that

$$\mathrm{tr}\Big\{\Phi\,\Phi\Big\} = 2\sum_{a=1}^{8}\phi_a^2 = 2\,(\pi^0)^2 + 2\,\eta^2 + 4\,\pi^+\pi^- + 4K^0\bar{K}^0 + 4K^+K^- . \tag{1.19}$$

Note that $U(x)$ transforms linearly under $SU(3)_L \times SU(3)_R$,

$$U \to U' = R\,U\,L^\dagger , \qquad R, L \in SU(3)_{R,L} , \tag{1.20}$$

whereas the Goldstone boson fields possess non-linear transformation properties.

According to the discrete C, P, T and chiral symmetries requirements, the most general Lagrangian is uniquely given by

$$\mathcal{L} = \frac{f^2}{4}\,\mathrm{tr}\Big\{D_\mu U^\dagger D^\mu U\Big\} + \frac{f^2 B_0}{2}\,\mathrm{tr}\Big\{\mathcal{M}\,U^\dagger + U\,\mathcal{M}^\dagger\Big\}, \tag{1.21}$$

where f is the pion decay constant in the chiral limit and B_0 is connected to the chiral quark condensate. In (1.21) the first term contains two derivatives[6] (which is equivalent to two powers of momentum) while the second term includes one power of the quark mass. The latter is responsible for the explicit symmetry breaking. The local $SU(3)_R \times SU(3)_L$ transformations lead to the covariant derivatives

$$\begin{aligned} D_\mu U &= \partial_\mu U - i\,r_\mu\,U + i\,U\,l_\mu , \\ D_\mu U^\dagger &= \partial_\mu U^\dagger + i\,U^\dagger\,r_\mu - i\,l_\mu\,U^\dagger , \end{aligned} \tag{1.22}$$

which transform in the same way as U in (1.20). The Lagrangian (1.21) is the leading term among an infinite number of terms which satisfy the symmetry constraints. In order to perform a systematic expansion, a power-counting scheme was introduced by Weinberg [Wei79]. The Lagrangian is organized according to the number of derivatives and powers of the quark masses involved in interaction terms,

$$\mathcal{L} = \mathcal{L}_2 + \mathcal{L}_4 + \ldots \tag{1.23}$$

where the subscript denotes the chiral power of the expansion. Consequently, at a given order there is only a finite number of terms, which has to be considered. Denoting by Q the expansion parameter which stands for the typical momentum of the process, one can summarize the general counting

$$\begin{aligned} U &\sim Q , \qquad \mathcal{M} \sim Q^2 , \qquad f_{\mu\nu}^{L/R} \sim Q , \\ D_\mu U &\sim Q , \qquad r_\mu, l_\mu \sim Q , \end{aligned} \tag{1.24}$$

[6] Note that in the mesonic sector due to parity conservation, only terms with an even number of derivatives are possible.

where we have introduced the field strength tensors that correspond to the gauge fields,

$$\begin{aligned} f^R_{\mu\nu} &= \partial_\mu r_\nu - \partial_\nu r_\mu - i\,[r_\mu, r_\nu]_- \\ f^L_{\mu\nu} &= \partial_\mu l_\nu - \partial_\nu l_\mu - i\,[l_\mu, l_\nu]_- \,. \end{aligned} \tag{1.25}$$

According to (1.24) the quark mass matrix $\mathcal{M}$ has order Q^2. It follows from the fact that at leading order $\mathcal{M}$ can be expressed in terms of the pion and kaon masses

$$\chi_0 \equiv 2B_0\,\mathcal{M} = \begin{pmatrix} m_\pi^2 & 0 & 0 \\ 0 & m_\pi^2 & 0 \\ 0 & 0 & 2m_K^2 - m_\pi^2 \end{pmatrix}, \tag{1.26}$$

and $m^2_{\pi,K} \sim Q^2$. Isospin breaking effects are neglected. All terms in (1.21) are of order Q^2 and correspond to the $\mathcal{L}_2$ in (1.23).

1.3 Chiral Lagrangian with vector mesons

In this section we will consider the inclusion of vector mesons in the chiral Lagrangian.

1.3.1 Relevant degrees of freedom

It seems quite natural to keep vector mesons as explicit degrees of freedom when aiming for a description of hadron physics in the resonance region. The light vector mesons play a crucial role in the hadrogenesis conjecture [LK01, LK04, LKK04, LK05, LS08, LL08, TLL12]. Together with the Goldstone bosons they are identified to be the "quasi-fundamental" hadronic degrees of freedom that are expected to generate the meson spectrum. For instance it was shown that the leading chiral interaction of Goldstone bosons with the light vector mesons generates an axial-vector meson spectrum that is quite close to the empirical one [LK04]. In addition we recall a resonance saturation mechanism [EGPdR89]. It was shown that the size of low energy constants (LECs) of Q^4 counter terms is basically saturated by light vector mesons. Therefore keeping the latter as explicit degrees of freedom, we extend this mechanism by taking into account the dynamics of the vector-meson propagator [KM01].

In this thesis we are going to further explore the dynamic role of light vector mesons in the chiral Lagrangian. The generating functional (1.13, 1.16) in the presence of vector mesons as explicit degrees of freedom is modified to

$$\exp\big(iZ[v,a,s,p]\big) = \int [DU]\,[D\Phi_{\mu\nu}]\,\exp\left(i\int d^4x\,\mathcal{L}_{\text{eff}}(U,\Phi_{\mu\nu};v,a,s,p)\right), \tag{1.27}$$

where a nonet of vector-meson fields is combined in the usual matrix $\Phi_{\mu\nu}$,

$$\Phi_{\mu\nu} = \begin{pmatrix} \rho^0_{\mu\nu} + \omega_{\mu\nu} & \sqrt{2}\,\rho^+_{\mu\nu} & \sqrt{2}\,K^+_{\mu\nu} \\ \sqrt{2}\,\rho^-_{\mu\nu} & -\rho^0_{\mu\nu} + \omega_{\mu\nu} & \sqrt{2}\,K^0_{\mu\nu} \\ \sqrt{2}\,K^-_{\mu\nu} & \sqrt{2}\,\bar{K}^0_{\mu\nu} & \sqrt{2}\,\phi_{\mu\nu} \end{pmatrix}. \tag{1.28}$$

We assume ideal $\phi - \omega$ mixing. The details of the antisymmetric tensor field representation of vector mesons are given in Appendix B.

1.3.2 Vector mesons

An introduction of higher-mass states in the chiral Lagrangian was first discussed in [CWZ69, CCWZ69]. There is a certain freedom in the choice of the $SU(3)_R \times SU(3)_L$ transformation rule for vector mesons. We follow the idea of the nonlinear realization of chiral symmetry in order to impose the correct low-energy behavior of the interaction terms in the Lagrangian. In this realization, the important ingredient is the compensating $SU(3)_V$ transformation K which is defined through the relation

$$u \to u' = R\,u\,K^\dagger = K\,u\,L^\dagger, \qquad u = \exp\left(i\frac{\Phi(x)}{2f}\right), \tag{1.29}$$

and leads to the following transformation of the vector-meson fields,

$$\Phi_{\mu\nu} \to \Phi'_{\mu\nu} = K\,\Phi_{\mu\nu}\,K^\dagger. \tag{1.30}$$

The matrix $K(L,R,U)$ is in general a non-linear function of L, R and $U(x)$. Its detailed form can be found in [CWZ69, CCWZ69]. In order to construct the most general Lagrangian it is useful to introduce new objects, transforming in the same way as vector fields [Kra90, Bir96],

$$\begin{aligned} U_\mu &= \frac{1}{2}u^\dagger\left(\partial_\mu U + ieA_\mu\,[\mathcal{Q},U]_-\right)u^\dagger, \\ \chi_\pm &= \frac{1}{2}(u\,\chi_0^\dagger\,u \pm u^\dagger\,\chi_0\,u^\dagger), \\ f^\pm_{\mu\nu} &= \frac{1}{2}(u\,f^L_{\mu\nu}\,u^\dagger \pm u^\dagger\,f^R_{\mu\nu}\,u), \end{aligned} \tag{1.31}$$

which together with the appropriate covariant derivatives

$$D_\mu X = \partial_\mu X + [\Gamma_\mu, X]_- + ieA_\mu\,[\mathcal{Q},X]_-, \tag{1.32}$$

form new building blocks. The chiral connection Γ_μ in (1.32) contains one derivative and has the following form

$$\Gamma_\mu = \frac{1}{2}\left(u^\dagger\,\partial_\mu u + u\,\partial_\mu u^\dagger\right). \tag{1.33}$$

It is important to mention, that the covariant derivative includes the interaction to the electromagnetic and pseudo-scalar fields. These terms are responsible for the lowest order interaction in the chiral expansion, the so-called Weinberg-Tomozawa ($\pi\,\pi\,h\,h$, h-hadron), Kroll-Ruderman ($\pi\,\gamma\,h\,h$) and "seagull" ($\gamma\,\gamma\,h\,h$) terms. The new objects in (1.31, 1.32) transform homogeneously under the local chiral transformations

$$X \to X' = K\,X\,K^\dagger. \tag{1.34}$$

Armed with this formalism one can incorporate vector mesons into the chiral Lagrangian. However, the constructed Lagrangian with light vector mesons will consist of an infinite number of terms. Similarly to the pure χPT case, an appropriate power-counting scheme is needed to make a systematic approximation.

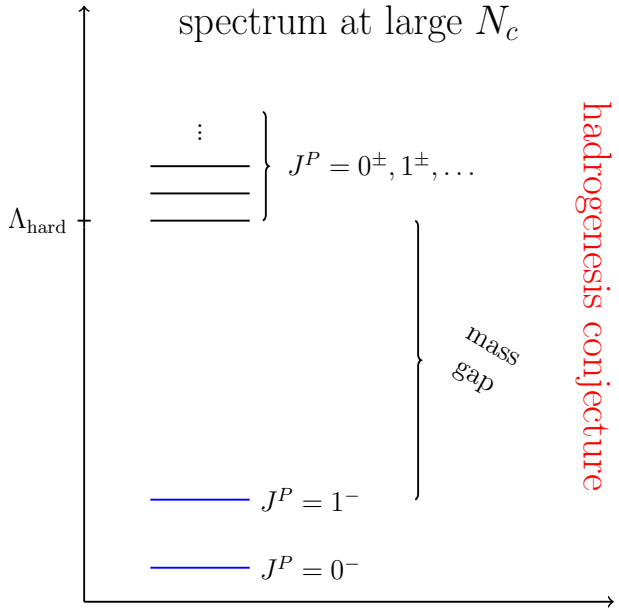

Figure 1.2.: The spectrum of mesons in the large N_c limit which is based on the hadrogenesis conjecture. The picture is taken from [TLL12].

1.3.3 The novel counting scheme

While it is straightforward to write down a chiral Lagrangian with explicit vector mesons, it is an open issue how to order the various terms. In a recent work a counting scheme was suggested based on the dynamical assumption of hadrogenesis [LL08, LK04, TLL12]. It was shown that an important step is the separation of scales. The expansion parameter in the theory is the soft scale divided by the hard scale. In pure χPT, soft scales are the typical momentum of the process and Goldstone boson masses, while the hard scale is the mass of the first non-Goldstone resonance, which is not part of the Lagrangian.

Scale separation is more complicated for the effective Lagrangian, which is used in nonperturbative coupled-channel calculations. First of all, light vector mesons are included explicitly in our Lagrangian. Secondly, as it will be shown in the Section 2.2, the chiral coupled-channel dynamics of Goldstone-boson scattering generates light scalar meson resonances ($J^P = 0^+$). At the same time, the leading chiral interaction of Goldstone bosons with the light vector mesons dynamically generates an axial-vector meson spectrum ($J^P = 1^+$) [LK04]. These findings suggest the hard scale to be significantly larger than in pure χPT. The latter assumption is a postulate of the hadrogenesis conjecture, which relies on the relevance of a few "quasi-fundamental" hadronic degrees of freedom (pseudo-scalar and vector meson fields), while the nearest $0^+, 1^+, 2^\pm$ states can be dynamically generated. Therefore, we expect to have a sizeable mass gap in the large N_c limit (see Fig. 1.2) between 0^-, 1^- and other resonances.

Based on these arguments, in [TLL12] the following hard scale

$$\Lambda_{\rm hard} \geq (2-3)\,\text{GeV} \tag{1.35}$$

was suggested. As a consequence the masses of light vector mesons (m_V) and pseudo-scalar mesons (m_P) can be treated as soft,

$$D_\mu,\, m_P,\, m_V \sim Q\,. \tag{1.36}$$

Note that a derivative is counted as Q not depending on the field it acts upon. The chiral counting for the new building blocks (1.31, 1.33) can be calculated straightforwardly from (1.24),

$$U_\mu \sim Q, \qquad \chi_\pm \sim Q^2, \qquad f_{\mu\nu} \sim Q^2.$$

Even though we have now a formal counting for vector mesons, in order to have a complete picture one has to explore loop effects. This study is beyond the scope of this thesis and will be done elsewhere. In the following we restrict ourselves to the leading order calculations.

1.3.4 Q^2 chiral Lagrangian

The most general Lagrangian can now be constructed with the help of the new building blocks (1.31, 1.33), the power-counting scheme (1.36, 1.37) and large N_c arguments [LL08]. The latter implies that interaction terms that involve a double trace in flavour space are suppressed by $1/N_c$ as compared to single-flavour trace interactions.

At order Q^2, the contributions to two-point functions for pseudo-scalar and vector mesons read [TLL12],

$$\begin{aligned}\mathcal{L}_2 &= f^2\,\mathrm{tr}\Big\{U^\mu\,U_\mu^\dagger + \frac{1}{2}\,\chi_+\Big\} - \frac{1}{4}\,\mathrm{tr}\Big\{(D^\mu\,\Phi_{\mu\alpha})(D_\nu\,\Phi^{\nu\alpha})\Big\} + \frac{1}{8}\,m_V^2\,\mathrm{tr}\Big\{\Phi^{\mu\nu}\,\Phi_{\mu\nu}\Big\} \\ &\quad + \frac{1}{8}\,b_D\,\mathrm{tr}\Big\{\Phi^{\mu\nu}\,\Phi_{\mu\nu}\,\chi_+\Big\} + \frac{1}{2}\,f_V\,\mathrm{tr}\Big\{\Phi^{\mu\nu}\,f_{\mu\nu}^+\Big\}, \end{aligned} \tag{1.37}$$

where f_V is the vector decay constant and parameter b_D determines the explicit breaking of chiral symmetry through the quark masses. At tree-level the vector meson masses are

$$\begin{aligned} m_\rho^2 &= m_\omega^2 = m_V^2 + b_D\,m_\pi^2, \\ m_{K^*}^2 &= m_V^2 + b_D\,m_K^2, \\ m_\phi^2 &= m_V^2 + b_D\,(2\,m_K^2 - m_\pi^2), \end{aligned} \tag{1.38}$$

which lead to the estimate of $m_V \simeq 0.764$ GeV and $b_D = 0.92 \pm 0.05$. The latter values reproduce the empirical vector meson masses with an uncertainty of less than 10 MeV. The parameter f_V,

$$f_V = 0.140 \pm 0.014 \text{ GeV} \tag{1.39}$$

was determined in [LL08] by the decay of the ρ_0, ω and ϕ mesons into di-electrons[7].

With respect to the chiral $SU(3)$ symmetry, the following terms are relevant for three-point vertices of order Q^2,

$$\begin{aligned}\mathcal{L}_3 &= \frac{i}{2}\,f_V\,h_P\,\mathrm{tr}\Big\{U_\mu\,\Phi^{\mu\nu}\,U_\nu\Big\} + \frac{i}{8}\,h_A\,\varepsilon^{\mu\nu\alpha\beta}\,\mathrm{tr}\Big\{\big[\Phi_{\mu\nu},\,(D^\tau\Phi_{\tau\alpha})\big]_+\,U_\beta\Big\} \\ &\quad - \frac{i}{4}\,\frac{m_V^2}{f_V}\,h_V\,\mathrm{tr}\Big\{\Phi_{\mu\tau}\,\Phi^{\mu\nu}\,\Phi^\tau{}_\nu\Big\} + \frac{i}{2}\,e_M\,\mathrm{tr}\Big\{\Phi^\alpha{}_\tau\,f_{\alpha\beta}^+\,\Phi^{\tau\beta}\Big\} \\ &\quad + \frac{i}{8}\,h_O\,\varepsilon^{\mu\nu\alpha\beta}\,\mathrm{tr}\Big\{\big[(D_\alpha\Phi_{\mu\nu}),\,\Phi_{\tau\beta}\big]_+\,U^\tau\Big\} + \frac{i}{4}\,b_A\,\varepsilon^{\mu\nu\alpha\beta}\,\mathrm{tr}\Big\{\Phi_{\mu\nu}\,\chi_-\,\Phi_{\alpha\beta}\Big\}. \end{aligned} \tag{1.40}$$

[7] Note that in [DGL11b, LL08] slightly different notations were used. The relations between e_V, g_D, g_F, h_P in [DGL11b, LL08] — denoted by *old* — and f_V, g_1, g_2, h_P used here and in [TLL12] are $f_V = \frac{0.776\,\text{GeV}}{4e}\,e_V$, $g_1 = g_D$, $g_2 = g_F$ and $h_P = \frac{0.776\,\text{GeV}}{f_V}\,h_P$[old]. $e \simeq 0.303$ is the positron charge.

Note that at this order there is no term which describes the direct decay of a vector meson into a Goldstone boson and photon. This is a next-to-leading order vertex and can be found in [LL08]. The term that includes coupling h_O does not vanish only for processes where at least one vector meson is off-shell (see Appendix B).

Finally, we present the relevant four-point vertices responsible for interactions of vector mesons and Goldstone bosons of order Q^2,

$$\begin{aligned}\mathcal{L}_4 \;=\; & \frac{1}{8} g_1 \,\mathrm{tr}\left\{\left[\Phi_{\mu\nu}, U_\alpha\right]_+ \left[U^\alpha, \Phi^{\mu\nu}\right]_+\right\} + \frac{1}{8} g_2 \,\mathrm{tr}\left\{\left[\Phi_{\mu\nu}, U_\alpha\right]_- \left[U^\alpha, \Phi^{\mu\nu}\right]_-\right\} \\ & + \frac{1}{8} g_3 \,\mathrm{tr}\left\{\left[U_\mu, U^\nu\right]_+ \left[\Phi_{\nu\tau}, \Phi^{\mu\tau}\right]_+\right\} + \frac{1}{8} g_4 \,\mathrm{tr}\left\{\left[U_\mu, U^\nu\right]_- \left[\Phi_{\nu\tau}, \Phi^{\mu\tau}\right]_-\right\} \\ & + \frac{1}{8} g_5 \,\mathrm{tr}\left\{\left[\Phi^{\mu\tau}, U_\mu\right]_- \left[\Phi_{\nu\tau}, U^\nu\right]_-\right\}. \end{aligned} \tag{1.41}$$

The complete leading-order Lagrangian that includes four-point vertices of vector mesons and the η' field can be found in [TLL12]. That work predicts a small mixing between the η and η', $\theta = \pm 2^\circ$, and therefore it is not taken into account in the present study.

To obtain the relevant terms it is useful to expand the building blocks (1.31, 1.33) in powers of Goldstone boson and vector meson fields,

$$\begin{aligned} U_\mu &= \frac{i}{2f}\,\partial_\mu \Phi - \frac{e}{2f} A_\mu \left[\mathcal{Q}, \Phi\right]_- + \mathcal{O}(\Phi^3), \\ D_\mu \Phi_{\alpha\beta} &= \partial_\mu \Phi_{\alpha\beta} + \frac{1}{8f^2}\left[\left[\Phi, \partial_\mu \Phi\right]_-, \Phi_{\alpha\beta}\right]_- + i\,e A_\mu \left[\mathcal{Q}, \Phi_{\alpha\beta}\right]_- + O(\Phi^4), \\ \Gamma_\mu &= \frac{1}{8f^2}\left[\Phi, \partial_\mu \Phi\right]_- + \mathcal{O}(\Phi^3), \\ \chi_+ &= \chi_0 - \frac{1}{8f^2}\left[\Phi, \left[\Phi, \chi_0\right]_+\right]_+ + \frac{1}{384 f^4}\left[\Phi, \left[\Phi, \left[\Phi, \left[\Phi, \chi_0\right]_+\right]_+\right]_+\right]_+ + \mathcal{O}\left(\Phi^6\right), \\ \chi_- &= \frac{i}{2f}\left[\chi_0, \Phi\right]_+ + \mathcal{O}\left(\Phi^3\right), \\ f_{\mu\nu}^+ &= -e\,\mathcal{Q} F_{\mu\nu} + \frac{e}{8f^2}\left[\Phi, \left[\Phi, \mathcal{Q}\right]_-\right]_- F_{\mu\nu} + \mathcal{O}\left(\Phi^4\right), \\ f_{\mu\nu}^- &= -\frac{i\,e}{2f}\left[\Phi, \mathcal{Q}\right]_- F_{\mu\nu} + \mathcal{O}\left(\Phi^3\right). \end{aligned} \tag{1.42}$$

As already pointed out, f may be identified with the pion-decay constant, $f_\pi = 92.4$ MeV, at leading order. A precise determination of f requires a chiral $SU(3)$ extrapolation of some data set. In [LK02] the value $f \simeq 90$ MeV was obtained from a detailed study of pion- and kaon-nucleon scattering data. At the same time, this value was used consistently in various applications of chiral Lagrangians to meson and baryon resonance physics [LK01, LKK04, LK05]. We will use $f = 90$ MeV throughout this thesis.

At first sight, the number of free parameters in (1.37, 1.40, 1.41) that have to be determined from experiment is quite large. However, it is important to stress that only a small part of these parameters contribute to specific physical processes. Most of the parameters are determined by the decay properties of the light vector mesons and Goldstone bosons and only few parameters

are left. Here we recall the values for the parameters determined from two and three body decays [LL08, LL09],

$$\begin{array}{lll} f_V\, h_P \simeq 0.225 \pm 0.023\,\mathrm{GeV}\,, & h_A \simeq 2.10\,, & b_A = 0.27 \pm 0.05\,, \\ h_V \simeq 0.084\,, & e_M \simeq 0.00\,. & \end{array} \tag{1.43}$$

As a result we expect coupled-channel calculations based on this Lagrangian to be highly predictive.

In the next chapter we will show how to extrapolate analytically subthreshold amplitudes to higher energies based on the scheme that implements constraints from micro-causality and exact unitarity [GL10]. First we illustrate the method for a schematic system (Yukawa-type interactions) where the exact solution is known. This will shed further light on its usefulness. Then we apply the scheme to Goldstone boson scattering and photon-fusion reactions. The tree-level partial-wave scattering amplitudes computed from the chiral Lagrangian (1.37, 1.40, 1.41) will be an important input for nonperturbative calculations.

2 Analytic extrapolation of the scattering amplitude

2.1 Yukawa-type interactions

In this section we examine the usefulness of the novel technique [GL10] for the case of non-relativistic Yukawa interactions. The method applied here allows to construct an analytic extrapolation of partial-wave scattering amplitudes fulfilling the unitarity condition. The conformal mapping technique helps to achieve a systematic approximation of the scattering amplitude.

For systems where the exact solution can easily be found, the method does not provide any benefits as compared to the existing theoretical approaches. However, for coupled-channel calculations based on the chiral Lagrangian, where it is already difficult to derive the interaction, our method appears to be very efficient. The Bethe-Salpeter equation, which describes the two-body scattering process in quantum field theory, is a four-dimensional integral equation which is hard to deal with. Moreover, if the interaction kernel is truncated in perturbation theory, where the electromagnetic gauge invariance is guaranteed order by order, the resulting scattering amplitude generally depends on the choice of gauge. This is due to the fact that by iterating the Bethe-Salpeter kernel, a lot of diagrams that are responsible for gauge invariance are missing. Additionally, when an interaction includes s-, t- and u-channel exchange processes the result of the Bethe-Salpeter equation depends on the field parametrization. This is a consequence of the dependence of the off-shell scattering amplitude on the parametrization of U in (1.17) [Sch03]. Contrary, our method is based on the generalized potential, which is an on-shell quantity. As a result, the generated scattering amplitudes will be gauge invariant and independent on the choice of field.

The calculations are made for non-relativistic Yukawa interactions of various strengths and ranges, where the exact solution is found from Lippmann-Schwinger equation. Though a quantitative description of realistic systems is not justified in terms of potential scattering, there are several important features kept in a Yukawa ansatz. It is well known that the analytic structure of the Yukawa partial wave amplitude is similar to the relativistic case. For instance, the nucleon-nucleon interaction has a long-range Yukawa part occurring from the one-pion exchange process. Importantly, a left-hand cut of the scattering amplitude is very close to threshold and therefore has a significant influence on the physical region. In this sense the pion-nucleon system is similar, because there is also a long-range component in the interaction given by the nucleon u-channel exchange.

2.1.1 Expansions with a Yukawa potential

We consider the nonrelativistic scattering of two particles with masses m_1 and m_2 due to a single Yukawa potential,

$$\langle \mathbf{k}'|V\,|\mathbf{k}\rangle = \frac{4\pi\, g}{(\mathbf{k}'-\mathbf{k})^2+\mu^2}\,, \tag{2.1}$$

where the coupling g and Yukawa mass μ characterize the strength and range of the interaction, respectively. The scattering process is determined by the t-matrix, satisfying the nonrelativistic Lippmann-Schwinger equation [BJ76]

$$t = V + V\,G\,t = V + V\,\frac{1}{E-H_0+i\epsilon}\,t\,, \tag{2.2}$$

where $E = q^2/(2\,m)$ is the energy in center-of-mass frame and $m = m_1\,m_2\,/(m_1+m_2)$ is the reduced mass. In the component notation Eq.(2.2) reads

$$\langle \mathbf{k}'|\,t(q^2)|\mathbf{k}\rangle = \langle \mathbf{k}'|V\,|\mathbf{k}\rangle + 2\,m\int \frac{d^3\mathbf{k}''}{(2\pi)^3}\,\frac{\langle \mathbf{k}'|V\,|\mathbf{k}''\rangle\,\langle \mathbf{k}''|\,t(q^2)|\mathbf{k}\rangle}{q^2-k''^2+i\,\epsilon}\,. \tag{2.3}$$

It is often convenient in low or intermediate energy physics to perform a partial-wave decomposition of the amplitude and the potential,

$$\begin{aligned}
\langle \mathbf{k}'|t(q^2)|\mathbf{k}\rangle &= 4\pi\sum_{l=0}^{\infty}(2l+1)\,P_l(\cos\theta)\,\langle k'|t_l(q^2)|k\rangle\,,\\
\langle k'|t_l(q^2)|k\rangle &= \frac{1}{4\pi}\int\frac{d\cos\theta}{2}\,P_l(\cos\theta)\,\langle \mathbf{k}'|t(q^2)|\mathbf{k}\rangle\,,\\
\langle \mathbf{k}'|V|\mathbf{k}\rangle &= 4\pi\sum_{l=0}^{\infty}(2l+1)\,P_l(\cos\theta)\,\langle k'|V_l|k\rangle\,,\\
\langle k'|V_l|k\rangle &= \frac{1}{4\pi}\int\frac{d\cos\theta}{2}\,P_l(\cos\theta)\,\langle \mathbf{k}'|V|\mathbf{k}\rangle\,,
\end{aligned} \tag{2.4}$$

where θ is the scattering angle in center-of-mass frame and l is the angular momentum. The partial-wave Lippmann-Schwinger equation takes the form

$$\langle\, k'|\,t_l(q^2)|k\rangle = \langle\, k'|V_l\,|k\rangle + \frac{4\,m}{\pi}\int_0^{\infty} k''^2\,dk''\,\frac{\langle k'|V_l\,|k''\rangle\,\langle\, k''|\,t_l(q^2)|k\rangle}{q^2-k''^2+i\,\epsilon}\,, \tag{2.5}$$

where q, k, k' correspond to the center-of-mass on-shell and initial and final off-shell momenta, respectively. The explicit form of the partial-wave Yukawa potential reads

$$\begin{aligned}
&\langle\, k'|V_l\,|k\rangle = \frac{g}{2\,k'k}\,Q_l\left(\frac{k^2+k'^2+\mu^2}{2\,k'k}\right)\,, \qquad Q_0(x) = \frac{1}{2}\,\log\frac{x+1}{x-1}\,,\\
&Q_l(x) = \frac{1}{2}\,P_l(x)\,\log\frac{x+1}{x-1} - \sum_{k=1}^{l}\frac{1}{k}\,P_{k-1}(x)\,P_{l-k}(x)\,,
\end{aligned} \tag{2.6}$$

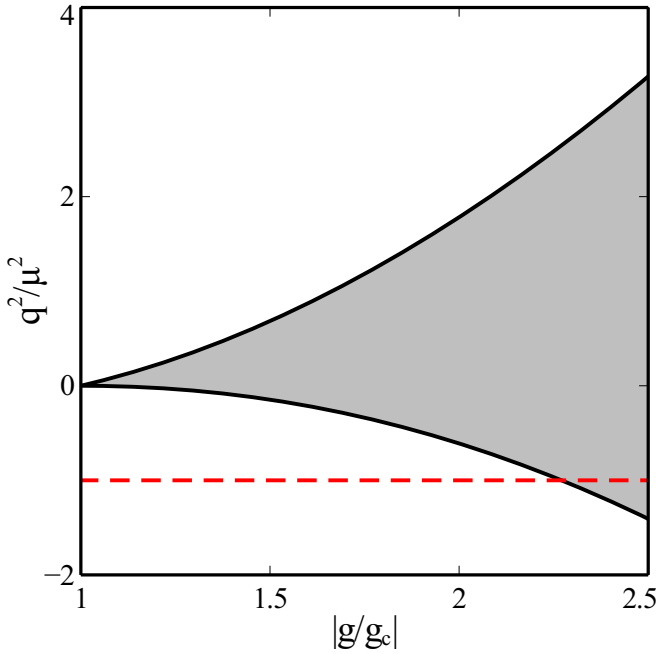

Figure 2.1.: The area of convergence (white) of the Born series for the s-wave Lippmann-Schwinger equation (2.5) with (2.6) in terms of q^2/μ^2 and $|g/g_c|$. For $|g/g_c| < 1$ the series converges for all energies. The branch point caused by the 2nd Born term is noted by the dashed curve.

where $Q_l(x)$ is the Legendre function of second kind, which is analytic everywhere except a cut between $x = \pm 1$.

The Born series, determined as a power expansion of the integral equation (2.5) in the coupling constant g,

$$\begin{aligned} \langle k'|\, t_l(q^2)|k\rangle &= t_l^{(1)} + t_l^{(2)} + \ldots \\ &= \langle\, k'|V_l\,|k\rangle + \frac{4\,m}{\pi}\int_0^\infty k''^2\, dk''\, \frac{\langle\, k'|V_l\,|k''\rangle\,\langle\, k''|\,V_l|k\rangle}{q^2 - k''^2 + i\,\epsilon} + \ldots, \end{aligned} \tag{2.7}$$

converges only for certain values of g and q^2 [Wei63, Lut00]. The convergence domain is determined by the condition that the kernel of the Lippmann-Schwinger equation has no eigenvalues outside the unit circle [Wei63]. The region where the system is perturbative is shown in Fig. 2.1 as a function of q^2/μ^2 and $|g/g_c|$ for the s-wave scattering. For coupling constants, $|g| < g_c$, smaller than the critical one, which is in case of s-wave [EW88]

$$g_c \simeq 1.68\,\frac{\mu}{2\,m}, \tag{2.8}$$

the series converges for all energies ($-\infty < q^2 < +\infty$). However, when the coupling constant is larger than its critical value the scattering amplitude is perturbative either for sufficiently small or large q^2. Within the shaded region of Fig. 2.1 the Born series (2.7) diverges. In the case of attraction ($g < 0$) the two particles form a bound state at $g = -g_c$ [EW88]. Note that even if the Born series fails to converge in the threshold region, the perturbation theory is still applicable for sufficiently large negative q^2.

In Fig. 2.2 the explicit calculation of the Born series to third order is presented. We show the scaled on-shell amplitude

$$\bar{t}_l\,(z) = 2\,m\,\mu\,\langle\, k'|\, t_l(q^2)|k\rangle\Big|_{k'=k=q} \qquad \text{with} \qquad z = \frac{q^2}{\mu^2}, \tag{2.9}$$

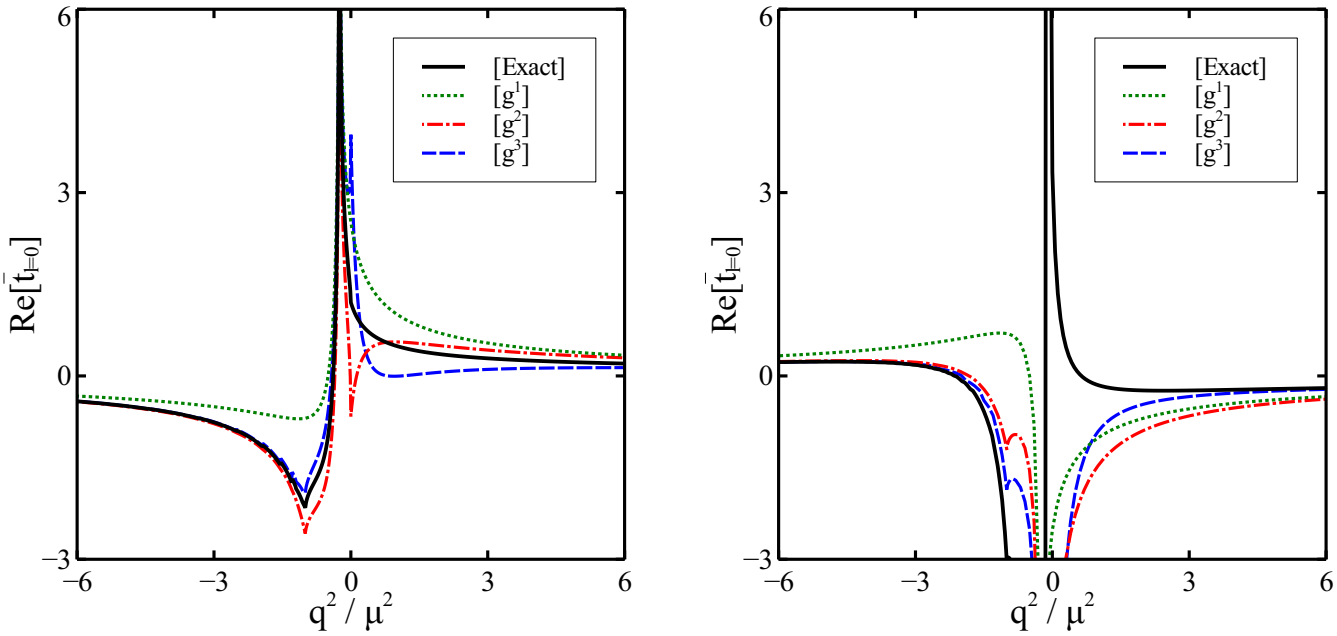

Figure 2.2.: S-wave scattering amplitude $\bar{t}_l$ for $g = \frac{3\,g_c}{2}$ (left-hand panel) and $g = -\frac{3\,g_c}{2}$ (right-hand panel). The solid curve follows with the exact solution of the Lippmann-Schwinger equation, while $[g^n]$ denotes the n-th Born approximation.

for $|g| = 3\,g_c/2$ and s-wave ($l = 0$). The dimensionless amplitude $\bar{t}_l(z)$ depends on $z = q^2/\mu^2$ and g/g_c only. The cases of a positive (repulsive) and a negative (attractive) coupling constant are shown in the left-hand and right-hand panels of Fig. 2.2, respectively. The convergence for large $|q^2/\mu^2|$ is clearly seen in the figure, while the near-threshold region cannot be described by the Born series. We also note the bound state structure arising for negative coupling constant. Similarly, one can consider higher partial waves, but in general they converge faster. The critical coupling constant is there much larger than for the case of s-wave scattering. Therefore in the following we restrict ourselves to considering s-waves only.

With this knowledge, we now turn to the question of how to construct a systematic approximation of the system in the non-perturbative region. Although for the Yukawa interaction this is a quite academic question, realistic systems are much more intricate and cannot be solved exactly. The idea is to explore the causality and unitarity constraints imposed on the scattering amplitude [GL10].

The scattering amplitude (2.9) suffers from kinematical constraints at $q^2 = 0$,

$$t_l(q^2 \simeq 0) \propto q^{2l}\,, \tag{2.10}$$

reflecting the angular momentum barrier. In order to ensure finite values of the partial-wave amplitude at threshold, we define a new scattering amplitude,

$$T_l(q^2) = -2\,m\,\sqrt{\Lambda^2+q^2}\left(\frac{\Lambda^2+q^2}{q^2}\right)^l \langle k'|\,t_l(q^2)|k\rangle\Big|_{k'=k=q}\,, \tag{2.11}$$

with the scale parameter Λ. The new amplitude vanishes at infinite momentum q^2 as

$$T_l(q^2) \to -\frac{g\,m}{2\sqrt{q^2}}\log\frac{q^2}{\mu^2} \qquad \text{for} \qquad q^2 \gg \Lambda^2\,. \tag{2.12}$$

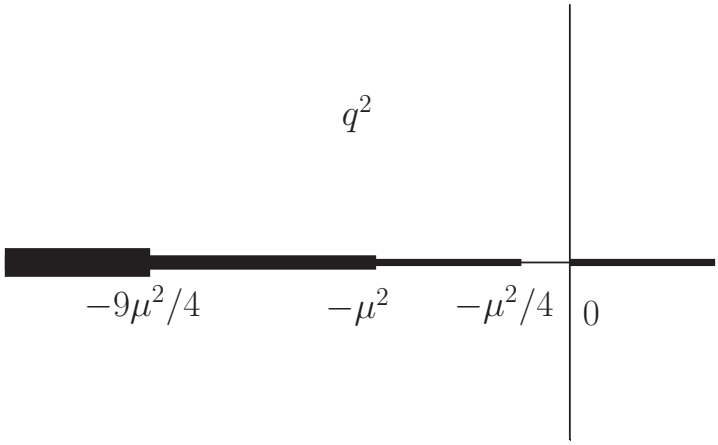

Figure 2.3.: Cut structure in the complex q^2-plane of the Yukawa partial-wave amplitude. The branch points at $q^2 = -\frac{1}{4}(n\,\mu)^2$ with $n = 1, 2, ...$ come from n-th Born terms and unitarity imposes a right-hand cut starting at $q^2 = 0$.

This is needed in order to obtain a well defined dispersive integral, discussed below. For energies above threshold, unitarity requires

$$\text{Im}\, T_l(q^2) = |T_l(q^2)|^2\, \rho_l(q^2)\,, \qquad \rho_l(q^2) = \left(\frac{q^2}{\Lambda^2 + q^2}\right)^{l+\frac{1}{2}}\,. \tag{2.13}$$

In this regard the parameter Λ describes the scale at which the phase-space factor $\rho_l(q^2)$ approaches unity. When the unitarity constraint is satisfied, the phase shifts $\delta_l(q^2)$ can be extracted from the partial-wave scattering amplitudes via,

$$T_l(q^2)\,\rho_l(q^2) = \frac{1}{2\,i}\left(e^{2\,i\,\delta_l(q^2)} - 1\right). \tag{2.14}$$

The analytic structure of the Yukawa partial-wave amplitude is well known (see Fig. 2.3 and e.g. [Tay83]). It has a sequence of left-hand branch points at $q^2 = -\frac{1}{4}(n\,\mu)^2$ $(n = 1, 2, ...)$ [Tay83] coming from n-th Born terms in addition to the branch point at $q^2 = -\Lambda^2$ caused by our normalization[1] (2.11). Moreover, unitarity imposes a cut in the region $q^2 > 0$. Knowing this, one can define the generalized potential $U_l(q^2)$,

$$U_l(q^2) = T_l(q^2) - \int_0^\infty \frac{dq'^2}{\pi}\,\frac{q^2 + \mu_M^2}{q'^2 + \mu_M^2}\,\frac{\rho(q'^2)}{q'^2 - q^2 - i\epsilon}\,|T_l(q'^2)|^2\,, \tag{2.15}$$

which is analytic everywhere above threshold and has the same left-hand cuts as $T_l(q^2)$. We insist on one subtraction in the partial-wave dispersion relation (2.15). This allows us to match the generalized potential and scattering amplitude at $q^2 = -\mu_M^2$ (see e.g. [Man63, GL10]).

An important step is to perform a perturbative expansion not of the scattering amplitude (standard Born series) but rather of the potential $U_l(q^2)$. The perturbative series is constructed

[1] The artificial singularity at $q^2 = -\Lambda^2$ does not have a significant effect on the results. This was checked by a variation of Λ.

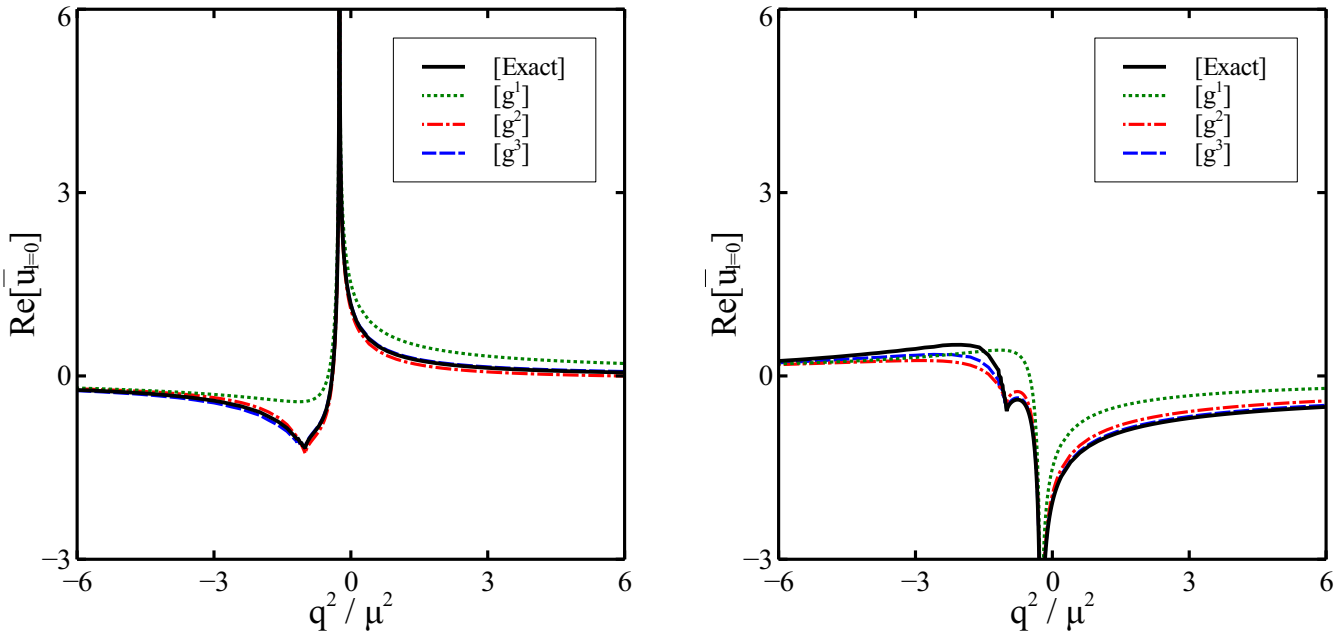

Figure 2.4.: S-wave generalized potential $\bar{u}_l$ for $g = \frac{3}{2} g_c$ (left) and $g = -\frac{3}{2} g_c$ (right). The solid curve follows with the exact solution of the Lippmann-Schwinger equation, while $[g^n]$ denotes the n-th Born approximation to the generalized potential (2.16) and (2.17). A variation of the parameter Λ from 3μ to 9μ is almost invisible on this figure and therefore we refrain from showing it.

by substituting $T_l(q^2) = \sum_k T_l^{(k)}(q^2)$ into the dispersion relation (2.15) and collecting terms of the same power of the coupling constant g

$$U_l(q^2) = \sum_k U_l^{(k)}(q^2), \tag{2.16}$$

where

$$\begin{aligned} U_l^{(1)}(q^2) &= T_l^{(1)}(q^2), \\ U_l^{(2)}(q^2) &= T_l^{(2)}(q^2) - \int_0^\infty \frac{dq'^2}{\pi} \frac{q^2+\mu_M^2}{q'^2+\mu_M^2} \frac{\rho(q'^2)}{q'^2 - q^2 - i\epsilon} |T_l^{(1)}(q'^2)|^2, \\ &\dots . \end{aligned}$$

Such an expansion converges also for the values of couplings larger than the critical one $|g| > g_c$ if the subtraction point μ_M is chosen inside the perturbative area of Fig. 2.1. Moreover such an expansion leads to *exact unitarity* for the scattering amplitude in contrast to Born approximation.

We take $|g| = \frac{3}{2} g_c$ and an s-wave scattering as before and also set the matching scale $\mu_M^2 = 10\,\mu^2$ well below the boundary of the nonperturbative domain. The variation of the parameter Λ will be discussed. In Fig. 2.4 we show the convergence for the generalized potential $\bar{u}_l$, which is normalized in the same way as $\bar{t}_l$,

$$\bar{u}_l(q^2) = -\frac{\mu}{\sqrt{\Lambda^2+q^2}} \left(\frac{\Lambda^2+q^2}{q^2} \right)^{-l} U_l(q^2). \tag{2.17}$$

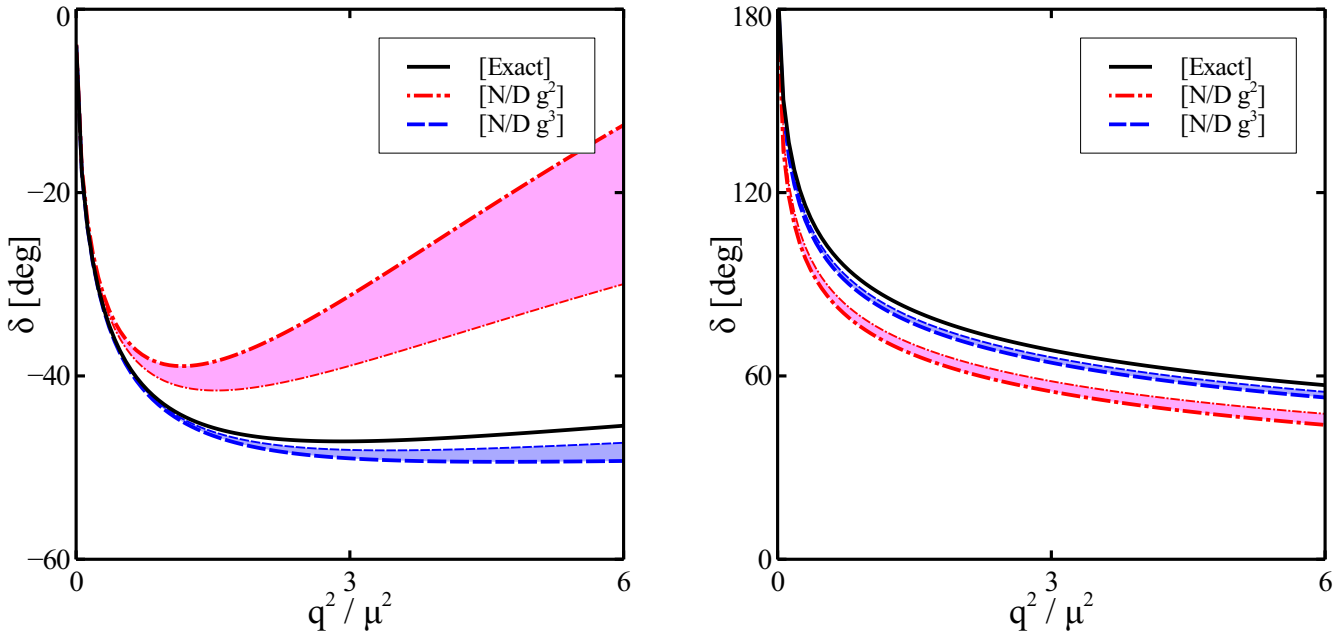

Figure 2.5.: S-wave phase shifts for $g = \frac{3}{2}\, g_c$ (left panel) and $g = -\frac{3}{2}\, g_c$ (right panel). The bands are caused by a variation of $3\,\mu < \Lambda < 9\,\mu$. The solid curve follows with the exact solution, while $[N/D\, g^n]$ denotes the n-th truncation of the generalized potential.

One comment concerning the bound states ($q^2 = -q_{B_i}^2$) is here in order. It is clear from the definition of $U_l(q^2)$ (2.15) that the sum $\sum_k U_l^{(k)}(q^2)$ does not converge to $U_l(q^2)$ but rather to $\tilde{U}_l(q^2)$,

$$\tilde{U}_l(q^2) = U_l(q^2) - \sum_i \frac{g_{B_i}^2\,(q^2+\mu_M^2)}{(q^2+q_{B_i}^2)(q_{B_i}^2-\mu_M^2)}\,, \tag{2.18}$$

with $E_{B_i} = q_{B_i}^2/(2\,m)$ and g_{B_i} are the binding energies and residues of possible bound states. As will be pointed out below, this term does not affect the further N/D solution.

The generalized potential $U_l(q^2)$ calculated for a given truncation can be used as an input for the nonlinear integral equation (2.15). We reconstruct the approximate scattering amplitude by means of the N/D technique [CM60, FW63]. In this method the scattering amplitude is expressed as a ratio of two functions

$$T_l(q^2) = \frac{N_l(q^2)}{D_l(q^2)}\,, \tag{2.19}$$

where $N_l(q^2)$ has only left-hand cuts, and $D_l(q^2)$ contains only right-hand cuts. These functions satisfy the following system of linear integral equations

$$\begin{aligned} N_l(q^2) &= U_l(q^2) + \int_0^\infty \frac{dq'^2}{\pi}\,\frac{q^2+\mu_M^2}{q'^2+\mu_M^2}\,\frac{N_l(q'^2)\,\rho_l(q'^2)\,(U_l(q'^2)-U_l(q^2))}{q'^2-q^2}\,, \\ D_l(q^2) &= 1 - \int_0^\infty \frac{dq'^2}{\pi}\,\frac{q^2+\mu_M^2}{q'^2+\mu_M^2}\,\frac{N_l(q'^2)\,\rho_l(q'^2)}{q'^2-q^2-i\epsilon}\,. \end{aligned} \tag{2.20}$$

Previous, but somewhat different, N/D applications to the case of Yukawa interactions were studied in [FK60, Lum64, CJ68].

In Fig. 2.5 we illustrate how the solution of the dispersion relation (2.15) with generalized potential truncated at various orders converges to the exact one. In order to have a more quantitative analysis we compare the phase shifts instead of scattering amplitudes. In both attractive and repulsive cases the third order of perturbative expansion of the generalized potential recovers the exact phase shifts uniformly in energy. This is in contrast to standard Born series which diverges in the threshold region (see Fig. 2.2). In Fig. 2.5 the bands display a variation of the parameter Λ from $3\,\mu$ to $9\,\mu$. One can see that the width of the band decreases systematically with increasing perturbative order and at cubic order the bands have almost disappeared.

Note that in the case of the attraction there is a bound state in the system. In the solution of the N/D equations (2.20) it appears as a zero in the D_l-function and consequently as a pole in the scattering amplitude T_l. Strictly speaking this indicates that the solution obtained from N/D (2.20) is not a solution of the dispersion relation (2.15), because the perturbative potential does not have a pole contribution. However, if one includes the corresponding pole term to the approximate potential,

$$\frac{g_B^2\,(q^2+\mu_M^2)}{(q^2+q_B^2)(q_B^2-\mu_M^2)}\,, \tag{2.21}$$

the Eq. (2.15) is satisfied. It is straightforward to show that adding such a pole term to the set of N/D equations (2.20) does not change the solution.

From Figs. 2.2 and 2.5 one can conclude that the constraints from analyticity and unitarity allow us to improve significantly the Born approximation, especially in the nonperturbative region.

2.1.2 Approximation for generalized potential

The case studied before is encouraging but a generalization to a more realistic situation would be a desired next step. In most effective field theories, like χPT, the systematic perturbative expansion can be performed only for small momentum. However, we stress that the N/D solution requires the knowledge of the generalized potential above threshold $q^2 > 0$ only. This, together with the fact that by definition the potential is analytic in that region, makes it possible to develop a controlled approximation.

We expect the scattering amplitude in the physical region to be affected largely by the closest cuts. In this respect we split the generalized potential into two parts[2],

$$U(q^2) = U_{\text{inside}}(q^2) + U_{\text{outside}}(q^2)\,, \tag{2.22}$$

where $U_{\text{inside}}(q^2)$ is characterized by the nearest cuts, while $U_{\text{outside}}(q^2)$ takes into account the effects from the more distant cuts. The closest branch cuts arise from one or two particle exchanges and can be evaluated explicitly in particular in χPT. In contrast, the discontinuities across the more distant left-hand cuts arise from many-particle exchanges and most frequently it is impossible to compute them.

[2] Here and in the following we suppress the index l to ease the notations.

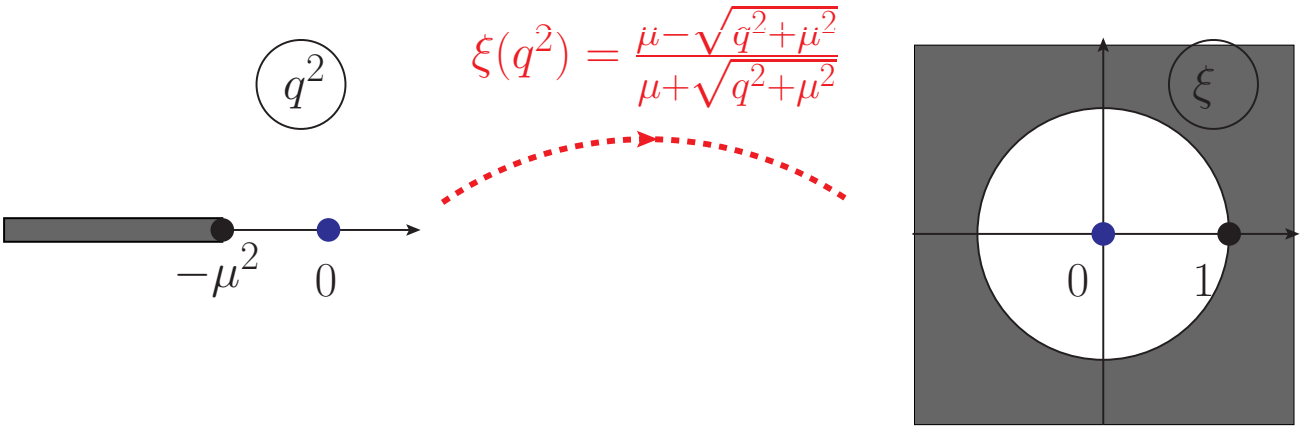

Figure 2.6.: The conformal mapping $q^2 \to \xi$ of $U_{\text{outside}}(q^2)$ which analytic structure is shown on the left. The branch point at $q^2 = -\mu^2$ is determined by the second Born term.

In the considered cases it is natural to calculate explicitly the part of the first Born branch cut from $-\mu^2 < q^2 < -\mu^2/4$ which is closest to the physical region. The known discontinuity across this cut and the Cauchy integral formula allow us to write,

$$U_{\text{inside}}(q^2) = g\, m \int_{-\mu^2}^{-\frac{\mu^2}{4}} \frac{dq'^2}{q'^2 - q^2} \frac{\sqrt{q'^2 + \Lambda^2}}{4q'^2}. \tag{2.23}$$

while the outside potential will be associated with the cuts for $q^2 < -\mu^2$.

If $U_{\text{outside}}(q^2)$ is known around $q^2 = 0$, we can analytically continue it onto $q^2 \in (0, \infty)$ using conformal mapping technique (see Appendix C for more details). The convergence radius of the standard Taylor series in q^2 is limited by the distance to the closest singularity at $q^2 = -\mu^2$. In order to go beyond and reconstruct the outside potential in the required region, we apply the transformation

$$\xi(q^2) = \frac{\mu - \sqrt{q^2 + \mu^2}}{\mu + \sqrt{q^2 + \mu^2}}, \tag{2.24}$$

which maps the cut plane onto a unit circle around $\xi = 0$ as shown in Fig. 2.6. The generalized potential is now approximated with

$$U(q^2) = U_{\text{inside}}(q^2) + \sum_{k=0}^{\infty} C_k \left[\xi(q^2)\right]^k, \tag{2.25}$$

where

$$C_k = \frac{d^k U_{\text{outside}}(q^2(\xi))}{k!\, d\xi^k}\bigg|_{\xi=0}. \tag{2.26}$$

We stress that the knowledge of the first n derivatives of $U_{\text{outside}}(q^2)$ at the expansion point $q^2 = 0$ is sufficient to calculate the n first coefficients of the ξ-expansion. By constructing the

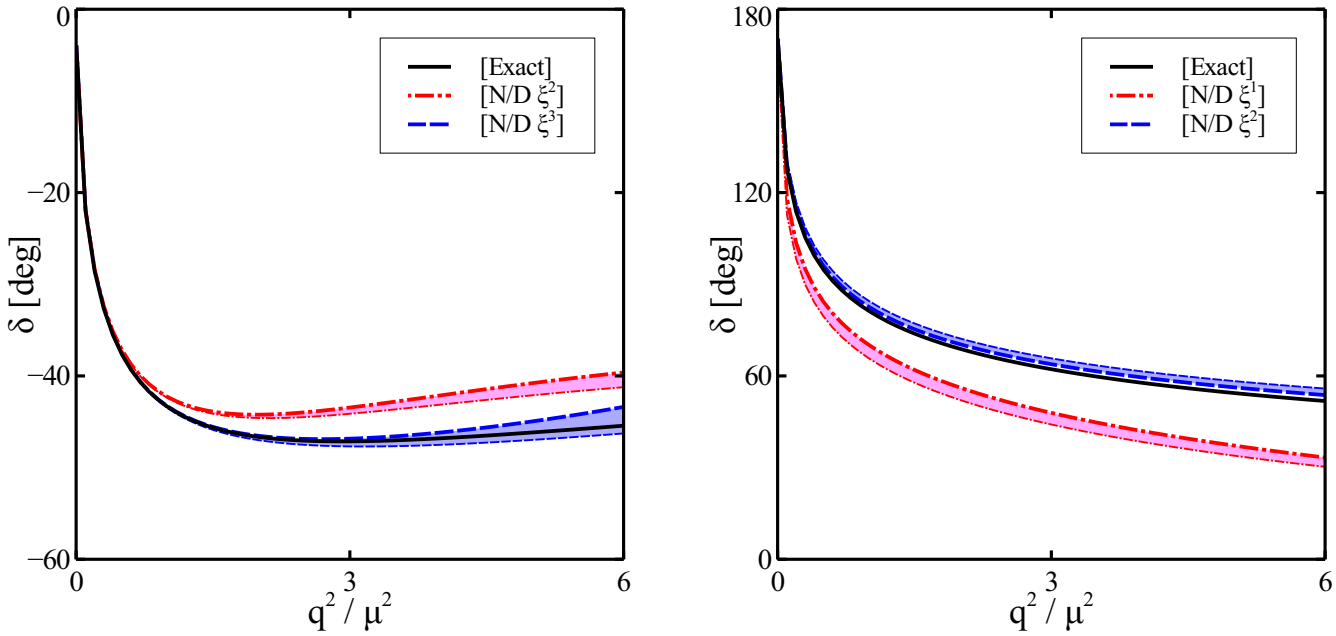

Figure 2.7.: S-wave phase shifts for $g = \frac{3}{2}\, g_c$ (left panel) and $g = -\frac{3}{2}\, g_c$ (right panel). The bands are caused by a variation of $3\,\mu < \Lambda < 9\,\mu$. The solid curve follows with the exact solution, while $[N/D\,\xi^n]$ denotes the corresponding truncation of the ξ-expansion (2.25).

conformal mapping (2.24, 2.25), we extend the radius of convergence of the standard power series into the complete cut plane.

The convergence properties of the ξ-expansion (2.25) are illustrated in Fig. 2.7 for the cases considered before. The conformal mapping technique is applied to the *exact* potential (2.15). In Fig. 2.7 we observe a rapid convergence and already the first three or four terms describe the exact phase shift very accurately. As in Fig. 2.5, the variation of the parameter Λ is reflected in the width of the bands.

We conclude that the information on the analytic structure of the generalized potential allows us to construct a controlled approximation (2.25) in application to realistic systems. In particular, the coefficients C_k can be calculated approximately within χPT or extracted directly from experiment.

2.1.3 Expansion after renormalization

The cases considered before still do not fully reflect a typical situation of effective field theories (EFTs). First of all, in EFTs the matching point cannot be chosen arbitrarily low as compared to Yukawa toy model. The matching scale is usually limited from below by the nonperturbative t- and u-channel effects. In order to take this into account we set $\mu_M = \mu$ in the following. Secondly, realistic systems usually include short- and long-range forces. The short-range ones are typically quite strong and nonperturbative while the long-range forces are week and perturbative. For instance the pion-exchange potential, which is responsible for the long-range part of NN interaction, has a coupling constant that is three times smaller than the critical value [EW88]. From another side there is often a strong short-range interaction which is crucial to produce bound states or resonances. The short-range dynamics is not resolved by EFTs. They become

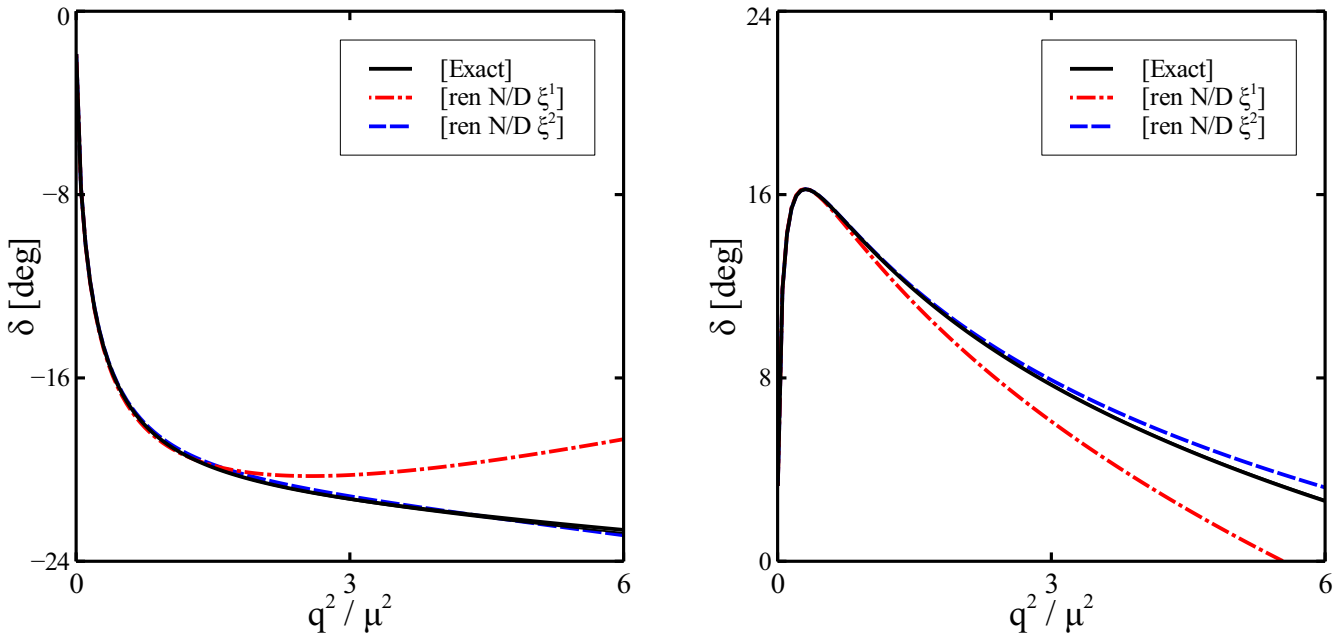

Figure 2.8.: Left-hand panel: repulsive short-range and long-range forces. Right-hand panel: repulsive short-range and attractive long-range forces. The thick solid curve denotes the exact solution, while the thin one corresponds to renormalization (2.30). Here the difference between these curves is invisible. The dashed and dash-dotted curves follow with (2.30) and truncated long-range potential $U_L(q^2)$ according to (2.25).

renormalized in order to satisfy the physical conditions. Thus, we separate the interaction into short (S) and long-range (L) parts,

$$\begin{aligned}\langle k'|V|k\rangle &= \langle k'|V_L|k\rangle + \langle k'|V_S|k\rangle \\ &= \frac{g_L}{4k'k}\log\frac{(k+k')^2+\mu_L^2}{(k-k')^2+\mu_L^2} + \frac{g_S}{4k'k}\log\frac{(k+k')^2+\mu_S^2}{(k-k')^2+\mu_S^2},\end{aligned} \tag{2.27}$$

where $\mu_S \gg \mu_L$. Later on, we will renormalize the short-range interaction in order to get a closer match with EFTs.

At first, we treat the strong short-range interaction exactly while the weak long-range part is considered perturbatively. Starting from ordinary Lippmann-Schwinger equation (2.2) in a compact matrix notation

$$t = \left[1-(V_L+V_S)\,G\right]^{-1}\left[V_L+V_S\right]$$

one obtains

$$t = t_S + (1+t_S\,G)\,V_L\sum_{n=0}^{\infty}\left[(G+G\,t_S\,G)\,V_L\right]^n(1+G\,t_S), \tag{2.28}$$

where $t_S = V_S + V_S\,G\,t_S$ is the corresponding t-matrix of the short-range potential V_S only. An important observation is that the left-hand cut begins at

$$q^2 = -\frac{1}{4}(n\,\mu_L + k\,\mu_S)^2, \tag{2.29}$$

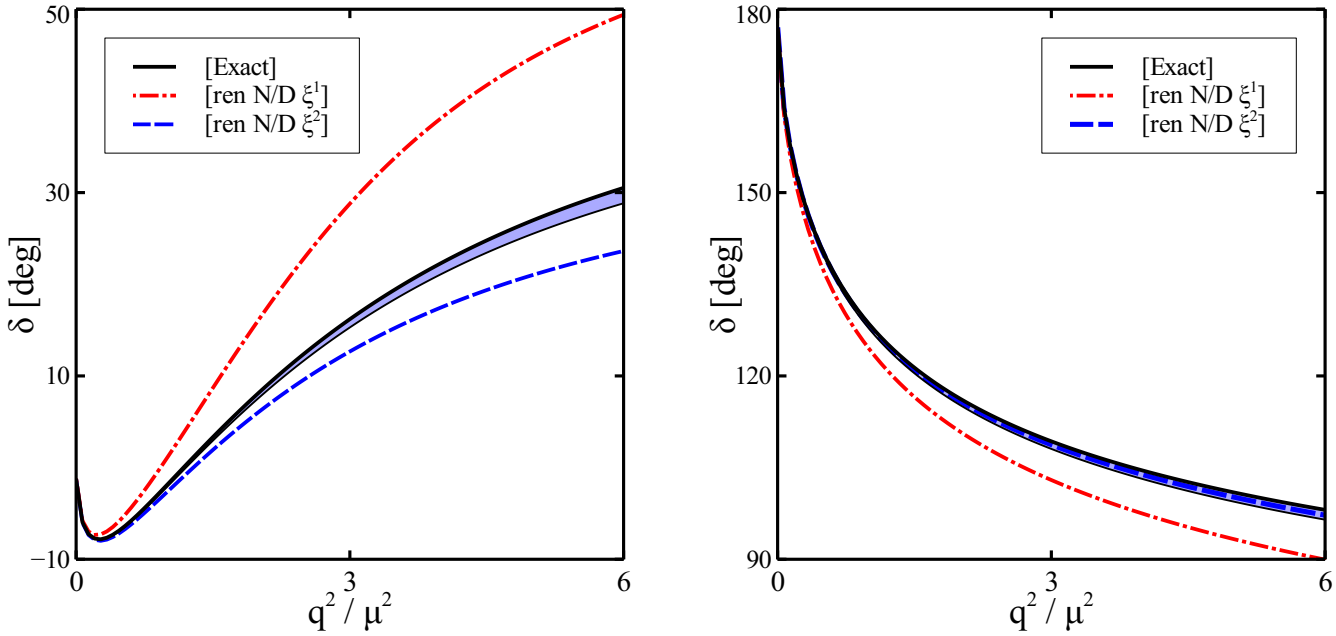

Figure 2.9.: Left-hand panel: attractive short- and repulsive long-range forces. Right-hand panel: attractive short- and long-range forces. Notations are the same as in Fig. 2.8.

caused by n long-range potentials V_L and k short-range structures t_S. Thus in the limit $\mu_S \to \infty$, we can implement the physical renormalization condition

$$U(q^2) \simeq U_L(q^2) + C_S \tag{2.30}$$

with

$$C_S = T(-\mu_M^2) - U_L(-\mu_M^2),$$

at least in the region required in (2.20). In Eq.(2.30) the generalized potential $U_L(q^2)$ is characterized by the long-range interaction and was studied in the previous sections. The size of the coupling constant g_S can be used to dial the value of the scattering amplitude at the matching point. This is nothing but the desired renormalization condition which we will insist on in the following. Due to this condition one may view our scheme as an analytic continuation of the scattering amplitude from the matching point further into the physical region.

For definiteness, we fix $\mu_S = 12\,\mu_L$ such that the short-range potential can be considered as pointlike in comparison with the long-range one. Moreover, we set

$$|g_S| = 0.95\, g_{c,S} \simeq 0.80\, \frac{\mu_S}{m}\,, \tag{2.31}$$

which corresponds to a quite strong interaction but not enough to form a bound state in the case of attraction. For the long-range potential we put $g_L = \pm\frac{1}{2}\, g_{cL}$. We note that the left-hand cut caused by the sort-range potential can be further weakened by a choice of parameter Λ,

$$\Lambda = \frac{1}{2}\,\mu_S\,, \tag{2.32}$$

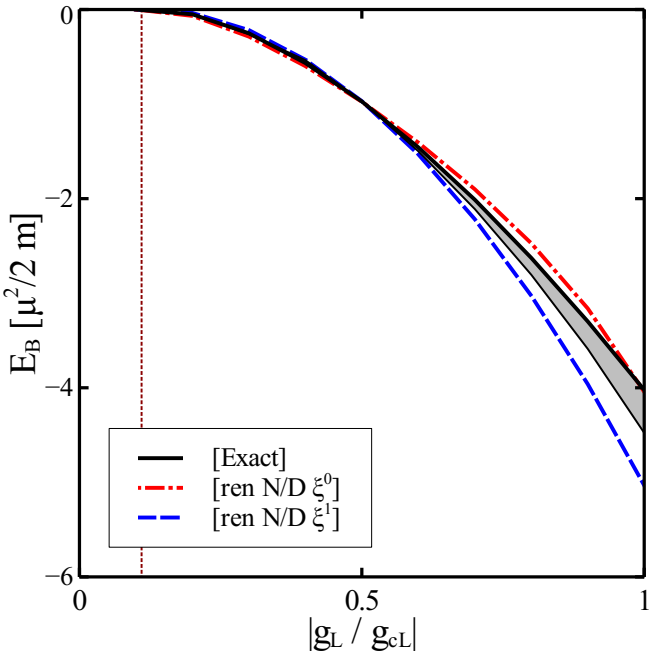

Figure 2.10.: Binding energy for the case of two attractive Yukawa potentials as a function of the coupling $|g_L/g_{cL}|$. The dashed line indicates the point when the first bound state is formed. Notations are the same as in Fig. 2.8.

providing a smooth behavior at the leading branch point $q^2 = -\mu_S^2/4$. Any other choices result in a logarithmic divergence at that point. In what follows we use (2.32) indicating a more rapid realization of (2.30) as $\mu_S \to \infty$.

We study various combinations of attractive and repulsive potentials. In Figs. 2.8 and 2.9 the exact phase shifts are compared with approximate solutions implied by renormalization (2.30) and ξ-expansion (2.25) of the long-range generalized potential $U_L(q^2)$. The bands demonstrate the accuracy of (2.30). For the repulsive short-range force the approximation (2.30) proves to be very accurate while we notice small discrepancies for the attractive short-range force (thick and thin solid curves in Figs. 2.8 and 2.9). In all considered cases already the second order approximation (three terms) in the conformal mapping (2.25) is able to produce a reasonable result.

Finally, we explore the system with two attractive potentials. The bound state is formed for $g_L < -0.11\, g_{cL}$. In Fig. 2.10 we plot the binding energy as a function of the long-range coupling g_L. We observe that already zeroth order in the conformal expansion describes the exact binding energy quite accurately even for large coupling constants.

We conclude that the novel scheme based on the causality and unitarity constraints lead to a systematic approximation that can be very useful for applications in effective field theories. In the next two sections Goldstone-boson scattering and photon-fusion reactions will be considered. In application of this scheme we will unitarize and extrapolate subthreshold partial-wave amplitudes, computed from the chiral Lagrangian (1.37, 1.40, 1.41), into the physical region.

2.2 Goldstone-boson scattering

In this section we study Goldstone-boson scattering which is a subject of wide interest in hadron physics [vBRM$^+$86, WI90, JPHS95, Roy71, ACGL01, CGL01, BDGM04, GMKP$^+$11]. In recent years there was a major progress in the understanding of QCD at low energies in the framework of chiral perturbation theory (χPT). A systematic expansion in terms of the meson momenta and masses perfectly describes the close-to-threshold region (usually $\sqrt{s} < 0.5$ GeV) [Wei79, GL84, KMSF95, BCE$^+$96, BCE$^+$97]. However, χPT faces problems in the resonance region and an extension to somewhat larger energies is achieved by coupled-channel unitarity techniques [OO97, BKM91, JOP00, GNP02]. The most noticeable computation has been done in [GNP02], where the inverse amplitude method (IAM) based on the one-loop χPT amplitudes was applied to produce s- and p-wave phase shifts below 1.2 GeV. At order $\mathcal{O}(Q^4)$ the eight low energy coupling constants were adjusted to reproduce the experimental data. This implies that the lowest scalar and vector mesons with $J^P = 0^+$ and 1^- are properly described by such an approach.

As emphasized in Section 1.3, we expect that the nature of scalar and vector mesons is different. While scalar mesons, in analogy to axial vector mesons, can be generated dynamically by the leading order terms of the chiral Lagrangian, the vector mesons are a consequence of the subleading counter terms and we assume that they belong to the large N_c ground states of QCD [LK04, LL08]. Therefore we keep vector mesons as explicit degrees of freedom and explore their dynamic role in the scattering of Goldstone bosons. Our starting point is the chiral Lagrangian (1.37, 1.40, 1.41) given in Section 1.3. We remind that in our counting scheme (see Subsection 1.3.3 and [TLL12]) the vector meson exchange processes appear at leading order already. Based on this Lagrangian we perform coupled-channel calculations, where we apply the novel unitarization scheme [GL10], discussed in the previous section for the case of non-relativistic Yukawa interaction.

Though the result of [GNP02] is encouraging, there is a certain limitation of IAM if applied to coupled-channel case. Usually the partial-wave scattering amplitudes possess not only right-hand unitary cuts but also unphysical left-hand cuts in the complex s-plane. Their positions depend on the channel and the exchange process. There is no universal branch point that characterizes all coupled-channel amplitudes. Consequently, due to matrix inversion performed in any algebraic method, there would be a mixture of the left-hand cuts of all involved channels. Though these cuts are unphysical, they may have a significant effect in the physical region - in particular when there are complicated overlapping cut structures or even anomalous threshold effects. In contrast to IAM, we treat left-hand singularities carefully and preserve the correct analytical structure of the reaction amplitudes.

2.2.1 Chiral Lagrangian

By expanding the leading order chiral Lagrangian (2.33), given in Subsection 1.3.4, in powers of the Goldstone-boson fields and collecting the terms relevant in our case, we obtain

$$\mathcal{L} = \frac{1}{48f^2}\,\mathrm{tr}\left\{[\Phi,\partial^\mu\Phi]_-\,[\Phi,\partial_\mu\Phi]_- + \Phi^4\,\chi_0\right\} - i\,\frac{f_V\,h_P}{8f^2}\,\mathrm{tr}\left\{\partial_\mu\Phi\,\Phi^{\mu\nu}\,\partial_\nu\Phi\right\}, \qquad (2.33)$$

where we remind that vector mesons are written in terms of the antisymmetric tensor field representation $\Phi_{\mu\nu} = -\Phi_{\nu\mu}$. In the Goldstone-boson sector this representation provides a trans-

parent resonance saturation mechanism for the Q^4 counter terms [EGPdR89]. We emphasize that the chiral Lagrangian (2.33) and therefore all the following results depend on two relevant and known parameters only: the chiral limit value of the pion decay constant $f \simeq 90$ MeV and the coupling $f_V\, h_P$ that characterizes the decay of vector mesons into a pair of Goldstone bosons. The latter was determined in [LL08, LL09] ,

$$f_V\, h_P \simeq 0.225 \pm 0.023\,\text{GeV}\,, \tag{2.34}$$

by analyzing two- and three-body decay properties of the light vector mesons at tree-level.

2.2.2 Isospin symmetry

In this thesis we assume an exact isospin symmetry everywhere. The $SU(3)$ Goldstone boson Φ and vector meson $\Phi_{\mu\nu}$ fields can be written in terms of their isospin symmetric components as

$$\begin{aligned}
\Phi &= \sum_i \Phi^i \lambda^i = \vec{\tau}\cdot\vec{\pi}(140) + \alpha^\dagger\cdot K(494) + K^\dagger(494)\cdot\alpha + \eta(547)\,\lambda_8\,,\\
\Phi_{\mu\nu} &= \sum_i \Phi^i_{\mu\nu} \lambda^i = \vec{\tau}\cdot\vec{\rho}_{\mu\nu}(770) + \alpha^\dagger\cdot K_{\mu\nu}(892) + K^\dagger_{\mu\nu}(892)\cdot\alpha\\
&\quad + \Big(\sqrt{\frac{2}{3}}\,\lambda_0 + \frac{1}{\sqrt{3}}\lambda_8\Big)\,\omega_{\mu\nu}(782) + \Big(\frac{1}{\sqrt{3}}\,\lambda_0 - \sqrt{\frac{2}{3}}\lambda_8\Big)\,\phi_{\mu\nu}(1020)\,,\\
\alpha^\dagger &= \frac{1}{\sqrt{2}}(\lambda_4 + i\,\lambda_5,\, \lambda_6 + i\,\lambda_7)\,, \quad \vec{\tau} = (\lambda_1,\, \lambda_2,\, \lambda_3)\,,
\end{aligned} \tag{2.35}$$

where η, $K = (K^+, K^0)^t$ and $\vec{\pi} = (\pi_1,\, \pi_2,\, \pi_3)$ are the isospin singlet, doublet and triplet fields, respectively. The numbers in braces indicate the approximate masses of pseudo-scalar and vector mesons. The explicit forms of the pion fields are

$$\pi_1 = \frac{\pi^+ + \pi^-}{\sqrt{2}}\,, \quad \pi_2 = i\,\frac{\pi^+ - \pi^-}{\sqrt{2}}\,, \quad \pi_3 = \pi^0\,. \tag{2.36}$$

The two-body scattering problem decouples into thirteen orthogonal channels specified by isospin (I), G-parity (G), and strangeness (S) quantum numbers,

$$(I^G, S) = (0,\pm2),\, (1,\pm2),\, (\tfrac{1}{2},\pm1),\, (\tfrac{3}{2},\pm1),\, (0^\pm,0),\, (1^\pm,0),\, (2,0)\,, \tag{2.37}$$

listed in Table 2.1. In order to construct them, we couple two-body isospin multiplets and perform an irreducible decomposition:

$$\begin{aligned}
&1\otimes 1 = 0\oplus 1\oplus 2, \qquad 1\otimes\frac{1}{2} = \frac{1}{2}\oplus\frac{3}{2}, \quad 1\otimes 0 = 1, \quad \frac{1}{2}\otimes\frac{1}{2} = 0\oplus 1\,,\\
&\tfrac{1}{2}\otimes 0 = \tfrac{1}{2}, \qquad 0\otimes 0 = 0\,.
\end{aligned} \tag{2.38}$$

For instance, the $|\pi\pi\rangle_{I=0}$ state is given by

$$\frac{1}{\sqrt{3}}\,(\pi_q\cdot\,\pi_p) = \frac{1}{\sqrt{3}}\left(\pi_q^+\,\pi_p^- + \pi_q^-\,\pi_p^+ + \pi_q^0\,\pi_p^0\right)\,, \tag{2.39}$$

Table 2.1.: The coupled-channel states (I^G, S) characterized by isospin (I), (G)-parity, and strangeness (S). The Pauli matrices σ_i act on isospin doublet fields $K, \bar{K}$ with for instance $K = (K^+, K^0)^t$.

$(0,-2)$	$(1,-2)$	$(\frac{1}{2},-1)$
$(\frac{1}{\sqrt{2}}\bar{K}_q\, i\,\sigma_2 \bar{K}_p^t)$	$(\frac{1}{\sqrt{2}}\bar{K}_q\,\vec{\sigma}\, i\,\sigma_2 \bar{K}_p^t)$	$\begin{pmatrix} (\frac{1}{\sqrt{3}}\pi_q\cdot\vec{\sigma}\, i\,\sigma_2 \bar{K}_p^t) \\ (\bar{K}_p\, i\,\sigma_2\,\eta_q) \end{pmatrix}$
$(\frac{3}{2},-1)$	$(0^+,0)$	$(0^-,0)$
$(\pi_q\cdot T\, i\,\sigma_2 \bar{K}_p^t)$	$\begin{pmatrix} \frac{1}{\sqrt{3}}(\pi_q\cdot\pi_p) \\ \frac{1}{2}(\bar{K}_q K_p + \bar{K}_p K_q) \\ (\eta_q\,\eta_p) \end{pmatrix}$	$\frac{1}{2}(\bar{K}_q K_p - \bar{K}_p K_q)$
$(1^+,0)$	$(1^-,0)$	$(2^+,0)$
$\begin{pmatrix} (\frac{1}{i\sqrt{2}}\pi_q\times\pi_p) \\ \frac{1}{2}(\bar{K}_q\vec{\sigma}\,K_p - \bar{K}_p\vec{\sigma}\,K_q) \end{pmatrix}$	$\begin{pmatrix} (\pi_q\,\eta_p) \\ \frac{1}{2}(\bar{K}_q\vec{\sigma}\,K_p + \bar{K}_p\vec{\sigma}\,K_q) \end{pmatrix}$	$\left(\frac{1}{2}(\pi_q^i\,\pi_p^j + \pi_q^j\,\pi_p^i) - \frac{1}{3}\,\delta_{ij}\,\pi_q\cdot\pi_p\right)$
$(0,2)$	$(1,2)$	$(\frac{1}{2},1)$
$(\frac{1}{\sqrt{2}}K_q^t\, i\,\sigma_2 K_p)$	$(\frac{1}{\sqrt{2}}K_q^t\,\sigma_2\, i\,\vec{\sigma}\,K_p)$	$\begin{pmatrix} (\frac{1}{\sqrt{3}}\pi_q\cdot\vec{\sigma}\,K_p) \\ (\eta_q K_p) \end{pmatrix}$
$(\frac{3}{2},1)$		
$(\pi_q\cdot T\,K_p)$		

where the subscripts p and q correspond to the initial four-momenta of two particles in the $P(p)+P(q)\to P(\bar{p})+P(\bar{q})$ scattering. This result up to a common sign reproduces the answer from standard Clebsch coefficients with the phase convention $|\pi^+\rangle = -|1,1\rangle$ [Gas83]. Note that the isoscalar structures $\frac{1}{\sqrt{2}}\bar{K}_q K_p$ and $\frac{1}{\sqrt{2}}\bar{K}_p K_q$ are not G-parity eigenstates, and therefore two new combinations were introduced,

$$\frac{1}{2}(\bar{K}_q K_p + \bar{K}_p K_q)\,, \qquad \frac{1}{2}(\bar{K}_q K_p - \bar{K}_p K_q)\,, \tag{2.40}$$

with ± 1 eigenvalues, respectively. The same idea also applies to the $I=1$ channel. In order to obtain states with negative strangeness, an antiparticle doublet is needed. The isospin symmetry group $SU(2)$ requires to define the kaon antiparticle doublet as

$$i\sigma_2 \bar{K}^t\,, \tag{2.41}$$

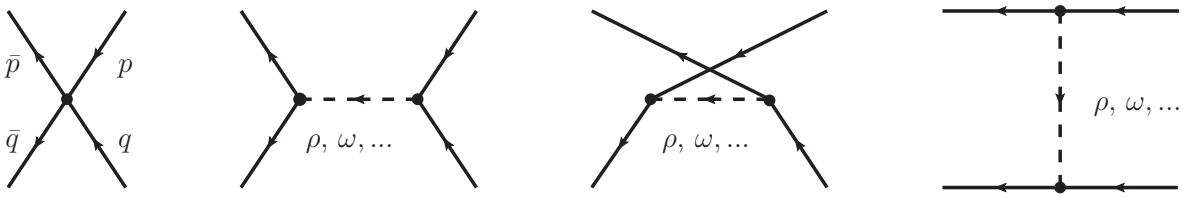

Figure 2.11.: Tree-level diagrams for Goldstone-boson scattering with the exchange of light vector mesons (dashed line) in the s-,t- and u-channels. p, q are the momenta of the incoming mesons and $\bar{p}$, $\bar{q}$ are the momenta of the outgoing mesons.

with $\bar{K} = (K^-, \bar{K}^0)$. Moreover in Table 2.1, the (4×2) matrices T_j describe the transition from isospin $1/2$ to $3/2$ states and are explicitly given by

$$T_1 = \begin{pmatrix} -\frac{1}{\sqrt{2}} & 0 \\ 0 & -\frac{1}{\sqrt{6}} \\ \frac{1}{\sqrt{6}} & 0 \\ 0 & \frac{1}{\sqrt{2}} \end{pmatrix}, \quad T_2 = \begin{pmatrix} \frac{i}{\sqrt{2}} & 0 \\ 0 & \frac{i}{\sqrt{6}} \\ \frac{i}{\sqrt{6}} & 0 \\ 0 & \frac{i}{\sqrt{2}} \end{pmatrix}, \quad T_3 = \begin{pmatrix} 0 & 0 \\ \sqrt{\frac{2}{3}} & 0 \\ 0 & \sqrt{\frac{2}{3}} \\ 0 & 0 \end{pmatrix}, \tag{2.42}$$

with the normalization $T T^\dagger = 1$ and $T_i^\dagger T_j = \delta_{ij} - \frac{1}{3}\sigma_i \sigma_j$.

In each of the isospin channels there are several meson-meson states coupled to each other. In Table 2.1 we have specified the states which contain the most relevant meson-meson information below 1.2 GeV. Here, we are neglecting multi-pion states which are only relevant for higher energies. As well, we neglect PV and VV states (P and V generically denote pseudo-scalar and light-vector mesons, respectively) which on account of the resonant nature of the vector states would significantly contribute to the multi-pion states.

2.2.3 Partial-wave amplitudes

Using the Lagrangian (2.33), we calculate the $P(p) + P(q) \to P(\bar{p}) + P(\bar{q})$ coupled-channel scattering amplitudes. At tree-level, the amplitude takes the form

$$\begin{aligned} T(s,t,u) = {} & \frac{C_s}{12f^2}\, s + \frac{C_t}{12f^2}\, t + \frac{C_u}{12f^2}\, u + \frac{C_\pi}{12f^2}\, m_\pi^2 + \frac{C_K}{12f^2}\, m_K^2 \\ & + \sum_{x=0}^{8} \frac{(f_V h_P)^2}{128 f^4} \frac{C_{s-ch}^{(x)}}{s - m_x^2} \left[(s + m_2^2 - m_1^2)(s + \bar{m}_2^2 - \bar{m}_1^2) + 2\,(t - m_2^2 - \bar{m}_2^2)\, s \right] \\ & + \sum_{x=0}^{8} \frac{(f_V h_P)^2}{128 f^4} \frac{C_{t-ch}^{(x)}}{t - m_x^2} \left[(t + m_2^2 - \bar{m}_2^2)(t + m_1^2 - \bar{m}_1^2) + 2\,(s - m_2^2 - m_1^2)\, t \right] \\ & + \sum_{x=0}^{8} \frac{(f_V h_P)^2}{128 f^4} \frac{C_{u-ch}^{(x)}}{u - m_x^2} \left[(u + m_2^2 - \bar{m}_1^2)(u + \bar{m}_2^2 - m_1^2) + 2\,(t - m_2^2 - \bar{m}_2^2)\, u \right], \end{aligned} \tag{2.43}$$

where the coefficients $C_{...}$ are presented in Tables 2.2 and 2.3 with respect to the coupled-channel states of Table 2.1. Note that we use a convention imposing the unitarity condition for identical and non-identical two-particle isospin states to be the same (see below (2.51) and

Table 2.2.: The coefficients C_s, C_t, C_u, C_π, C_K and $C^{(x)}_{s-ch}$ of the amplitude (2.43) that characterize the contact and s-channel vector meson exchange contributions of the Goldstone-boson scattering with respect to the coupled-channel states $\left(I^G, S\right)$ of Table 2.1. The numbers in the column "ch = ab" correspond to the out-states (a) and in-states (b) of Table 2.1.

$\left(I^G, S\right)$	ch.	C_s	C_t	C_u	C_π	C_K	$C^{(\rho)}_{s-ch}$	$C^{(K^*)}_{s-ch}$	$C^{(\omega)}_{s-ch}$	$C^{(\phi)}_{s-ch}$
(0,-2)	11	0	0	0	0	0	0	0	0	0
(1,-2)	11	-4	2	2	0	4	0	0	0	0
$\left(\frac{1}{2}, -1\right)$	11	5	2	-7	2	2	0	-6	0	0
	12	-3	6	-3	2	-2	0	-6	0	0
	22	-3	6	-3	-2	6	0	-6	0	0
$\left(\frac{3}{2}, -1\right)$	11	-4	2	2	2	2	0	0	0	0
$(0^+, 0)$	11	8	-4	-4	10	0	0	0	0	0
	12	$2\sqrt{3}$	$-\sqrt{3}$	$-\sqrt{3}$	$2\sqrt{3}$	$2\sqrt{3}$	0	0	0	0
	13	0	0	0	$2\sqrt{3}$	0	0	0	0	0
	22	6	-3	-3	0	12	0	0	0	0
	23	6	-3	-3	-2	6	0	0	0	0
	33	0	0	0	$-\frac{14}{3}$	$\frac{32}{3}$	0	0	0	0
$(0^-, 0)$	11	0	9	-9	0	0	0	0	-4	-8
$(1^+, 0)$	11	0	6	-6	0	0	-8	0	0	0
	12	0	$3\sqrt{2}$	$-3\sqrt{2}$	0	0	$-4\sqrt{2}$	0	0	0
	22	0	3	-3	0	0	-4	0	0	0
$(1^-, 0)$	11	0	0	0	4	0	0	0	0	0
	12	$2\sqrt{6}$	$-\sqrt{6}$	$-\sqrt{6}$	$2\sqrt{\frac{2}{3}}$	$-2\sqrt{\frac{2}{3}}$	0	0	0	0
	22	4	-2	-2	0	8	0	0	0	0
$(2^+, 0)$	11	-4	2	2	4	0	0	0	0	0

(2.52)). The tree-level scattering amplitude is given by the Weinberg-Tomozawa and the s-, t- and u-channel vector meson exchange terms. In Fig. 2.11 the set of diagrams that we take into account is depicted. The sums in (2.43) run over all members of the light vector nonet (1.28).

Partial-wave amplitudes are constructed by an average

$$T_J(s) = \int_{-1}^{+1} \frac{d\cos\theta}{2} \left(\frac{s}{\bar{p}_{\rm cm}\, p_{\rm cm}}\right)^J T(s,t,u)\, P_J(\cos\theta) \tag{2.44}$$

over the scattering angle θ in the center-of-mass frame. In Eq. (2.44) J denotes the total angular momentum and $p_{\rm cm}$ and $\bar{p}_{\rm cm}$ are the initial and final relative momenta, respectively. The conventions we use for kinematics are given in Appendix D. The factor $(s/\bar{p}_{\rm cm}\, p_{\rm cm})^J$ in (2.44) is required to avoid kinematical singularities at threshold and to arrive at a proper normalization

Table 2.3.: The coefficients $C^{(x)}_{t-ch}$ and $C^{(x)}_{u-ch}$ of the amplitude (2.43) that characterize the t- and u-channel vector meson exchange contributions of the Goldstone-boson scattering with respect to the coupled-channel states $\left(I^G, S\right)$ of Table 2.1.

$\left(I^G, S\right)$	ch.	$C^{(\rho)}_{t-ch}$	$C^{(K^*)}_{t-ch}$	$C^{(\omega)}_{t-ch}$	$C^{(\phi)}_{t-ch}$	$C^{(\rho)}_{u-ch}$	$C^{(K^*)}_{u-ch}$	$C^{(\omega)}_{u-ch}$	$C^{(\phi)}_{u-ch}$
(0,-2)	11	-3	0	1	2	-3	0	1	2
(1,-2)	11	1	0	1	2	-1	0	-1	-2
$\left(\frac{1}{2}, -1\right)$	11	-8	0	0	0	0	2	0	0
	12	0	0	0	0	0	-6	0	0
	22	0	0	0	0	0	-6	0	0
$\left(\frac{3}{2}, -1\right)$	11	4	0	0	0	0	-4	0	0
$(0^+, 0)$	11	-8	0	0	0	8	0	0	0
	12	0	-2 $\sqrt{3}$	0	0	0	2 $\sqrt{3}$	0	0
	13	0	0	0	0	0	0	0	0
	22	-3	0	-1	-2	3	0	1	2
	23	0	-6	0	0	0	6	0	0
	33	0	0	0	0	0	0	0	0
$(0^-, 0)$	11	-3	0	-1	-2	-3	0	-1	-2
$(1^+, 0)$	11	-4	0	0	0	-4	0	0	0
	12	0	$-2\sqrt{2}$	0	0	0	$-2\sqrt{2}$	0	0
	22	1	0	-1	-2	1	0	-1	-2
$(1^-, 0)$	11	0	0	0	0	0	0	0	0
	12	0	-2 $\sqrt{6}$	0	0	0	2$\sqrt{6}$	0	0
	22	1	0	-1	-2	-1	0	1	2
$(2^+, 0)$	11	4	0	0	0	-4	0	0	0

of the partial-wave amplitudes. From (2.43) and (2.44) we obtain the following results[3] for $J = 0$,

$$
\begin{aligned}
T_{J=0}(s) = {} & \frac{C_s}{12f^2}s + \frac{C_\pi}{12f^2}m_\pi^2 + \frac{C_K}{12f^2}m_K^2 \\
& + \frac{C_t}{24f^2}\left[m_1^2 + m_2^2 + \bar{m}_1{}^2 + \bar{m}_2^2 - s - \frac{m_2^2 - m_1^2}{s}\left(\bar{m}_2^2 - \bar{m}_1^2\right)\right] \\
& + \frac{C_u}{24f^2}\left[m_1^2 + m_2^2 + \bar{m}_1{}^2 + \bar{m}_2^2 - s + \frac{m_2^2 - m_1^2}{s}\left(\bar{m}_2^2 - \bar{m}_1^2\right)\right] \\
& + \sum_{x=0}^{8}\frac{(f_V h_P)^2 C^{(x)}_{t-ch}}{32f^4}\, h_t^{(0)}(s) + \sum_{x=0}^{8}\frac{(f_V h_P)^2 C^{(x)}_{u-ch}}{32f^4}\, h_u^{(0)}(s),
\end{aligned}
\tag{2.45}
$$

[3] Note that in what follows, meson-meson interactions are considered only for s- and p-waves. The result for the d-wave amplitude is needed for the photon-fusion reactions, elaborated in Section 2.3.

$J=1$,

$$T_{J=1}(s) = \frac{C_t}{18f^2}s - \frac{C_u}{18f^2}s + \sum_{x=0}^{8}\frac{(f_V h_P)^2}{96f^4}\frac{C_{s-ch}^{(x)}}{s-m_x^2}s^2 + \sum_{x=0}^{8}\frac{(f_V h_P)^2\, C_{t-ch}^{(x)}}{32f^4}h_t^{(1)}(s) + \sum_{x=0}^{8}\frac{(f_V h_P)^2\, C_{u-ch}^{(x)}}{32f^4}h_u^{(1)}(s)\,, \tag{2.46}$$

and $J=2$,

$$T_{J=2}(s) = \sum_{x=0}^{8}\frac{(f_V h_P)^2\, C_{t-ch}^{(x)}}{32f^4}h_t^{(2)}(s) + \sum_{x=0}^{8}\frac{(f_V h_P)^2\, C_{u-ch}^{(x)}}{32f^4}h_u^{(2)}(s)\,, \tag{2.47}$$

where the contributions from the t- and u-channel vector meson exchanges follow with

$$\begin{aligned} h_u^{(J)}(s) &= \int_{-1}^{+1}\frac{s^J\,dx}{8\,(p_{cm}\bar{p}_{cm})^J}\frac{1}{u-m_x^2}\Big[(u+m_2^2-\bar{m}_1^2)(u+\bar{m}_2^2-m_1^2) \\ &\quad +2(t-m_2^2-\bar{m}_2^2)\,u\Big]P_J(x)\,, \\ h_t^{(J)}(s) &= \int_{-1}^{+1}\frac{s^J\,dx}{8\,(p_{cm}\bar{p}_{cm})^J}\frac{1}{t-m_x^2}\Big[(t+m_2^2-\bar{m}_2^2)(t+m_1^2-\bar{m}_1^2) \\ &\quad +2(s-m_2^2-m_1^2)\,t\Big]P_J(x)\,, \end{aligned} \tag{2.48}$$

and

$$\begin{aligned} u &= \frac{1}{2}\left[m_1^2+m_2^2+\bar{m}_1^2+\bar{m}_2^2-s+\frac{m_2^2-m_1^2}{s}(\bar{m}_2^2-\bar{m}_1^2)\right]-2\,x\,p_{cm}\bar{p}_{cm}\,, \\ t &= \frac{1}{2}\left[m_1^2+m_2^2+\bar{m}_1^2+\bar{m}_2^2-s-\frac{m_2^2-m_1^2}{s}(\bar{m}_2^2-\bar{m}_1^2)\right]+2\,x\,p_{cm}\bar{p}_{cm}\,, \\ \sqrt{s} &= \sqrt{p_{cm}^2+m_1^2}+\sqrt{p_{cm}^2+m_2^2}=\sqrt{\bar{p}_{cm}^2+\bar{m}_1^2}+\sqrt{\bar{p}_{cm}^2+\bar{m}_2^2}\,. \end{aligned} \tag{2.49}$$

We note that for identical bosons of spin zero the system must be symmetric or antisymmetric under the interchange of the two particles. This depends on the angular momentum J and implies additional selection rules. For instance, the allowed possibilities for two pions are: if $I=0,2$ (the isospin states are symmetric under interchange $p\longleftrightarrow q$) then J must be even, and if $I=1$ then J must be odd. In Table 2.4 a complete set of selection rules for the Goldstone-boson scattering according to the isospin channels (I^G,S) can be found.

2.2.4 Dynamics of coupled channels

The coupled-channel partial-wave amplitudes $T_{ab}^J(s)$ will be determined in the same manner as in our previous Section, namely as solutions of the non-linear integral equation

$$T_{ab}^J(s) = U_{ab}^J(s) + \int_{\mu_{thr}^2}^{\infty}\frac{d\bar{s}}{\pi}\frac{s-\mu_M^2}{\bar{s}-\mu_M^2}\frac{\Delta T_{ab}^J(\bar{s})}{\bar{s}-s-i\epsilon}\,, \tag{2.50}$$

Table 2.4.: Selection rules for the Goldstone-boson scattering with respect to the coupled-channel states (I^G, S) of Table 2.1.

$(0,-2)$	$(1,-2)$	$(\frac{1}{2},-1)$	$(\frac{3}{2},-1)$	$(0^+,0)$	$(0^-,0)$	$(1^+,0)$	$(1^-,0)$	$(2^+,0)$
odd J	even J	$\begin{pmatrix} \text{any } J \\ \text{any } J \end{pmatrix}$	any J	$\begin{pmatrix} \text{even } J \\ \text{even } J \\ \text{even } J \end{pmatrix}$	odd J	$\begin{pmatrix} \text{odd } J \\ \text{odd } J \end{pmatrix}$	$\begin{pmatrix} \text{any } J \\ \text{even } J \end{pmatrix}$	even J

which is generalized for the case of several coupled-channel states. The generalized potential, $U^J_{ab}(s)$, contains left-hand cuts only and a and b are the coupled-channel indices (in our case $\pi\pi$, KK etc.). Unitarity implies that the discontinuity along the right hand cut is given by[4]

$$\begin{aligned} \Delta T^J_{ab}(s) &= \frac{1}{2i}\left(T^J_{ab}(s+i\epsilon) - T^J_{ab}(s-i\epsilon)\right) \\ &= \text{Im}\, T^J_{ab}(s) = \sum_{c,d} T^J_{ac}(s)\,\rho^J_{cd}(s)\,T^{J*}_{db}(s), \end{aligned} \tag{2.51}$$

where the phase-space function $\rho^J_{cd}(s)$ is a real diagonal matrix and the sum runs over the various intermediate states. In our normalization, the phase space matrix

$$\begin{aligned} \rho^J_{cd}(s) &= \frac{1}{8\pi}\left(\frac{p_{cm}}{\sqrt{s}}\right)^{2J+1} \Theta(s-\mu^2_{\text{thr}})\,\delta_{cd}\,, \\ p^2_{cm} &= \frac{(s-(m_1+m_2)^2)(s-(m_1-m_2)^2)}{4s} \end{aligned} \tag{2.52}$$

approaches a finite value in the high-energy limit. Combining (2.51) and (2.50) we obtain the following non-linear integral equation

$$T^J_{ab}(s) = U^J_{ab}(s) + \sum_{c,d}\int_{\mu^2_{thr}}^{\infty} \frac{d\bar{s}}{\pi}\frac{s-\mu^2_M}{\bar{s}-\mu^2_M}\,\frac{T^J_{ac}(\bar{s})\,\rho^J_{cd}(\bar{s})\,T^{J*}_{db}(\bar{s})}{\bar{s}-s-i\epsilon}\,. \tag{2.53}$$

The matching scale μ^2_M is identified with the smallest two-body threshold accessible in a sector with given isospin, G-parity and strangeness (I^G, S),

$$\mu^2_M = (m_1+m_2)^2_{\text{min}}\,. \tag{2.54}$$

For a given generalized potential $U^J_{ab}(s)$ we use (2.53) to reconstruct the final partial-wave scattering amplitudes $T^J_{ab}(s)$ that would satisfy coupled-channel unitarity and micro-causality conditions. However, the crossing symmetry constraint is not automatically fulfilled [GLP11]. We remind that in the case of exact crossing symmetry a crossed reaction can be uniquely reconstructed from the direct reaction amplitude (for instance $KK \to \pi\pi$ process relates to $K\pi \to K\pi$

[4] Note that in pure χPT the unitarity can only be satisfied perturbatively, i.e. $\text{Im}\, T_2 = 0$, $\text{Im}\, T_4 = T_2\,\rho\, T_2, ...$, where $T = T_2 + T_4 + ...$ and T_2 corresponds to order Q^2.

in s, t, u representation). In order to do that, one has to evaluate the direct reaction amplitude at energies below the s-channel threshold. In this sense, the crossing symmetry is strongly connected to left-hand cuts of the scattering amplitude. At first, now imagine that we approximated the generalized potential at energies above the s-channel threshold only (a necessary condition to solve (2.53)). Then from (2.53) the final scattering amplitude would also be valid above threshold only and as a consequence we are not able to compute the crossed channel in the physical region. The latter can be obtained by setting up the analogous dispersion relation (2.53) for the crossed reaction. That means the crossing symmetry effects dominantly amplitudes at subthreshold energies where we match our result with χPT. In turn, χPT satisfies the exact crossing symmetry at any order of the expansion. In a second step, let us imagine that we approximated the generalized potential at energies $s \geq \Lambda_0^2$, i.e. we included a small subthreshold region. The coincidence of the crossing transformed amplitudes and the amplitudes from the crossed reaction in that specific subthreshold region defines the desired constraint. Note that a non-empty coincidence region requires Λ_0^2 to be sufficiently distinct from the s-channel unitarity branch point. In our scheme a measure for the amount of crossing-symmetry violation is the strength of non-perturbative contributions to the subthreshold scattering amplitudes.

The non-linear integral equation (2.53) may not have a solution at all or have (infinitely) many solutions. In order to pick out the right one, we match the final amplitude with the result of chiral perturbation theory:

$$T^J_{ab}(\mu_M^2) = U^J_{ab}(\mu_M^2)\,. \tag{2.55}$$

As pointed above, this condition implies a significant suppression of a possible crossing violation. In order to produce a solution of (2.53) the generalized potential is needed above threshold only and its behavior has to be bounded asymptotically (some logarithmic structures). However in χPT, partial-wave amplitudes are reliable in subthreshold region only and at high energy they are basically polynomials in some powers of s. To overcome this difficulty we use the conformal mapping technique described in Section 2.1 and in [GL10, DGL11a] (see also Appendix C for more details). Based on the knowledge of $U^J_{ab}(s)$ around an expansion point we can analytically extrapolate the potential into the required region. The expansion point $\mu^2_{ab,E}$ should lie within the region where $U^J_{ab}(s)$ can be computed safely in χPT (2.43). We follow [GL10] and define μ_E between the initial and final thresholds,

$$\mu_E = \frac{1}{2}(m_1 + m_2 + \bar{m}_1 + \bar{m}_2)\,. \tag{2.56}$$

A standard Taylor series around μ_E^2 converges in a small area, which is determined by the location of the nearest left-hand singularity. In our case, the left-hand singularities nearest to the physical region are defined by the two Goldstone boson t- and u-channel exchange processes. In order to analytically continue the potential up to some cutoff scale Λ_s^2, we apply the conformal map suggested in [GL10],

$$\xi(s) = \frac{a\,(\Lambda_s^2 - s)^2 - 1}{(a - 2\,b)(\Lambda_s^2 - s)^2 + 1}\,, \quad a = \frac{1}{(\Lambda_s^2 - \mu_E^2)^2}, \quad b = \frac{1}{(\Lambda_s^2 - \Lambda_0^2)^2}\,, \tag{2.57}$$

where the parameter Λ_0^2 is generally determined by the condition that the mapping domain touches the nearest left-hand singularity. The numbers of Λ_0^2 with respect to the coupled-channel states of Table 2.1 can be found in Table 2.5.

Table 2.5.: The positions of the nearest left-hand branch points to the physical region for Goldstone-boson scattering, that are determined by the t- or u-channel exchange of Goldstone boson pairs.

$\left(I^G, S\right)$	ch.	μ_E^2	Λ_0^2	Description
$(0,-2)$	11	$4m_K^2$	$4(m_K^2-m_\pi^2)$	t,u-ch (2π)
$(1,-2)$	11	$4m_K^2$	$4(m_K^2-m_\pi^2)$	t,u-ch (2π)
$\left(\frac{1}{2},-1\right)$	11	$(m_\pi+m_K)^2$	$m_K^2-m_\pi^2$	t-ch (2π)
	12	$\frac{1}{4}(m_\pi+2m_K+m_\eta)^2$	$\frac{m_\eta^2 m_\pi+m_K^3}{m_K+m_\pi}-m_K m_\pi$	u-ch (πK)
	22	$(m_K+m_\eta)^2$	$m_\eta^2+m_K^2-2m_\pi^2$ $+2\sqrt{(m_\eta^2-m_\pi^2)(m_K^2-m_\pi^2)}$	t-ch (2π)
$\left(\frac{3}{2},-1\right)$	11	$(m_\pi+m_K)^2$	$m_K^2-m_\pi^2$	t-ch (2π)
$(0^+,0)$	11	$4m_\pi^2$	0	t,u-ch (2π)
	12	$(m_\pi+m_K)^2$	0	t,u-ch (πK)
	13	$(m_\pi+m_\eta)^2$	0	t,u-ch $(\pi\eta)$
	22	$4m_K^2$	$4(m_K^2-m_\pi^2)$	t,u-ch (2π)
	23	$(m_K+m_\eta)^2$	$\frac{(m_\eta^2-m_\pi^2)((2m_K^2+m_\pi^2)^2-m_\eta^2)}{(m_K+m_\pi)^2}$	t,u-ch (πK)
	33	$4m_\eta^2$	$4(m_\eta^2-m_\pi^2)$	t,u-ch (2π)
$(0^-,0)$	11	$4m_K^2$	$4(m_K^2-m_\pi^2)$	t,u-ch (2π)
$(1^+,0)$	11	$4m_\pi^2$	0	t,u-ch (2π)
	12	$(m_\pi+m_K)^2$	0	t,u-ch (πK)
	22	$4m_K^2$	$4(m_K^2-m_\pi^2)$	t-ch (2π)
$(1^-,0)$	11	$(m_\pi+m_\eta)^2$	$m_\eta^2-m_\pi^2$	t-ch (2π)
	12	$\frac{1}{4}(m_\pi+2m_K+m_\eta)^2$	$\frac{m_K(m_\eta^2-m_\pi^2)}{m_K+m_\pi}$	t,u-ch (πK)
	22	$4m_K^2$	$4(m_K^2-m_\pi^2)$	t,u-ch (2π)
$(2^+,0)$	11	$4m_\pi^2$	0	t,u-ch (2π)

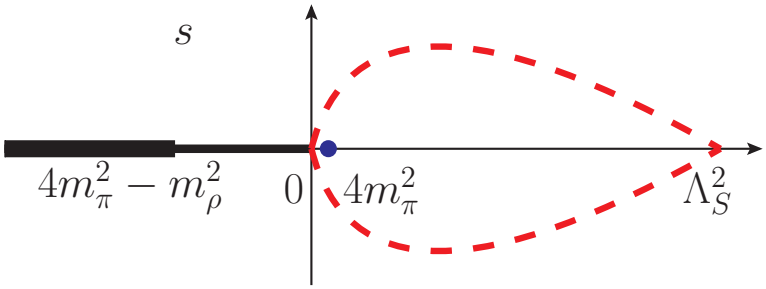

Figure 2.12.: Left-hand cut structure in the complex s-plane of the partial-wave two-pion scattering amplitude. The branch point of the ρ-meson exchange is located at $\Lambda_0^2 = 4m_\pi^2 - m_\rho^2$, while the two-pion exchange cut starts at $\Lambda_0^2 = 0$. The dashed line indicates the convergence region of the expansion (2.58).

Within this domain the generalized potential can be approximated by[5]

$$U(s) = \sum_{k=0}^{\infty} c_k \, \xi^k(s) \qquad \text{for} \quad s < \Lambda_s^2 \,, \tag{2.58}$$

where the coefficient c_k depends on the form of the conformal map (2.57) and the first k derivatives of $U(s)$ at μ_E^2 ($\xi(\mu_E^2) = 0$)

$$c_k = \frac{d^k U(s(\xi))}{k!\, d\xi^k}\bigg|_{\xi=0} . \tag{2.59}$$

In our analysis the generalized potential $U(s)$ at the expansion point is identified with the tree-level partial-wave amplitude (2.45-2.47) computed from the chiral Lagrangian (2.33). The input parameters are just the masses of the pseudo-scalar and vector mesons, f and $f_V\, h_P$. We stress that the scattering amplitude truncated at any chiral order will contribute to the generalized potential via its derivatives at the expansion point[6]. As a result, all left-hand cut structures are 'integrated' out systematically. The sensitivity to the expansion order of $U(s)$ will be shown in the results section.

With the help of (2.58) we approximated the generalized potential in the region $\Lambda_0^2 < s < \Lambda_s^2$ (see Fig. 2.12). For energies $s > \Lambda_s^2$, we may simply cut off the integral in (2.53) at $\bar{s} = \Lambda_s^2$. However, it is advantageous not to do so, since that would induce rapid variations of the amplitudes close to and below $s = \Lambda_s^2$. While the precise form of the generalized potential at $s > \Lambda_s^2$ should not influence the reaction amplitudes in the target region, where we have a controlled expansion, it is useful to minimize its residual influence on the target region. This is the case if the outside potential is smoothly extended for $s > \Lambda_s^2$ by a constant (see [GL10]). We note that because of the specific form of $\xi(s)$, namely $\xi'(\Lambda_s^2) = 0$, this is a smooth procedure.

[5] Here and in the following for notational convenience we suppress the J index. Where not needed we also do not show the couple-channel indices a, b.

[6] However if one computes the chiral amplitude at next-to-leading order (one loop) then it is natural to calculate explicitly the contribution from the nearest cut (the so-called $U_{\text{inside}}(s)$ part). See Subsection 2.1.2 and [GL10] for more details.

With the approximated generalized potential (2.58) it remains to solve (2.53) in the interested isospin sectors. Based on N/D method [CM60] the partial-wave scattering amplitude can be decomposed into the form

$$T_{ab}(s) = \sum_c D^{-1}_{ac}(s) N_{cb}(s)\,, \tag{2.60}$$

where the contributions of left- and right-hand singularities are separated respectively into $N_{ab}(s)$ and $D_{ab}(s)$ functions,

$$\begin{aligned} N_{ab}(s) &= U_{ab}(s) + \sum_{c,d} \int_{\mu^2_{\rm thr}}^{\infty} \frac{d\bar{s}}{\pi} \frac{s-\mu_M^2}{\bar{s}-\mu_M^2} \frac{N_{ac}(\bar{s})\,\rho_{cd}(\bar{s})\,[U_{db}(\bar{s}) - U_{db}(s)]}{\bar{s}-s}\,, \\ D_{ab}(s) &= \delta_{ab} - \sum_c \int_{\mu^2_{thr}}^{\infty} \frac{d\bar{s}}{\pi} \frac{s-\mu_M^2}{\bar{s}-\mu_M^2} \frac{N_{ac}(\bar{s})\rho_{cb}(\bar{s})}{\bar{s}-s-i\epsilon}\,. \end{aligned} \tag{2.61}$$

The system of linear equations (2.61) is nothing but a generalization of (2.20) to the relativistic coupled-channel case.

Since in the p-wave scattering vector mesons show up as poles above the s-channel threshold [OO99,SGBDV10], one *Castillejo-Dalitz-Dyson pole* (CDD) [CDD56] has to be included explicitly in order to solve Eq.(2.53). In this case the coupled-channel unitarity is guaranteed with the ansatz [GL10]

$$D_{ab}(s) = \delta_{ab} - \frac{s-\mu_M^2}{s-M^2_{CDD}} R^{(D)}_{ab} - \sum_c \int_{\mu^2_{thr}}^{\infty} \frac{d\bar{s}}{\pi} \frac{s-\mu_M^2}{\bar{s}-\mu_M^2} \frac{N_{ac}(\bar{s})\rho_{cb}(\bar{s})}{\bar{s}-s-i\epsilon}\,, \tag{2.62}$$

where M_{CDD} is a CDD pole mass parameter and $R^{(D)}$ is a coupling matrix. In accordance with (2.60) and (2.62) one can write the corresponding linear integral equation for $N_{ab}(s)$

$$\begin{aligned} N_{ab}(s) = U^{\rm eff}_{ab}(s) &- \frac{s-\mu_M^2}{s-M^2_{CDD}} \left[R^{(B)}_{ab} + \sum_c R^{(D)}_{ac}\, U^{\rm eff}_{cb}(s) \right] \\ &+ \sum_{c,d} \int_{\mu^2_{\rm thr}}^{\infty} \frac{d\bar{s}}{\pi} \frac{s-\mu_M^2}{\bar{s}-\mu_M^2} \frac{N_{ac}(\bar{s})\,\rho_{cd}(\bar{s})\,[U^{\rm eff}_{db}(\bar{s}) - U^{\rm eff}_{db}(s)]}{\bar{s}-s}\,, \end{aligned} \tag{2.63}$$

with

$$\begin{aligned} U^{\rm eff}_{ab}(s) &= U_{ab}(s) + \frac{g_a\, m^2\, g_b}{s-m^2} \frac{s-\mu_M^2}{m^2-\mu_M^2}\,, \\ R^{(D)}_{ab} &= \frac{m^2-M^2_{CDD}}{m^2-\mu_M^2} \left(\delta_{ab} - {\rm Re} \sum_c \int_{\mu^2_{\rm thr}}^{\infty} \frac{d\bar{s}}{\pi} \frac{m^2-\mu_M^2}{\bar{s}-\mu_M^2} \frac{N_{ac}(\bar{s})\,\rho_{cb}(\bar{s})}{\bar{s}-m^2-i\epsilon} \right)\,, \\ R^{(B)}_{ab} &= -\frac{\mu_M^2 - M^2_{CDD}}{(\mu_M^2-m^2)^2}\, g_a\, m^2\, g_b - {\rm Re} \sum_{c,d} \int_{\mu^2_{thr}}^{\infty} \frac{d\bar{s}}{\pi} \frac{\bar{s}-M^2_{CDD}}{\bar{s}-\mu_M^2} \frac{N_{ac}(\bar{s})\,\rho_{cd}(\bar{s})}{(\bar{s}-m^2-i\epsilon)^2}\, g_d\, m^2\, g_b \\ &\quad + (m^2 - M^2_{CDD})\, {\rm Re} \sum_{c,d} \int_{\mu^2_{\rm thr}}^{\infty} \frac{d\bar{s}}{\pi} \frac{N_{ac}(\bar{s})\,\rho_{cd}(\bar{s})\,U^{\rm eff}_{db}(\bar{s})}{(\bar{s}-\mu_M^2)(\bar{s}-m^2-i\epsilon)}\,. \end{aligned} \tag{2.64}$$

The merit of the ansatz (2.62, 2.63, 2.64) lies in its specification of the CDD pole parameters, $R^{(D)}$ and $R^{(B)}$, in terms of the parameters g_a and m, characterizing a possible pole term of the generalized potential in the physical region. The coupling g_a is completely fixed by the condition that the effective potential $U^{\rm eff}_{ab}(s)$ is regular at $s = m^2$. From Eq.(2.46), one can determine

$$g_a\, g_b = -\frac{(m_V\, h_P)^2}{96\, f^4}\, m^2\, \left(C_{s-ch}\right)_{ab}\,. \tag{2.65}$$

The numerical value of M_{CDD} is irrelevant. By construction (2.60-2.64), the final scattering amplitude does not depend on it.

The set of coupled-channel integral equations (2.61) can be solved numerically by the method of matrix inversion. After solving the linear integral equation for $N_{ab}(s)$, we compute $D_{ab}(s)$ and finally the partial-wave scattering amplitude is produced with (2.60). The N/D calculation with a CDD pole can be performed in a similar way. The only difference is in solving the linear equation for $N_{ab}(s)$ one has also simultaneously determine $R^{(D)}_{ab}$, $R^{(B)}_{ab}$ matrices by (2.63, 2.64).

The elements $T_{ab}(s)$ of the partial-wave unitary scattering amplitude can be expressed in terms of the phase shifts and the inelasticity. In the case of two coupled-channel states it holds

$$\begin{aligned} &1 + 2\,i\,T_{11}\,\rho_{11} = \eta\, e^{2\,i\,\delta_1}, \\ &1 + 2\,i\,T_{22}\,\rho_{22} = \eta\, e^{2\,i\,\delta_2}, \\ &2\,i\,T_{12}\,\sqrt{\rho_{11}\,\rho_{22}} = \eta\, e^{i\,(\delta_1+\delta_2)}\,, \end{aligned} \tag{2.66}$$

where the phase-space function ρ_{ab} is given in (2.52). In Eq.(2.66) δ_1, δ_2 are the phase shifts for the $a = b = 1$ and $a = b = 2$ channels (for instance $\pi K \to \pi K$ and $\eta K \to \eta K$ in the $(I^G, S) = (\frac{1}{2}, 1)$ sector) and η is the inelasticity ($\eta \le 1$). Inelasticity is equal to unity when elastic unitarity holds. From the above relations and the optical theorem, one has

$$\begin{aligned} &\delta_1 = \frac{1}{2}\,{\rm Arg}(1 + 2\,i\,T_{11}\,\rho_{11})\,, \\ &\frac{1-\eta^2}{4} = {\rm Im}(T_{11})\rho_{11} - |T_{11}|^2\,\rho_{11}\,, \end{aligned} \tag{2.67}$$

while in the one-channel case $\delta_1 = {\rm Arg}(T_{11})$. It is straightforward to generalize (2.66) to the case of n coupled-channel states. We remind that expressions (2.66, 2.67) are given for a particular choice of J and I. In the following the notation δ_{IJ} for phase shifts will be used.

2.2.5 Numerical results

In this subsection we compare the evaluated phase shifts with the available experimental data. The numerical results depend on the choice of different parameters. As noted before, we use $f = 90$ MeV everywhere. Small variations around that value lead to very similar results. We fix the cutoff parameter introduced in (2.57) to $\Lambda_s = 1.6$ GeV unless otherwise specified. The dependence on Λ_s is rather soft and will be discussed later. The value of Λ_s sets the scale from where on s-channel physics is integrated out. In our analysis the system is characterized further by the order at which the conformal expansion (2.58) is truncated. Typically taking the first few terms is sufficient to achieve a good approximation of the generalized potential. A large

number of terms would be justified if the left-hand cut structures are modeled very accurately, or a large number of counter terms are considered. If the experimental data were more accurate and complete, one would try to fix the coefficients c_k in (2.58) directly from the data set in a model independent way. In our approach the chiral amplitude possesses t- and u-channel vector meson exchange terms. The latter imply specific correlations of the expansion coefficients.

Channels J=1, $(I^G, S) = (0^-, 0), (1^+, 0), (1/2, 1)$

We start with the p-wave scattering, where one CDD pole structure is requested due to the s-channel vector meson exchange process. Within our unitarization scheme we identify the expressions of (1.38) with the mass parameter m in (2.64) and set it equals to the empirical mass of vector mesons. The parameter $f_V\, h_P$, given in (2.34), has an uncertainty of $\sim 10\%$. We determine

$$f_V h_P \simeq 0.23\,\mathrm{GeV} \tag{2.68}$$

as to obtain an accurate description of the $(I^G, S) = (1^+, 0)$ and $(I, S) = (\frac{1}{2}, 1)$ sectors which are dominated by the s-channel ρ and K^* exchanges. We conclude that the tree-level expressions for the vector meson masses survive the unitarization. This justifies our procedure to use physical vector meson masses in the driving expressions (2.43). In Figs. 2.13 and 2.14 we compare the calculated p-wave phase shifts with experimental data. In both $\pi\pi$ and πK channels a remarkable agreement with the data up to about 1.2 GeV is achieved. The positions of ρ and K^* mesons are well reproduced. Our results for $J = 1$ are insensitive to the choice of Λ_s and the number of terms kept in (2.58). This is clearly seen in Figs. 2.13 and 2.14 (upper panels). The inelasticities in these sectors are approximately equal to unity in the range $\sqrt{s} < 1.2$ GeV. This is a consequence of a very small mixture of $\pi\pi$ with $K\bar{K}$ and πK with ηK in $I = 1$ and $I = 1/2$ sectors, respectively.

Channels J=0, $(I^G, S) = (1/2, 1), (3/2, 1), (0^+, 0), (1^-, 0), (2^+, 0)$

We turn to study the s-wave scattering with isospins $I = 1/2,\ 3/2,\ 0,\ 1,\ 2$. Our results are presented in Figs. 2.13 and 2.14. The sensitivity to the truncation order in the ξ-expansion (2.58) is shown in Fig. 2.13. In all cases we observe a convergence and already the first four terms reproduce the empirical data within the error bars from different experimental groups. We conclude from this result that indeed the vector meson exchanges contributions provide a quite accurate approximation for the leading coefficients in the conformal expansion (2.58). In the isoscalar sector the coupled-channel dynamics are crucially important. Three different channels, $\pi\,\pi$, $K\,\bar{K}$ and $\eta\,\eta$ contribute to our analysis. In Fig. 2.13 we show the $\pi\,\pi \to \pi\,\pi$ and $\pi\,\pi \to K\,\bar{K}$[7] phase shifts. The main features of the data have been recovered. However, the $f_0(980)$ resonance structure is reproduced with some quantitative discrepancies. The inelasticity in the $\pi\pi \to K\bar{K}$ reaction is somewhat underestimated, although the data sets are controversial.

The dependence of the scattering phases on a variation of Λ_s from 1.4 GeV to 1.8 GeV is shown in Fig. 2.14. In all cases this causes a rather small error band, where with decreasing the number of terms in the conformal expansion (2.58) the error bands decrease as well.

[7] This is actually $\delta_{\pi\pi\to\pi\pi} + \delta_{K\bar{K}\to K\bar{K}}$.

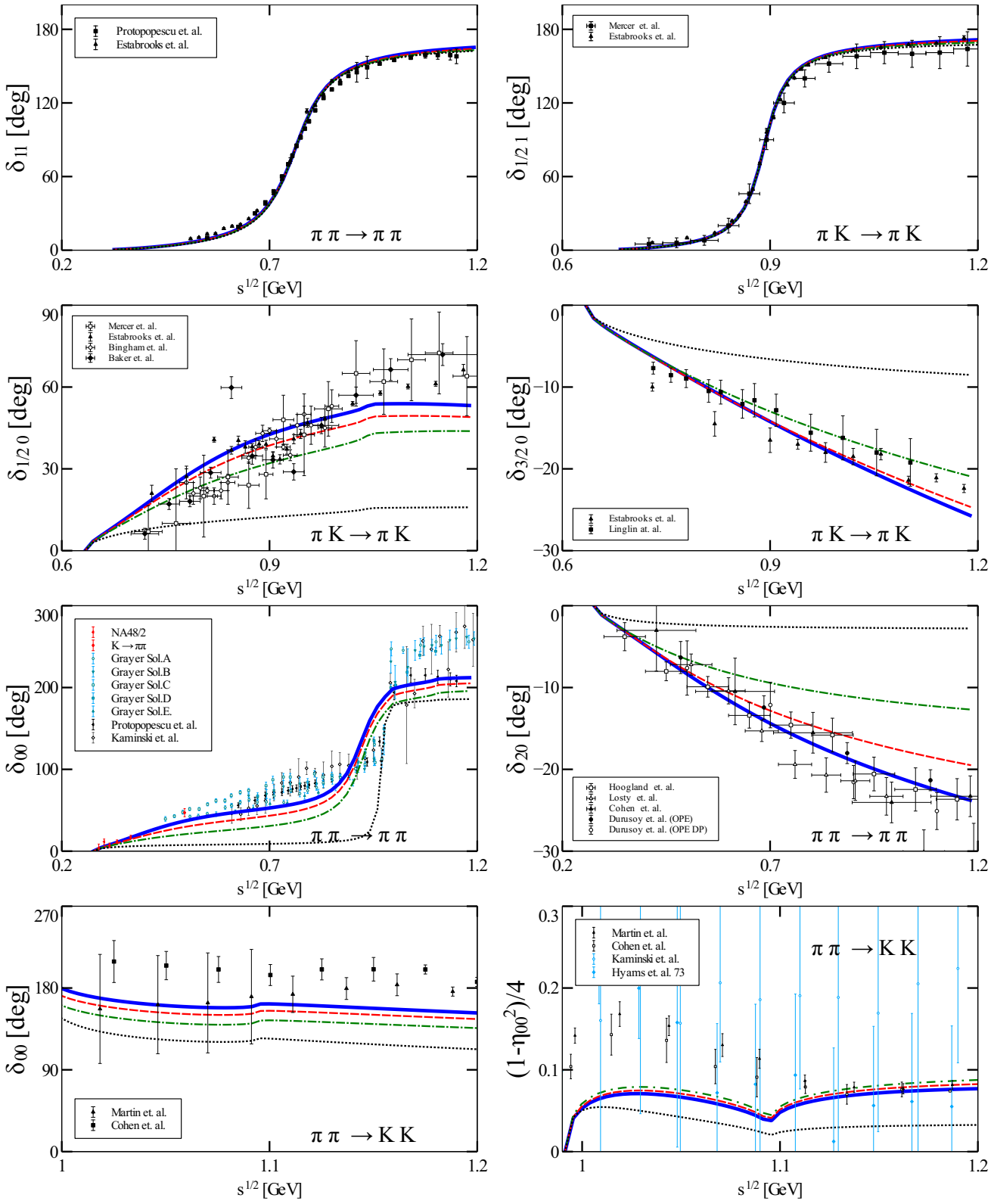

Figure 2.13.: Phase shifts δ_{IJ} (in degrees) as a function of energy. The dotted, dash-dotted, dashed and solid lines correspond to a truncation in the expansion (2.58) at order 0, 1, 2, 3 respectively. The data are taken from [PAGBG$^+$73, EM74, MAC$^+$71, ECM$^+$78, BDD$^+$72, BBC$^+$75, LCD$^+$73, HPG$^+$77, LCF$^+$74, CAD$^+$80, DBG$^+$73, GHJ$^+$74, KLR97, BCK$^+$08, CEP09, MO79, KLR02, HJW$^+$73].

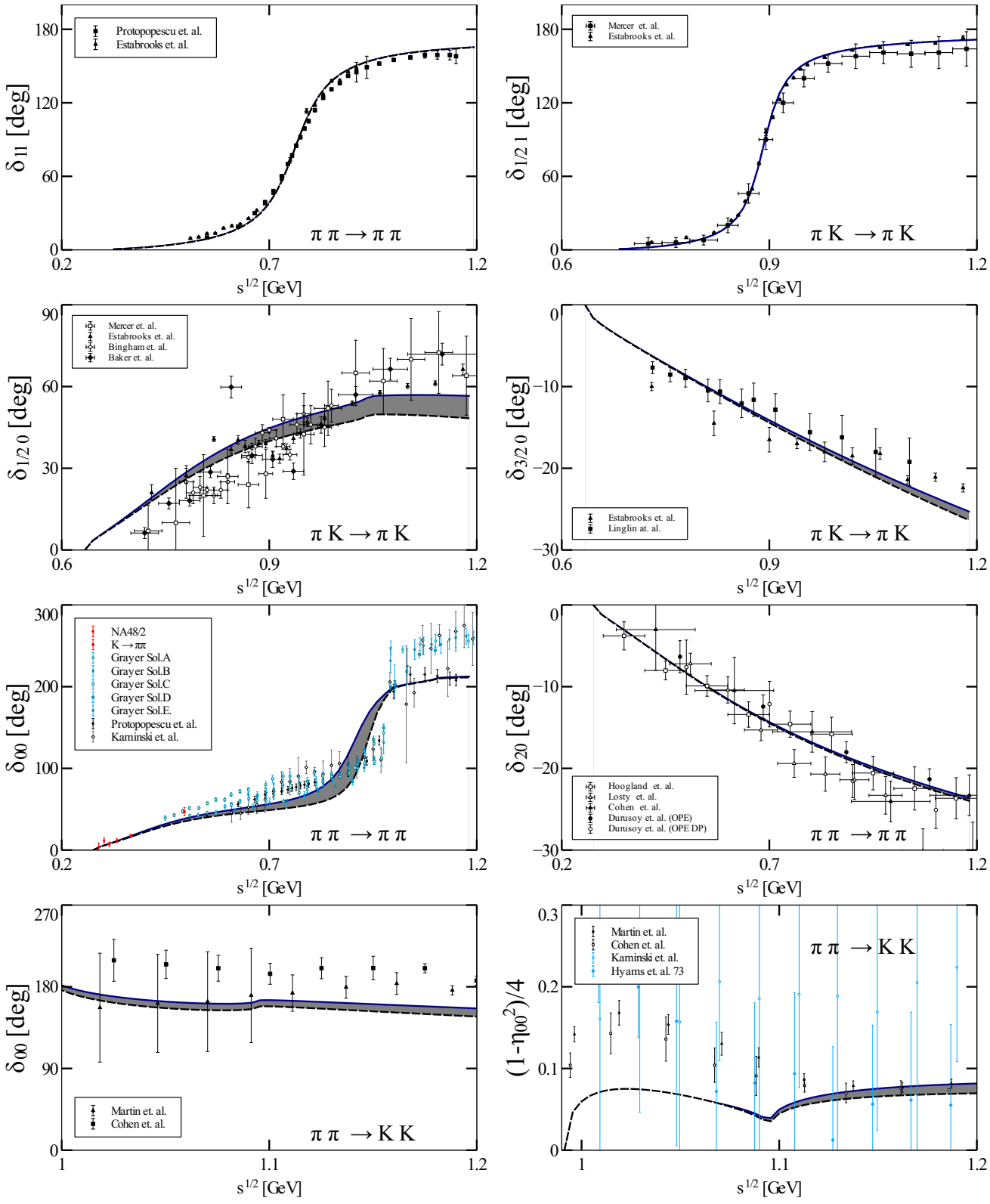

Figure 2.14.: Phase shifts δ_{IJ} (in degrees) as a function of energy. The various bands are implied by a variation of the parameter Λ_s with 1.4 GeV (dashed line) $< \Lambda_s <$ 1.8 GeV (solid line). In (2.58) we used 4-term approximation. The data are taken from [PAGBG$^+$73, EM74, MAC$^+$71, ECM$^+$78, BDD$^+$72, BBC$^+$75, LCD$^+$73, HPG$^+$77, LCF$^+$74, CAD$^+$80, DBG$^+$73, GHJ$^+$74, KLR97, BCK$^+$08, CEP09, MO79, KLR02, HJW$^+$73].

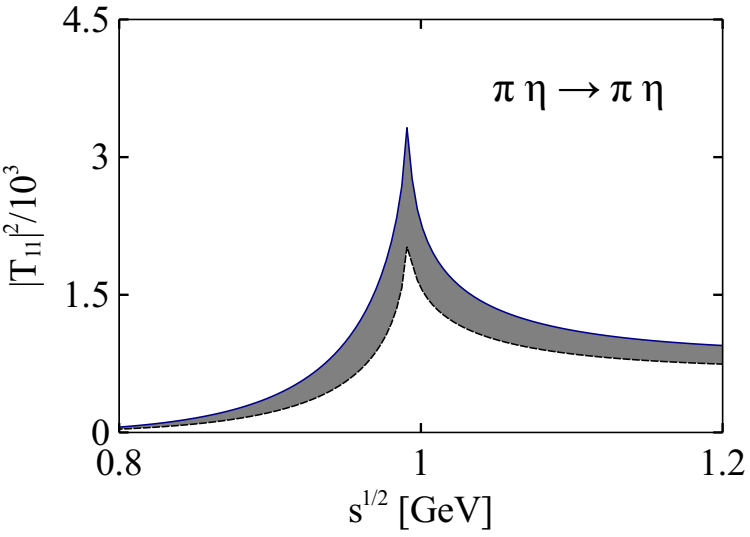

Figure 2.15.: Modulus squared of the scattering amplitude $|T_{11}|^2$ with $J = 0$ and $(I^G, S) = (1^-, 0)$. The band is implied by a variation of parameter Λ_s with 1.4 GeV (dashed line) $< \Lambda_s <$ 1.8 GeV (solid line). In (2.58) we used a 4-term approximation.

We finally discuss the $\pi\eta$ scattering in the $(I^G, S) = (1^-, 0)$ sector. In contrast to the $\pi\pi$ channel, there is no elastic $\pi\eta$ scattering data available. Therefore in Fig. 2.15 we plot the modulus squared of the scattering amplitude. We observe a peak around 1 GeV which can be associated with the $a_0(980)$ resonance. The width is around 50 MeV. This result is consistent with the empirical data [N$^+$10], $M_{a_0} = 980 \pm 10$ MeV and $\Gamma^{\rm Full}_{a_0} = 50$ to 100 MeV. It is important to stress that the $f_0(980)$ and $a_0(980)$ resonances appear due to the introduction of the $K\bar{K}$ channel in addition to $\pi\pi$ in $I = 0$ and $\pi\eta$ in $I = 1$ sectors. They strongly couple to the $K\bar{K}$-channel and disappear if it is omitted.

Our results are in general agreement with analyses based on the Roy-Steiner equations [ACGL01, CGL01, BDGM04]. Since in our approach we have no free parameters (the only two relevant parameters, $f = 90$ MeV and $f_V h_P = 0.23$ GeV, were fixed before in [LL08]) we find this agreement very satisfactory. We conclude that with our approach we further consolidated the dynamical role of light vector-meson degrees of freedom. In the next section we extend the analysis of Goldstone-boson scattering to the case of photon-fusion reactions.

2.3 Photon-fusion reactions

We now turn to the case of photon-fusion reactions $\gamma\gamma \to PP$ (with $PP = \pi^0\pi^0$, $\pi^+\pi^-$, $K^0\bar{K}^0$, K^+K^-, $\eta\eta$ and $\pi^0\eta$), which is a subject to study in nonperturbative QCD [PMUW08, OR08, GMM10,HPS11,MWZ$^+$09]. Traditionally, chiral perturbation theory (χPT) is applied to describe low-energy dynamics. The one- and two-loop calculations of the scattering amplitude were performed in [BC88, DHL88] and [GIS05, GIS06], respectively. However, in χPT the systematic expansion can be accomplished only in the close-to-threshold region and χPT cannot serve as an appropriate framework in the resonance region, where exact coupled-channel unitarity plays an important role. In the previous sections it was shown that in order to extend the validity of χPT to higher energies one can use the constraints from micro-causality and coupled-channel unitarity. The aim of the present section is to obtain a unified description of the reactions $\gamma\gamma \to \pi^0\pi^0$, $\pi^+\pi^-$, $K^0\bar{K}^0$, K^+K^-, $\eta\eta$ and $\pi^0\eta$, using the same approach.

A key aspect of photon-fusion reactions is the creation mechanism of scalar ($J^{PC} = 0^{++}$) and tensor ($J^{PC} = 2^{++}$) resonances. In particular, one finds the relatively narrow[8] scalar states $f_0(980)$ and $a_0(980)$ [OO98, PMUW08, MWZ$^+$09]. In the present study we focus on energies below $\sqrt{s} = 1.2$ GeV, where these resonances appear to dominate. In Section 2.2 both $f_0(980)$ and $a_0(980)$ were dynamically generated within the novel unitarization approach from coupled-channel $PP \to PP$ interactions. We remind that in the $\pi\eta$ channel there is no elastic scattering data. However, the $\pi\eta$ channel can be populated by the inelastic photon-fusion reaction. We will demonstrate in the following that the dynamical generation of $a_0(980)$ is in remarkable agreement with the empirical data on $\gamma\gamma \to \pi\eta$ reaction.

An important ingredient of the coupled-channel $PP \to PP$ calculations performed in Section 2.2 is the chiral Lagrangian supplemented with light vector-meson degrees of freedom. The latter appear there as exchange particles, but not as states in the coupled channels. However, at higher energies in accordance with the hadrogenesis conjecture [LL08, LK04, TLL12], we expect the tensor resonances $f_2(1270)$ and $a_2(1320)$ to be naturally generated within our approach from vector-vector interactions. In principle, the partial-wave projection for reactions involving vector mesons has been carried out in [LV12]. Nevertheless, in the present study we concentrate on lower energies and consider scattering and rescattering of the type $\gamma\gamma \to PP$ and $PP \to PP$, respectively, but disregard $PP \leftrightarrow VV, VP$. The coupled-channel dynamics of VV type and correspondingly the description of $f_2(1270)$ and $a_2(1320)$ resonances is beyond the scope of the present thesis.

Concerning experiment, the study of photon-fusion processes $\gamma\gamma \to hh$ (h-hadron) is available in e^+e^- colliders via the reaction $e^+e^- \to e^+e^- + hh$ [B$^+$90, B$^+$92, M$^+$90, A$^+$86, A$^+$90, B$^+$89, A$^+$85]. The Belle Collaboration has recently reported high-statistics data on $\gamma\gamma \to \pi^+\pi^-$, $\pi^0\pi^0$, $\pi\eta$ [U$^+$09b, M$^+$07, U$^+$09a] and the first measurement of $\eta\eta$ production [U$^+$10]. The reaction $\gamma\gamma \to \pi^0\eta$ is linked to the decay $\eta \to \pi^0\gamma\gamma$ by crossing symmetry. Recently, the invariant-mass spectra of the two photons from this decay have been obtained at AGS [Pra07, P$^+$08] and at MAMI [Pra07, Unv10]. This information will allow us to adjust few unknown parameters which show up in the interaction Lagrangian with two vector-meson fields.

[8] compared e.g. with the ρ-meson

2.3.1 Chiral interaction

We recall the leading-order chiral Lagrangian with explicit vector mesons (1.37, 1.40, 1.41) (see Section 1.3). Expanding the building blocks in powers of the Goldstone-boson field, the relevant part for the photon-fusion processes takes the simple form

$$\begin{aligned}
\mathcal{L} \;=\; & -\frac{e^2}{2} A^\mu A_\mu \,\mathrm{tr}\left\{\Phi\, \mathcal{Q}\, \left[\Phi, \mathcal{Q}\right]_-\right\} + i\,\frac{e}{2} A^\mu \,\mathrm{tr}\left\{\partial_\mu \Phi \left[\mathcal{Q}, \Phi\right]_-\right\} - e\, f_V\, \partial_\mu A_\nu \,\mathrm{tr}\left\{\Phi^{\mu\nu}\, \mathcal{Q}\right\} \\
& - i\,\frac{f_V\, h_P}{8 f^2}\,\mathrm{tr}\left\{\partial_\mu \Phi\, \Phi^{\mu\nu}\, \partial_\nu \Phi\right\} + \frac{e\, f_V}{8 f^2}\,\partial_\mu A_\nu \,\mathrm{tr}\left\{\Phi^{\mu\nu}\left[\Phi, \left[\Phi, \mathcal{Q}\right]_-\right]_-\right\} \\
& + \frac{e\, f_V\, h_P}{8 f^2} A_\nu \,\mathrm{tr}\left\{\left[\partial_\mu \Phi\,,\, \Phi^{\mu\nu}\right]_- \left[\mathcal{Q}, \Phi\right]_-\right\} - \frac{1}{16 f^2}\,\mathrm{tr}\left\{\partial^\mu \Phi_{\mu\alpha}\left[\left[\Phi, \partial_\nu \Phi\right]_-, \Phi^{\nu\alpha}\right]_-\right\} \\
& - \frac{b_D}{64 f^2}\,\mathrm{tr}\left\{\Phi^{\mu\nu}\, \Phi_{\mu\nu}\left[\Phi, \left[\Phi, \chi_0\right]_+\right]_+\right\} - \frac{g_1}{32 f^2}\,\mathrm{tr}\left\{\left[\Phi_{\mu\nu}\,, \partial_\alpha \Phi\right]_+ \left[\partial^\alpha \Phi, \Phi^{\mu\nu}\right]_+\right\} \\
& - \frac{g_2}{32 f^2}\,\mathrm{tr}\left\{\left[\Phi_{\mu\nu}\,, \partial_\alpha \Phi\right]_- \left[\partial^\alpha \Phi, \Phi^{\mu\nu}\right]_-\right\} - \frac{g_3}{32 f^2}\,\mathrm{tr}\left\{\left[\partial_\mu \Phi\,, \partial^\nu \Phi\right]_+ \left[\Phi_{\nu\tau}\,, \Phi^{\mu\tau}\right]_+\right\} \\
& - \frac{g_5}{32 f^2}\,\mathrm{tr}\left\{\left[\Phi^{\mu\tau}, \partial_\mu \Phi\right]_- \left[\Phi_{\nu\tau}\,, \partial^\nu \Phi\right]_-\right\} - \frac{h_A}{16 f}\,\epsilon_{\mu\nu\alpha\beta}\,\mathrm{tr}\left\{\left[\Phi^{\mu\nu}, \partial_\tau \Phi^{\tau\alpha}\right]_+ \partial^\beta \Phi\right\} \\
& - \frac{b_A}{16 f}\,\epsilon_{\mu\nu\alpha\beta}\,\mathrm{tr}\left\{\left[\Phi^{\mu\nu}, \Phi^{\alpha\beta}\right]_+ \left[\chi_0, \Phi\right]_+\right\} - \frac{h_O}{16 f}\,\epsilon_{\mu\nu\alpha\beta}\,\mathrm{tr}\left\{\left[\partial^\alpha \Phi^{\mu\nu}, \Phi^{\tau\beta}\right]_+ \partial_\tau \Phi\right\},
\end{aligned} \tag{2.69}$$

where the Goldstone-boson field Φ, the vector-meson field $\Phi_{\mu\nu}$, the charge matrix $\mathcal{Q}$, and the mass matrix χ_0 are given in Eqs. (1.18), (1.28), (1.15) and (1.26), respectively. In principle, in the hadrogenesis conjecture also the singlet eta field is part of the "quasi-fundamental" hadronic degrees of freedom. It can be included in the flavour matrix of Φ in a straightforward way [TLL12]. However, as discussed before, we do not include vector channels in our coupled-channel approach. Consequently, we also do not include channels with the η' which would appear in the same energy regime. Vector mesons are important, nonetheless, as they contribute as exchange particles to the coupled channels $\gamma\gamma$ and PP. On the other hand, this is not the case for the η'. Consequently, here we have not considered the eta singlet explicitly in our Lagrangian.

Finally, we shall discuss the coupling constants appearing in (2.69). Combining (2.68) with the parameter set given in (1.43) we obtain:

$$\begin{array}{lll}
f_V = 0.140 \pm 0.014\ \mathrm{GeV}, & h_A \simeq 2.10, & b_A = 0.27, \\
h_P\, f_V = 0.23\,\mathrm{GeV}, & b_D = 0.92, & f \simeq 0.90\ \mathrm{GeV}.
\end{array} \tag{2.70}$$

The values of the other parameters g_{1-3}, g_5 and h_O have not been determined so far. Assuming that they are of natural size we will study in Subsection 2.3.4 the impact of variations of these parameters on the photon-fusion processes and on the related decay $\eta \to \pi^0\gamma\gamma$.

2.3.2 Invariant amplitudes and partial-wave decomposition

The T-matrix element for photon-fusion reactions is determined as

$$\left\langle P(\bar{p})\, P(\bar{q})\right|\, T\, \left|A(k_1, \lambda_1) A(k_2, \lambda_2)\right\rangle \;=\; (2\pi)^4 \delta^4(k_1 + k_2 - \bar{p} - \bar{q})\; T^{\mu\nu}\, \epsilon_\mu(k_1, \lambda_1)\, \epsilon_\nu(k_2, \lambda_2)$$

Table 2.6.: The coupled-channel states I^G characterized by isospin I and G-parity G. The Pauli matrices σ_i act on isospin-doublet fields $K, \bar{K}$ with for instance $K = (K^+, K^0)^t$. Note that in particular the neutral ($I_3 = 0$) two-pion state with isospin two is given by $\frac{1}{\sqrt{6}}(2\,\pi_p^0\,\pi_q^0 - \pi_p^+\,\pi_q^- - \pi_p^-\,\pi_q^+)$.

0^+	1^-	2^+
$\begin{pmatrix} (\gamma\,\gamma) \\ \frac{1}{\sqrt{3}}(\pi_q \cdot \pi_p) \\ \frac{1}{2}(\bar{K}_q\,K_p + \bar{K}_p\,K_q) \\ (\eta_q\,\eta_p) \end{pmatrix}$	$\begin{pmatrix} (\gamma\,\gamma) \\ (\pi_q\,\eta_p)_{I_3=0} \\ \frac{1}{2}(\bar{K}_q\,\vec{\sigma}\,K_p + \bar{K}_p\,\vec{\sigma}\,K_q)_{I_3=0} \end{pmatrix}$	$\begin{pmatrix} (\gamma\,\gamma) \\ \left(\frac{1}{2}(\pi_q^i\,\pi_p^j + \pi_q^j\,\pi_p^i) - \frac{1}{3}\,\delta_{ij}\,\pi_q \cdot \pi_p\right)_{I_3=0} \end{pmatrix}$

where $k_{1,2}$, $\epsilon_{1,2}$ are the momenta and the polarization vectors of the incoming photons, respectively, and $\bar{p}$, $\bar{q}$ are the momenta of the outgoing mesons.

In general, the two-body scattering problem decouples into orthogonal channels specified by isospin, G-parity, parity and strangeness quantum numbers. For the case at hand, with two photons in the initial state and two pseudoscalars in the final state, parity is always positive (see below) and strangeness is always zero. In each of the channels, finally specified by isospin I and G-parity G, there are several meson-meson states coupled to each other. In Table 2.6 we have specified the states which contain the most relevant meson-meson information below 1.2 GeV. This table extends the isospin table of two Goldstone boson scattering given in Section 2.2.4 by the inclusion of two-photon states. As discussed before, we neglect PV and VV states which are only relevant for higher energies.

Lorentz covariance and gauge invariance lead to a decomposition of the scattering amplitude $T^{\mu\nu}$ into Lorentz tensors $L_i^{\mu\nu}$ and invariant amplitudes F_i,

$$\begin{aligned} T^{\mu\nu} &= F_1(s,t,u)\,L_1^{\mu\nu} + F_2(s,t,u)\,L_2^{\mu\nu}\,, \\ L_1^{\mu\nu} &= k_1^\nu\,k_2^\mu - (k_1\cdot k_2)\,g^{\mu\nu}\,, \\ L_2^{\mu\nu} &= (\Delta^2\,(k_1\cdot k_2) - 2\,(k_1\cdot\Delta)\,(k_2\cdot\Delta))\,g^{\mu\nu} - \Delta^2\,k_1^\nu\,k_2^\mu - 2(k_1\cdot k_2)\,\Delta^\mu\,\Delta^\nu \\ &\quad +2(k_2\cdot\Delta)\,k_1^\nu\,\Delta^\mu + 2(k_1\cdot\Delta)\,k_2^\mu\,\Delta^\nu\,, \end{aligned} \tag{2.71}$$

where $\Delta = \bar{p} - \bar{q}$ and $T^{\mu\nu}$ satisfies the Ward identities

$$k_{1\mu}\,T^{\mu\nu} = k_{2\nu}\,T^{\mu\nu} = 0\,. \tag{2.72}$$

The motivation for choosing these particular Lorentz structures is twofold. First, the corresponding invariant amplitudes are independent and free of kinematical singularities or zeros. Second, in order to simplify further calculations we have chosen the Lorentz tensors such that the following property holds:

$$L_1^{\mu\nu}\,L_{2\,\mu\nu} = 0\,. \tag{2.73}$$

The invariant amplitudes F_1 and F_2 are analytic functions of s, t and u except for dynamical cuts. Furthermore, a $t-u$ crossing symmetry is satisfied due to the Bose statistics of the two photons.

It is useful to introduce the helicity components of the scattering amplitude and decompose each of them into their partial waves,

$$\begin{aligned}\phi_{++} &= T^{\mu\nu}\,\epsilon_\mu(k_1,+1)\,\epsilon_\nu(k_2,+1) = \sum_{\text{even } J\geq 0}(2J+1)\,t^{(J)}_{++}\,d^{(J)}_{00}(\cos\theta)\,,\\ \phi_{+-} &= T^{\mu\nu}\,\epsilon_\mu(k_1,+1)\,\epsilon_\nu(k_2,-1) = \sum_{\text{even } J\geq 2}(2J+1)\,t^{(J)}_{+-}\,d^{(J)}_{20}(\cos\theta)\,,\end{aligned} \tag{2.74}$$

where $d^{(J)}_{\lambda,\bar\lambda}(\cos\theta)$ are Wigner rotation functions and θ is the center-of-mass scattering angle. The polarization vectors of two photons in the center-of-mass frame can be found in Appendix D. Note that the partial-wave expansion involves only even $J \geq \lambda$ and positive parity $P = +$ [BLP82]. This constraint arises from the combination of Bose symmetry of the two initial massless photons with the possible J, P quantum numbers of the two Goldstone bosons in the final state.

The invariant amplitudes $F_{1,2}$ can be expressed in terms of the helicity amplitudes ϕ_{++}, ϕ_{+-},

$$\begin{pmatrix} F_1 \\ F_2 \end{pmatrix} = \begin{pmatrix} -\frac{2}{s} & 0 \\ 0 & \frac{1}{2s\,\bar p^2_{cm}\,(x^2-1)} \end{pmatrix} \begin{pmatrix} \phi_{++} \\ \phi_{+-} \end{pmatrix}, \tag{2.75}$$

where $\bar p_{\rm cm}$ is the final center-of-mass relative momentum and $x = \cos\theta$. For unpolarized photons the differential cross section is given by

$$\frac{d\sigma}{d\cos\theta} = \frac{\beta}{32\,\pi\,s}\,\frac{1}{4}\left(2\,|\phi_{++}|^2 + 2\,|\phi_{+-}|^2\right), \tag{2.76}$$

where $\beta = 2\,\bar p_{cm}/\sqrt{s}$. If two identical particles appear in the final state (neutral pions, for instance) one has to include an additional factor of $1/2$ in (2.76) or perform the integration only over $\theta \in [0,\,\pi/2]$.

According, to (2.74) the partial-wave helicity amplitudes $t^{(J)}_{++}$, $t^{(J)}_{+-}$ can be computed in terms of the invariant amplitudes $F_{1,2}$ as

$$\begin{aligned} t^{(J)}_{++}(s) &= -\int \frac{dx}{4}\,s\,F_1(s,x)\,d^{(J)}_{00}(x)\,,\\ t^{(J)}_{+-}(s) &= \int \frac{dx}{2}\,2\,\bar p^2_{cm}\,s\,\left(x^2-1\right)\,F_2(s,x)\,d^{(J)}_{20}(x)\,, \end{aligned} \tag{2.77}$$

with the help of the useful identities for the Wigner rotation functions [VMK88]

$$\begin{aligned} d^{(J)}_{00}(x) &= P_J(x)\,,\\ d^{(J)}_{20}(x) &= \frac{2\,x\,P'_J(x)}{\sqrt{(J-1)\,J\,(J+1)\,(J+2)}} - \sqrt{\frac{J\,(J+1)}{(J-1)\,(J+2)}}\,P_J(x)\,. \end{aligned} \tag{2.78}$$

In order to avoid kinematical singularities and zeros in the partial-wave amplitudes at threshold, we rescale (2.77) by a phase-space factor $(p_{cm}\,\bar p_{cm})^J$,

$$\begin{aligned} T^{(J)}_{++} &= \frac{s^J}{(p_{cm}\,\bar p_{cm})^J}\,t^{(J)}_{++}\,,\\ T^{(J)}_{+-} &= \frac{s^J}{(p_{cm}\,\bar p_{cm})^J}\,t^{(J)}_{+-}\,, \end{aligned} \tag{2.79}$$

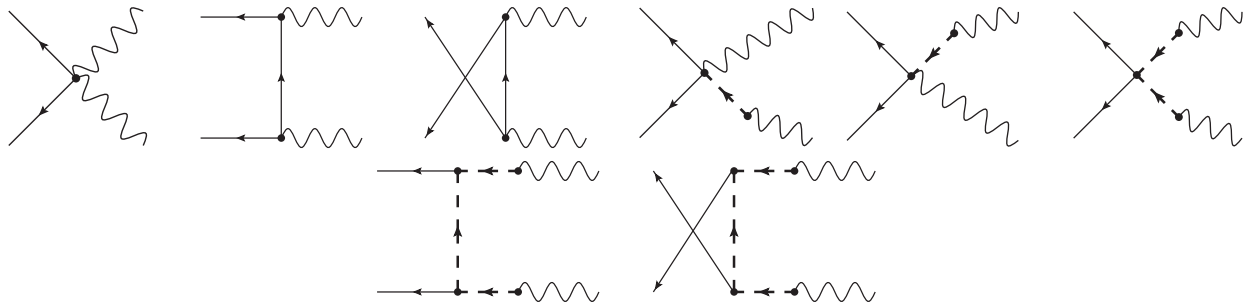

Figure 2.16.: Tree-level diagrams for $\gamma\gamma \to PP$ reactions with the exchange of pseudo-scalar (solid line) and light vector (dashed line) mesons.

and also multiply by s^J to ensure a finite limit of the phase-space matrices at large energy.

The invariant amplitudes (2.71) computed from the chiral Lagrangian (2.69) read

$$
\begin{aligned}
F_1 \;=\;& \frac{e^2\,C_{SG}}{2s} - \sum_{x\in[8]} \frac{e^2\,(m_x^4 - t\,u)\,C_0^{(x)}}{2s^2\,(t-m_x^2)} + \sum_{x\in[9]} \left(\frac{e^2\,f_V^2}{8\,f^2}\,\frac{C_1^{(x)}}{m_x^2} - \frac{e^2\,f_V^2\,h_P}{8\,f^2}\,\frac{C_{h_P}^{(x)}}{m_x^2} \right) \\
&+ \sum_{x,y\in[9]} \frac{e^2\,f_V^2}{32\,f^2}\,\frac{1}{m_x^2\,m_y^2} \\
&\quad \times \left(\left(g_1\,C_{g_1}^{(x,y)} + g_2\,C_{g_2}^{(x,y)} + g_3\,C_{g_3}^{(x,y)} + g_5\,C_{g_5}^{(x,y)} \right) (s - \bar{m}_1^2 - \bar{m}_2^2) - \frac{1}{2}\,b_D\,C_{b_D}^{(x,y)} \right) \\
&+ \sum_{x,y,z\in[9]} \frac{e^2\,f_V^2}{16\,f^2}\,\frac{1}{m_x^2\,m_y^2} \left(\frac{1}{16}\,\frac{t^2}{m_z^2}\,h_O^2\,C_{h_O}^{(x,y,z)} + \frac{t-2\,m_z^2}{m_z^2}\,\frac{1}{t-m_z^2}\,b_A^2\,C_{b_A}^{(x,y,z)} \right. \\
&\qquad \left. - \frac{1}{16}\,\frac{t^2}{t-m_z^2}\,h_A^2\,C_{h_A}^{(x,y,z)} + \frac{1}{2}\,\frac{t}{t-m_z^2}\,b_A\,h_A\,C_{b_A h_A}^{(x,y,z)} + \frac{1}{2}\,\frac{t}{m_z^2}\,b_A\,h_O\,C_{b_A h_O}^{(x,y,z)} \right) \\
&+ (t \longleftrightarrow u), \qquad (2.80) \\
F_2 \;=\;& -\sum_{x\in[8]} \frac{e^2\,C_0^{(x)}}{8s\,(t-m_x^2)} - \sum_{x,y\in[9]} \frac{e^2\,f_V^2}{64\,f^2}\,\frac{1}{m_x^2\,m_y^2} \left(g_3\,C_{g_3}^{(x,y)} + g_5\,C_{g_5}^{(x,y)} \right) \\
&+ \sum_{x,y,z\in[9]} \frac{e^2\,f_V^2}{64\,f^2}\,\frac{1}{m_x^2\,m_y^2} \left(\frac{1}{16}\,\frac{t}{m_z^2}\,h_O^2\,C_{h_O}^{(x,y,z)} + \frac{1}{m_z^2}\,\frac{1}{t-m_z^2}\,b_A^2\,C_{b_A}^{(x,y,z)} \right. \\
&\qquad \left. + \frac{1}{16}\,\frac{t}{t-m_z^2}\,h_A^2\,C_{h_A}^{(x,y,z)} - \frac{1}{2}\,\frac{1}{t-m_z^2}\,b_A\,h_A\,C_{b_A h_A}^{(x,y,z)} + \frac{1}{m_z^2}\,b_A\,h_O\,C_{b_A h_O}^{(x,y,z)} \right) \\
&+ (t \longleftrightarrow u),
\end{aligned}
$$

where the sum runs over the octet of Goldstone bosons ([8]) or the vector-meson nonet ([9]) and $m_{x,y,z}$ denotes their respective masses. The coefficients $C_{\dots}$ are presented in Tables 2.7, 2.8, 2.9, and 2.10 with respect to the coupled-channel states of Table 2.6. In Fig. 2.16 the set of tree-level diagrams that gives nonzero contributions is depicted. We remind that for the isospin states which contain identical particles (e.g. $|\pi\,\pi\rangle$, $|\eta\,\eta\rangle$, ...) we use a convention where the unitarity condition for identical and non-identical two-particle states are the same.

The conventions of Table 2.6 imply the following relations between scattering amplitudes in isospin and particle bases,

$$
\begin{aligned}
T_{\gamma\gamma\to\pi^+\pi^-} &= 2\left(\frac{1}{\sqrt{3}}\,T^{I=0}_{\gamma\gamma\to\pi\pi} - \frac{1}{\sqrt{6}}\,T^{I=2}_{\gamma\gamma\to\pi\pi}\right),\\
T_{\gamma\gamma\to\pi^0\pi^0} &= 2\left(\frac{1}{\sqrt{3}}\,T^{I=0}_{\gamma\gamma\to\pi\pi} + \sqrt{\frac{2}{3}}\,T^{I=2}_{\gamma\gamma\to\pi\pi}\right),\\
T_{\gamma\gamma\to\pi^0\eta} &= \sqrt{2}\;T^{I=1}_{\gamma\gamma\to\pi\eta}, \qquad T_{\gamma\gamma\to\eta\eta} = 2\,T^{I=0}_{\gamma\gamma\to\eta\eta},\\
T_{\gamma\gamma\to K^+K^-} &= T^{I=0}_{\gamma\gamma\to K\bar K} + T^{I=1}_{\gamma\gamma\to K\bar K},\\
T_{\gamma\gamma\to K^0\bar K^0} &= T^{I=0}_{\gamma\gamma\to K\bar K} - T^{I=1}_{\gamma\gamma\to K\bar K},
\end{aligned}
\tag{2.81}
$$

where the factor 2 reflects our normalization for two-body states with identical particles.

The partial-wave amplitudes obtained from (2.79, 2.77) and (2.80) at tree-level will serve as an input for the nonperturbative coupled-channel calculations to which we turn next.

2.3.3 Dynamics of coupled channels

The partial-wave reaction amplitudes satisfy the dispersion-integral representation,

$$
T^J_{ab}(s) \;=\; U^J_{ab}(s) + \sum_{c,d}\int_{\mu^2_{\rm thr}}^{\infty}\frac{d\bar s}{\pi}\frac{s-\mu_M^2}{\bar s-\mu_M^2}\,\frac{T^J_{ac}(\bar s)\,\rho^J_{cd}(\bar s)\,T^{J*}_{db}(\bar s)}{\bar s - s - i\epsilon}\,,
\tag{2.82}
$$

where the phase-space matrix $\rho^J_{cd}(s)$ is diagonal in c and d. In (2.82) the coupled-channel indices a and b run over the various channel $\gamma\gamma$, $\pi\pi$, $K\bar K$ etc. While the hadronic part of the phase-space matrix is given in (2.52), intermediate states with two photons are neglected in this work. Numerically they are largely suppressed, being proportional to e^4 at least. Therefore the two-dimensional phase-space matrix for the two-photon states need not to be specified here.

Our approach satisfies the electromagnetic gauge-invariance constraint. This follows from the on-shell condition for the generalized potential, for which we will construct a systematic approximation in the following. The on-shell reaction amplitude will then be derived in application of (2.82). Owing to the matching scale μ_M in (2.82) the nonperturbative coupled-channel calculation and the results from a perturbative application of the chiral Lagrangian smoothly connect at $s=\mu_M^2$. This is discussed in detail in Section 2.2 and [GL10]. Here, we identify μ_M with the smallest two-body hadronic threshold value and thereby assume the applicability of χPT at $s=\mu_M^2$.

Following Sections 2.1 and 2.2 the generalized potential $U^J_{ab}(s)$ is extrapolated to higher energies in a controlled manner by applying conformal mapping techniques. For the photon-fusion processes the generalized potential is split into two contributions[9],

$$
U(s) \;=\; U_{\rm inside}(s) + U_{\rm outside}(s)\,,
\tag{2.83}
$$

where $U_{\rm inside}(s)$ contains the contributions from close-by left-hand cuts and $U_{\rm outside}(s)$ the contributions from far-distant left-hand cuts. While the former can be explicitly calculated from

[9] In the following we do not display any more the angular-momentum superscript J explicitly. Where not needed we also do not display the channel index ab.

Table 2.7.: The coefficients C_{SG}, $C_0^{(x)}$ and $C_1^{(x)} = 2\,C_{h_P}^{(x)}$ of the invariant amplitudes (2.80) with respect to the coupled-channel states I^G of Table 2.6. The numbers in the column "ch = ab" correspond to the out-states (a) and in-states (b) of Table 2.6. Note, that non-appearing ones are zero.

I^G	ch.	C_{SG}	$C_0^{(\pi)}$	$C_0^{(K)}$	$C_1^{(\rho)}$	$C_1^{(\omega)}$	$C_1^{(\phi)}$
0^+	21	$-\frac{8}{\sqrt{3}}$	$-\frac{8}{\sqrt{3}}$	0	$\frac{16}{\sqrt{3}}$	0	0
	31	-4	0	-4	4	$\frac{4}{3}$	$\frac{8}{3}$
1^-	31	-4	0	-4	4	$\frac{4}{3}$	$\frac{8}{3}$
2^+	21	$4\sqrt{\frac{2}{3}}$	$4\sqrt{\frac{2}{3}}$	0	$-8\sqrt{\frac{2}{3}}$	0	0

Table 2.8.: The coefficients $C_{b_A h_A}^{(x,y,z)} = C_{b_A h_O}^{(x,y,z)}$. See the caption of Table 2.7 for more details.

		$C_{b_A h_A}^{(x,y,z)}$					
I^G	ch.	(ρ,ρ,ρ)	(ρ,ρ,ω)	(ρ,ρ,K^*)	(ρ,ω,ρ) (ω,ρ,ω)	(ρ,ω,K^*) (ω,ρ,K^*)	(ρ,ϕ,K^*) (ϕ,ρ,K^*)
0^+	21	0	$\frac{32\,m_\pi^2}{\sqrt{3}}$	0	0	0	0
	31	0	0	$32\,m_K^2$	0	0	0
	41	$\frac{32\,m_\pi^2}{3}$	0	0	0	0	0
1^-	21	0	0	0	$\frac{32}{3}\sqrt{\frac{2}{3}}\,m_\pi^2$	0	0
	31	0	0	0	0	$\frac{16\,m_K^2}{3}$	$-\frac{32\,m_K^2}{3}$
2^+	21	0	$32\sqrt{\frac{2}{3}}\,m_\pi^2$	0	0	0	0
		(ω,ω,ρ)	(ω,ω,ω)	(ω,ω,K^*)	(ω,ϕ,K^*) (ϕ,ω,K^*)	(ϕ,ϕ,K^*)	(ϕ,ϕ,ϕ)
0^+	21	$\frac{32\,m_\pi^2}{3\sqrt{3}}$	0	0	0	0	0
	31	0	0	$\frac{16\,m_K^2}{9}$	$-\frac{32\,m_K^2}{9}$	$\frac{64\,m_K^2}{9}$	0
	41	0	$\frac{32\,m_\pi^2}{27}$	0	0	0	$\frac{32}{27}(16\,m_K^2 - 8\,m_\pi^2)$

Table 2.9.: The coefficients $C_{b_A}^{(x,y,z)}$ and $C_{h_A}^{(x,y,z)} = C_{h_O}^{(x,y,z)}$. See the caption of Table 2.7 for more details.

$C_{b_A}^{(x,y,z)}$

I^G	ch.	(ρ,ρ,ρ)	(ρ,ρ,ω)	(ρ,ρ,K^*)	(ρ,ω,ρ) (ω,ρ,ω)	(ρ,ω,K^*) (ω,ρ,K^*)	(ρ,ϕ,K^*) (ϕ,ρ,K^*)
0^+	21	0	$\frac{64\,m_\pi^4}{\sqrt{3}}$	0	0	0	0
	31	0	0	$32\,m_K^4$	0	0	0
	41	$\frac{64\,m_\pi^4}{3}$	0	0	0	0	0
1^-	21	0	0	0	$\frac{64}{3}\sqrt{\frac{2}{3}}\,m_\pi^4$	0	0
	31	0	0	0	0	$\frac{32\,m_K^4}{3}$	$-\frac{64\,m_K^4}{3}$
2^+	21	0	$64\sqrt{\frac{2}{3}}\,m_\pi^4$	0	0	0	0
		(ω,ω,ρ)	(ω,ω,ω)	(ω,ω,K^*)	(ω,ϕ,K^*) (ϕ,ω,K^*)	(ϕ,ϕ,K^*)	(ϕ,ϕ,ϕ)
0^+	21	$\frac{64\,m_\pi^4}{3\sqrt{3}}$	0	0	0	0	0
	31	0	0	$\frac{32\,m_K^4}{9}$	$-\frac{64\,m_K^4}{9}$	$\frac{128\,m_K^4}{9}$	0
	41	0	$\frac{64\,m_\pi^4}{27}$	0	0	0	$\frac{64}{27}(32\,m_K^4 - 32\,m_\pi^2\,m_K^2 + 8\,m_\pi^4)$

$C_{h_A}^{(x,y,z)}$

I^G	ch.	(ρ,ρ,ρ)	(ρ,ρ,ω)	(ρ,ρ,K^*)	(ρ,ω,ρ) (ω,ρ,ω)	(ρ,ω,K^*) (ω,ρ,K^*)	(ρ,ϕ,K^*) (ϕ,ρ,K^*)
0^+	21	0	$\frac{16}{\sqrt{3}}$	0	0	0	0
	31	0	0	8	0	0	0
	41	$\frac{16}{3}$	0	0	0	0	0
1^-	21	0	0	0	$\frac{16}{3}\sqrt{\frac{2}{3}}$	0	0
	31	0	0	0	0	$\frac{8}{3}$	$-\frac{16}{3}$
2^+	21	0	$16\sqrt{\frac{2}{3}}$	0	0	0	0
		(ω,ω,ρ)	(ω,ω,ω)	(ω,ω,K^*)	(ω,ϕ,K^*) (ϕ,ω,K^*)	(ϕ,ϕ,K^*)	(ϕ,ϕ,ϕ)
0^+	21	$\frac{16}{3\sqrt{3}}$	0	0	0	0	0
	31	0	0	$\frac{8}{9}$	$-\frac{16}{9}$	$\frac{32}{9}$	0
	41	0	$\frac{16}{27}$	0	0	0	$\frac{128}{27}$

Table 2.10.: The coefficients $C_{g_1}^{(x,y)}$, $C_{g_2}^{(x,y)}$, $C_{g_3}^{(x,y)}$, $C_{g_5}^{(x,y)}$ and $C_{b_D}^{(x,y)}$. See the caption of Table 2.7 for more details.

I^G	ch.	(ρ,ρ)	(ρ,ω) (ω,ρ)	(ρ,ϕ) (ϕ,ρ)	(ω,ω)	(ω,ϕ) (ϕ,ω)	(ϕ,ϕ)
				$C_{g_1}^{(x,y)}$			
0^+	21	$\frac{16}{\sqrt{3}}$	0	0	$\frac{16}{3\sqrt{3}}$	0	0
	31	8	0	0	$\frac{8}{9}$	$-\frac{16}{9}$	$\frac{32}{9}$
	41	16/3	0	0	$\frac{16}{27}$	0	$\frac{128}{27}$
1^-	21	0	$\frac{16}{3}\sqrt{\frac{2}{3}}$	0	0	0	0
	31	0	$\frac{8}{3}$	$-\frac{16}{3}$	0	0	0
2^+	21	$16\sqrt{\frac{2}{3}}$	0	0	0	0	0
				$C_{g_2}^{(x,y)}$			
0^+	21	$\frac{32}{\sqrt{3}}$	0	0	0	0	0
	31	8	0	0	$\frac{8}{9}$	$\frac{16}{9}$	$\frac{32}{9}$
1^-	31	0	$\frac{8}{3}$	$\frac{16}{3}$	0	0	0
2^+	21	$-16\sqrt{\frac{2}{3}}$	0	0	0	0	0
				$C_{g_3}^{(x,y)}$			
0^+	21	$4\sqrt{3}$	0	0	$\frac{4}{3\sqrt{3}}$	0	0
	31	4	0	0	$\frac{4}{9}$	0	$\frac{16}{9}$
	41	$\frac{4}{3}$	0	0	$\frac{4}{27}$	0	$\frac{32}{27}$
1^-	21	0	$\frac{4}{3}\sqrt{\frac{2}{3}}$	0	0	0	0
	31	0	$\frac{4}{3}$	0	0	0	0
				$C_{g_5}^{(x,y)}$			
0^+	21	$-\frac{8}{\sqrt{3}}$	0	0	0	0	0
	31	-2	0	0	$-\frac{2}{9}$	$-\frac{4}{9}$	$-\frac{8}{9}$
1^-	31	0	$-\frac{2}{3}$	$-\frac{4}{3}$	0	0	0
2^+	21	$4\sqrt{\frac{2}{3}}$	0	0	0	0	0
				$C_{b_D}^{(x,y)}$			
0^+	21	$32\sqrt{3}\,m_\pi^2$	0	0	$\frac{32}{3\sqrt{3}}\,m_\pi^2$	0	0
	31	$32\,m_K^2$	0	0	$\frac{32}{9}\,m_K^2$	0	$\frac{128}{9}\,m_K^2$
	41	$\frac{32}{3}\,m_\pi^2$	0	0	$\frac{32}{27}\,m_\pi^2$	0	$\frac{32}{27}\left(16\,m_K^2-8\,m_\pi^2\right)$
1^-	21	0	$\frac{32}{3}\sqrt{\frac{2}{3}}\,m_\pi^2$	0	0	0	0
	31	0	$\frac{32}{3}\,m_K^2$	0	0	0	0

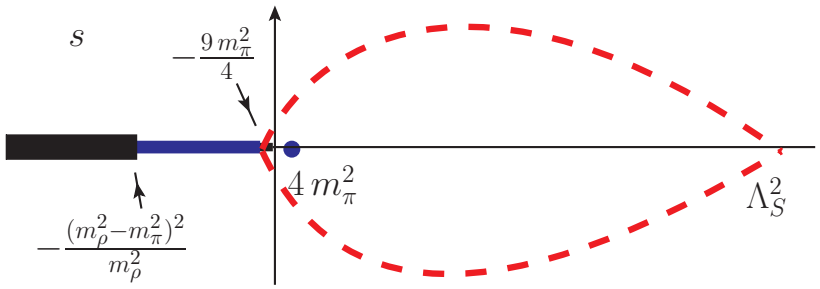

Figure 2.17.: Left-hand cut structure in the complex s-plane of the $\gamma\gamma \to \pi\pi$ partial-wave amplitude. The branch point of the ρ-meson exchange is located at $\Lambda_0^2 = -(m_\rho^2 - m_\pi^2)^2/m_\rho^2$, while one- and two-pion exchange cuts start at $\Lambda_0^2 = 0,\ -9\,m_\pi^2/4$, respectively. The dashed line identifies the convergence region of the conformal expansion (2.84).

the chiral Lagrangian in a perturbative application, the latter reflect short distance physics that needs to be parameterized systematically and efficiently. For the specific example reaction $\gamma\gamma \to \pi\,\pi$ the separation of "inside" and "outside" is implied by the dashed line in Fig. 2.17.

The outside potential is approximated in the same manner as in Section 2.2. The power series in a conformal variable $\xi(s)$ is constructed such as to ensure convergence for any value of s inside the area bounded by the dashed line of Fig. 2.17,

$$U_{\text{outside}}(s) \;=\; \sum_{k=0}^{n} c_k\,\xi^k(s) \quad \text{for} \quad s < \Lambda_s^2\,, \tag{2.84}$$

where the coefficients c_k are uniquely determined by the first k derivatives of $U_{\text{outside}}(s)$ at the expansion point $s = \mu_E^2$. We identify this expansion point with the mean of the initial and the final thresholds. The form of the function $\xi(s)$ is the same as in (2.57). It is uniquely determined by the positions of the closest left-hand branch point Λ_0^2, the expansion point μ_E^2 and the upper limit of the convergence region Λ_s^2 (see Fig. 2.17). The quantities μ_E^2 and Λ_0^2 are collected in Table 2.11 for the isospin states of Table 2.6.

To be specific, the "inside" part of the potential receives contributions from the one-pion (kaon) exchange processes only. We evaluate the contributions from the cuts starting from

$$\begin{aligned} -\frac{9\,m_\pi^2}{4} < s < 0 \qquad & \text{for} \quad \gamma\gamma \to \pi\pi\,, \\ -m_\pi^2\,\frac{(m_\pi + 2\,m_K)^2}{(m_\pi + m_K)^2} < s < 0 \quad & \text{for} \quad \gamma\gamma \to K\bar{K}\,, \end{aligned} \tag{2.85}$$

following the procedure outlined in Appendix B of [GL10]. According to Table 2.7 there are no more cases to be considered. The coefficients c_k in the outside part of the potential are computed by evaluating the first n derivatives of the partial-wave amplitudes as determined via (2.77, 2.78) by the tree-level result (2.80).

Via (2.83) we obtain an approximated generalized potential for energies $\Lambda_0^2 < s < \Lambda_s^2$. While the inside part of the potential is defined for $s > \Lambda_s^2$ also, the outside part is undefined for

Table 2.11.: The positions of the closest left-hand branch points of $U_{\text{outside}}(s)$ for $\gamma\gamma \to PP$ that are determined by the t- and u-channel exchange processes. The numbers in the column "ch.=ab" correspond to the out-states (a) and in-states (b) of Table 2.6.

I^G	ch.	μ_E^2	μ_M^2	Λ_0^2	Description
0^+	21	m_π^2	$4m_\pi^2$	$-\frac{9m_\pi^2}{4}$	t,u-ch (2π)
	31	m_K^2	$4m_\pi^2$	$-\frac{m_\pi^2(m_\pi+2m_K)^2}{(m_\pi+m_K)^2}$	t,u-ch (πK)
	41	m_η^2	$4m_\pi^2$	0	t,u-ch (2π)
1^-	21	$\frac{1}{4}(m_\pi+m_\eta)^2$	$(m_\pi+m_\eta)^2$	$\frac{3}{4}(m_\eta^2-4m_\pi^2)$	t,u-ch (2π)
	31	m_K^2	$(m_\pi+m_\eta)^2$	$-\frac{m_\pi^2(m_\pi+2m_K)^2}{(m_\pi+m_K)^2}$	t,u-ch (πK)
2^+	21	m_π^2	$4m_\pi^2$	$-\frac{9m_\pi^2}{4}$	t,u-ch (2π)

$s > \Lambda_s^2$ by (2.84). For energies larger than the cutoff scale Λ_s^2 the outside potential is set to a constant [GL10]. We remind that due to the particular form of the conformal map (2.57), the outside potential and its derivative are continuous at $s = \Lambda_s^2$.

Following the results of Section 2.2, we choose $n = 3$ in (2.84) and $\Lambda_s = 1.6\,\text{GeV}$. The variation of the parameter Λ_s in the range 1.4 GeV to 1.8 GeV is small and will be shown later.

A crucial observation behind our summation scheme is the fact that the computation of the partial-wave scattering amplitude from (2.82) at energies larger than threshold also requires only the knowledge of the generalized potential at energies larger than threshold. More generally, depending on where we want to compute the partial-wave scattering amplitudes, it suffices to construct a controlled approximation of the generalized potential in a specific region of the complex plane only. This is always achieved with (2.83, 2.84) and the desired solution of (2.82) can be found by the N/D ansatz [CM60] (see Section 2.2 for more details).

2.3.4 Results and discussions

In this section we present our results for the cross sections[10] of the reactions $\gamma\gamma \to \pi^0\pi^0$, $\pi^+\pi^-$, $K^0\bar{K}^0$, K^+K^-, $\eta\eta$ and $\pi^0\eta$, evaluated with the $J = 0, 2$ partial-wave amplitudes. We have checked that the contributions from the higher partial waves are negligible in the energy range $\sqrt{s} < 1.2$ GeV.

We use the set of parameters given in (2.70) for all the numerical results. However, the remaining five parameters g_1, g_2, g_3, g_5 and h_O have to be determined. Our strategy is to use

[10] Usually the experimental results are limited to a range of $|x| \le Z$ with $x = \cos\theta$. In this case the cross section is given by $\sigma = 2\int_0^Z \frac{d\sigma}{dx}\,dx$.

the empirical data on the reactions $\gamma\gamma \to \pi^0\pi^0$, $\pi^+\pi^-$ and $\pi^0\eta$ and in addition the differential and integrated data for the decay $\eta \to \pi^0\gamma\gamma$. The results for the cross sections of the reactions $\gamma\gamma \to K^0\bar{K}^0$, K^+K^- and $\eta\,\eta$ are then pure predictions.

On account of crossing symmetry, the decay amplitude for $\eta \to \pi^0\gamma\gamma$ can be easily obtained from $\gamma\gamma \to \pi^0\eta$ by considering π^0 and photons as outgoing particles. To get the decay amplitude it is enough to replace

$$\begin{aligned} s &= (k_1+k_2)^2 \to (\bar{k}_1+\bar{k}_2)^2 = M_{\gamma\gamma}^2\,, \\ t &= (p-k_1)^2 \to (p_\pi+\bar{k}_1)^2 = M_{\gamma_1\pi}^2\,, \\ u &= (p-k_2)^2 \to (p_\pi+\bar{k}_2)^2 = M_{\gamma_2\pi}^2\,, \end{aligned} \tag{2.86}$$

in the invariant amplitudes (2.80). The differential decay rate is given by [N$^+$10]

$$d\Gamma = \frac{1}{(2\pi)^3}\,\frac{1}{32\,m_\eta^3}\sum_{pol}|T_{\eta\to\pi^0\gamma\gamma}|^2\,dM_{\gamma\gamma}^2\,dM_{\gamma_2\pi}^2\,, \tag{2.87}$$

where the phase-space boundaries are

$$\begin{aligned} 0 \;\le\; M_{\gamma\gamma}^2 \;&\le\; (m_\eta - m_\pi)^2\,, \\ (M_{\gamma_2\pi}^2)_{\min} \;\le\; M_{\gamma_2\pi}^2 \;&\le\; (M_{\gamma_2\pi}^2)_{\max}\,, \end{aligned} \tag{2.88}$$

with

$$\begin{aligned} (M_{\gamma_2\pi}^2)_{\min} &= (E_\gamma^* + E_\pi^*)^2 - \left(E_\gamma^* + \sqrt{E_\pi^{*2} - m_\pi^2}\right)^2\,, \\ (M_{\gamma_2\pi}^2)_{\max} &= (E_\gamma^* + E_\pi^*)^2 - \left(E_\gamma^* - \sqrt{E_\pi^{*2} - m_\pi^2}\right)^2\,. \end{aligned}$$

Here, $E_\gamma^* = M_{\gamma\gamma}/2$ and $E_\pi^* = (m_\eta^2 - M_{\gamma\gamma}^2 - m_\pi^2)/2M_{\gamma\gamma}$ are the energies of photon and pion, respectively, in the rest frame of the two-photon system. For the integrated partial decay width one has to include the degeneracy factor of 1/2 to account for the fact that one has two indistinguishable photons in the final state. To obtain the *decay* amplitude we use directly the tree-level result (2.80). Since we are here in the low-energy decay region, we assume that coupled-channel effects are less important. For the *reaction* amplitudes we use, of course, the full rescattering formalism outlined in the previous section.

In a first step, we use the reaction data of $\gamma\gamma \to \pi^0\pi^0$, $\pi^+\pi^-$ and $\pi^0\eta$ to correlate the five free parameters. Having matched the data with the coupled-channel calculations leads to the following relations:

$$\begin{aligned} g_1 &= 0.900 - 0.200\,g_3 + 0.038\,h_O^2 + 0.128\,h_O\,, \\ g_2 &= -1.50 - 0.27\,g_3 + 0.25\,g_5\,. \end{aligned} \tag{2.89}$$

This leaves us with three free parameters. If they are varied within the range g_3, g_5, $h_O \in [-5,5]$ one obtains the cross sections depicted in Fig. 2.18. A detailed discussion of the cross sections will be given below. To get a feeling for the influence of the five parameters we also provide the cross sections for the case where all these five parameters are put to zero, see the dashed lines

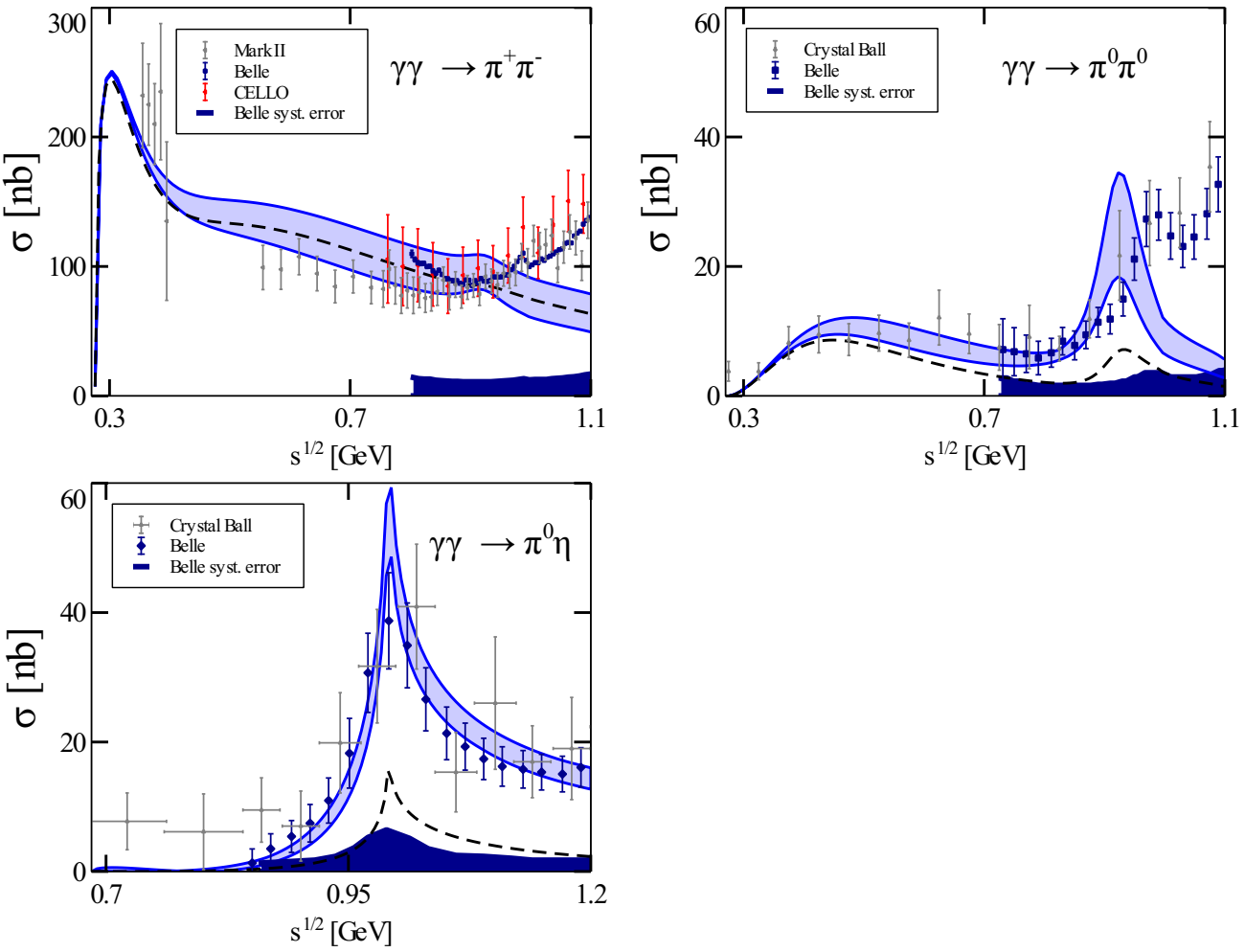

Figure 2.18.: Total cross sections for $\gamma\gamma \to \pi^+\pi^-$ with $|\cos\theta| < 0.6$ (top left), $\gamma\gamma \to \pi^0\pi^0$ with $|\cos\theta| < 0.8$ (top right) and $\gamma\gamma \to \pi^0\eta$ with $|\cos\theta| < 0.9$ (bottom). A variation of parameters g_3, g_5, $h_O \in [-5,5]$ using (2.89) is reflected by the various bands. The dashed curves correspond to the case of $g_i = h_O = 0$. The data are taken from [M$^+$90, U$^+$09b, B$^+$90, B$^+$92, M$^+$07, A$^+$86, U$^+$09a].

in Fig. 2.18. Obviously, one would significantly underestimate the data in both neutral channels $\pi^0\pi^0$ and $\pi^0\eta$ without the parameters g_i and h_O. Note, however, that the qualitative structure does not depend so much on these parameters.

We continue with a determination of the remaining parameters using the existing data on $\eta \to \pi^0\gamma\gamma$ decay. The present experimental status for $\eta \to \pi^0\gamma\gamma$ decay is the following: The Particle Data Group [N$^+$10] gives the branching ratio $\Gamma_{\eta\to\pi^0\gamma\gamma}/\Gamma_\eta = (2.7\pm0.5)\cdot10^{-4}$ and the full width $\Gamma_\eta = (1.30\pm0.07)\,\mathrm{keV}$. This results in a partial decay width of $\Gamma_{\eta\to\pi^0\gamma\gamma} \approx (0.35\pm0.09)\,\mathrm{eV}$. Theoretical studies have been performed in [ABBC92, OPR03, OPR08].

For the decay $\eta \to \pi^0\gamma\gamma$ three of the yet undetermined parameters contribute, namely g_1, g_3 and h_O. Using the relation (2.89) for g_1, we adjust g_3 and h_O to the partial decay width and to the two-photon invariant-mass distribution depicted in Fig. 2.19. In this way, we find

$$g_3 = -4.88\,, \qquad h_O = 3.27\,, \tag{2.90}$$

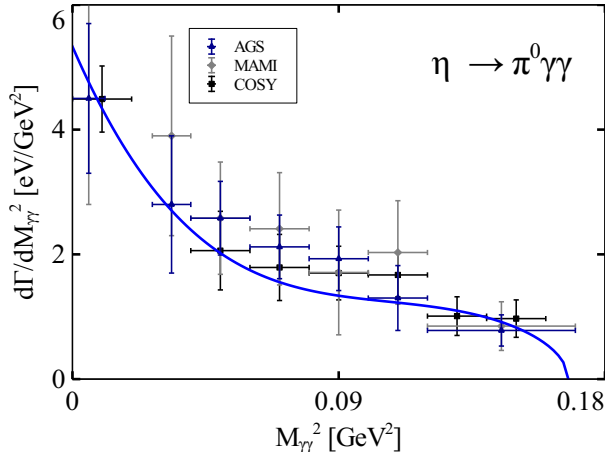

Figure 2.19.: The result for $d\Gamma(\eta \to \pi^0\gamma\gamma)/dM^2_{\gamma\gamma}$ compared to the data from [Pra07, P$^+$08, Lal10]. Parameters are chosen according to (2.89) and (2.90). Note that the parameters g_2 and g_5 do not contribute to this decay.

which implies $g_1 = 2.70$ and $g_2 = -0.18 + 0.25\, g_5$. The fit yields

$$\Gamma_{\eta\to\pi^0\gamma\gamma} = 0.310\,\text{eV} \tag{2.91}$$

for the integrated partial decay width, in good agreement with the experimental value.

We have determined four of our five free parameters. In the following we will show results where the remaining free parameter g_5 is varied in the range $g_5 \in [-5, 5]$. Note that the achieved determination of the parameters is also crucial for the possible future investigations. Originally all these parameters concern interactions between two vector mesons and an odd (h_O) or even (g_i, $i = 1, 2, 3, 5$) number of Goldstone bosons. In the future one can explore also the importance of vector-meson channels for the coupled-channel problems (cf. the corresponding discussion in the beginning of this section and [LV12]). There the coupling constants h_O and g_i enter directly and mediate, e.g., the transition from two vector to two pseudo-scalar mesons. For the following reason these coupling constants are also important for our case at hand, in spite of the fact that we do not consider the vector-meson channels: The neutral vector mesons couple directly to photons; see also Fig. 2.16. Therefore, the coupling constants h_O and g_i enter also the transition amplitudes from two photons to two pseudoscalars. In turn, data on such interactions between hadrons and electromagnetism can be used to constrain purely hadronic coupling constants. This resembles the determination of h_A from the decay $\omega \to \gamma\pi^0$ in [LL08]. Note, however, that in our formalism this line of reasoning does not lead automatically to strict vector-meson dominance, but rather to an improved version thereof [TL10, TLL12].

We now turn to a detailed discussion of the various two-meson channels populated by photon fusion. The first highlight is the $\pi^0\eta$ channel depicted in Fig. 2.20. Here our formalism shows a dynamically generated scalar-isovector resonance which is in full quantitative agreement with the experimental data; see also [OO97, OO98, DMOR11] where similar findings have been reported. In our approach we find that this $a_0(980)$ resonance coincides with the two-kaon threshold and emerges from rescattering and coupled-channel effects between $\pi^0\eta$ and $K\bar{K}$. We compare our full coupled-channel result with a pure tree-level calculation based on (2.80). The latter is also depicted in Fig. 2.20 and, of course, does not show a resonance shape, in obvious disagreement with the experimental data. We stress again that according to the hadrogenesis

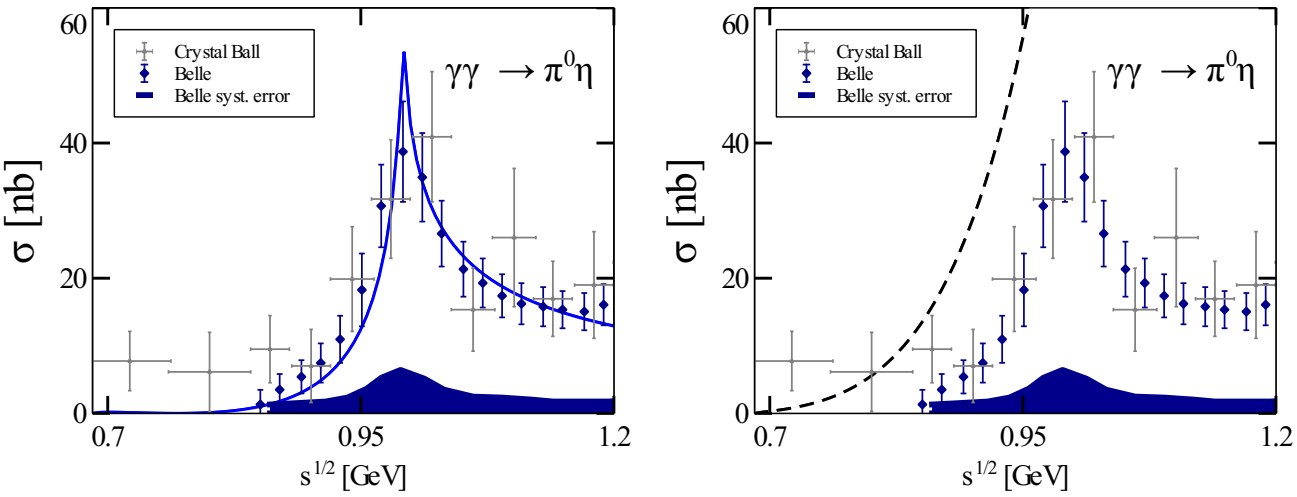

Figure 2.20.: Total cross sections for $\gamma\gamma \to \pi^0\eta$ using (2.89), (2.90) together with $g_5 \in [-5,5]$. The full result is shown on the left and the tree-level result on the right. The tree-level result does not depend on g_5. Also the dependence of the full result on g_5 is very weak. It is caused by the cross-channel effect $\gamma\gamma \to K\bar{K} \to \pi^0\eta$. See the figure caption of Fig. 2.18 for more details.

conjecture [LK01, LK04, LKK04, LK05, LS08, LL08, TLL12] the low-lying scalar resonances are supposed to be generated dynamically. A realization of this suggestion is seen in Fig. 2.20. We recall from our previous discussion about Fig. 2.18 that the location of the resonance does not depend on the choice of the coupling constants g_i and h_O. Only the height of the curve is sensitive to these parameters. This provides confidence in the robustness of our interpretation of the lowest-lying scalar-isovector resonance.

The cross sections for the two-pion channels are depicted in Fig. 2.21. Obviously both channels $\pi^+\pi^-$ and $\pi^0\pi^0$ are well described up to energies of about $\sqrt{s} \approx 0.9\,\text{GeV}$. Then our calculations show a distinct peak, most pronounced in the neutral channel. After this peak our theory curves decrease while the data continue to rise. Two issues need to be disentangled here, namely the location of the $f_0(980)$ in the s-wave and the rise towards the tensor mesons in the d-wave. To do this, we compare our results also to the partial-wave analysis of [PMUW08] as shown in Fig. 2.22. For the d-waves (bottom panels) we observe reasonable agreement up the point in energy where the peak from the isoscalar tensor meson starts out. As already stressed in the introduction we expect that in the spirit of the hadrogenesis conjecture this peak will be generated by vector-vector channels. But since this is beyond the present work we cannot expect to obtain a reasonable description of the d-wave beyond about 0.9 GeV. Below this energy the agreement is very satisfying. Turning to the s-wave, we observe also good agreement for isospin $I = 2$ (top right panel in Fig. 2.22). For the isoscalar channel (top left) some disagreement with the results of [PMUW08] is observed. Most notably our peak for the $f_0(980)$ is slightly shifted to lower energies, i.e. this dynamically generated scalar-isoscalar state is somewhat overbound in our approach. This has already been observed in Section 2.2 (see Fig. 2.13). Whether this is due to higher-order effects in the scattering kernel or due to missing vector-vector channels remains to be seen.

For the energy range below 0.9 GeV we deduce from Fig. 2.21 that we have obtained an overall good description of the reaction data. This is completely in line with the complementary

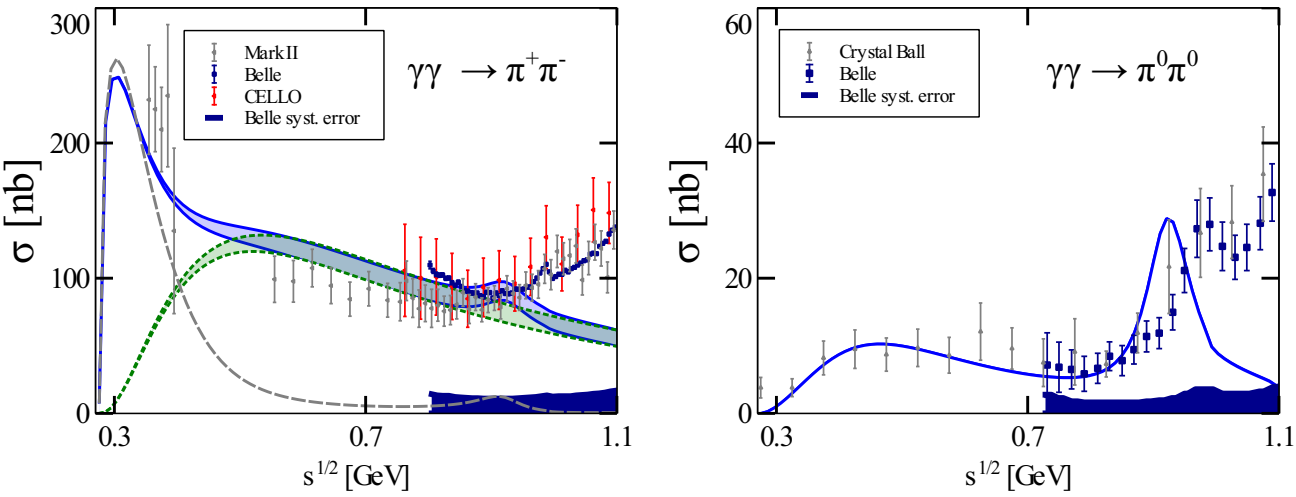

Figure 2.21.: Total cross sections for the reactions $\gamma\gamma \to \pi^+\pi^-$ (left) and $\gamma\gamma \to \pi^0\pi^0$ (right) using (2.89) and (2.90). The variation of $g_5 \in [-5,5]$ is indicated by the bands. For the charged pions (left) the s-wave (long-dashed) and d-wave (short-dashed) are shown separately. See the figure caption of Fig. 2.18 for more details.

information contained in the pion phase shifts as addressed in Section 2.2.4. In Fig. 2.23 we compare our calculations to the results from chiral perturbation theory (χPT) [BC88, DHL88, GIS05, GIS06]. We observe a satisfying agreement. Note that even without vector mesons our calculations contain multi-loop diagrams by the achieved resummation in the s-channel. On the other hand, our calculation does not contain all one-loop diagrams in the t- and u-channel which enter χPT at next-to-leading order. In view of these differences one can be satisfied with the agreement and conclude that the numerically most important corrections from the χPT point of view are included in our approach. At larger energies pure χPT stops working and resummations must be incorporated in one or the other way [OO97, OO98, GNP02, DGL11b, DL12].

Finally, we show in Fig. 2.24 the result of a tree-level calculation based on our amplitudes (2.80). Obviously the charged-pion channel is fairly insensitive to rescattering effects, i.e. to a large extent dominated by the one-pion exchange, which is responsible for the steep rise of the cross section at low energies. The neutral-pion channel, however, which does not have the corresponding one-pion exchange, is dominated by loop/rescattering effects. In this channel the tree-level calculation fails already at low energies.

While the previously discussed channels have been used to some extent to fix our free parameters, the channels which we discuss in the following are pure predictions. Unfortunately, the data situation is rather poor in all three channels $\gamma\gamma \to K^+K^-$, $K^0\bar{K}^0$ and $\eta\eta$, but we will see that it is a non-trivial task to match the available data points. We restrict ourselves to the energy region close to threshold, i.e. to $\sqrt{s} \leq 1.2\,\text{GeV}$. There, we expect the s-wave to dominate, such that we do need to worry about the tensor mesons.

The reaction $\gamma\gamma \to K^+K^-$ is depicted in the top left panel of Fig. 2.25. Other theory approaches have been reported in [OO98, AS11, LYZ99]. Unfortunately there is only one data point with a large energy uncertainty in the considered energy interval. Nonetheless, this data point is significantly lower than generic tree-level calculations. For comparison we show two types of such tree-level calculations. The dashed line is obtained if our Lagrangian is used di-

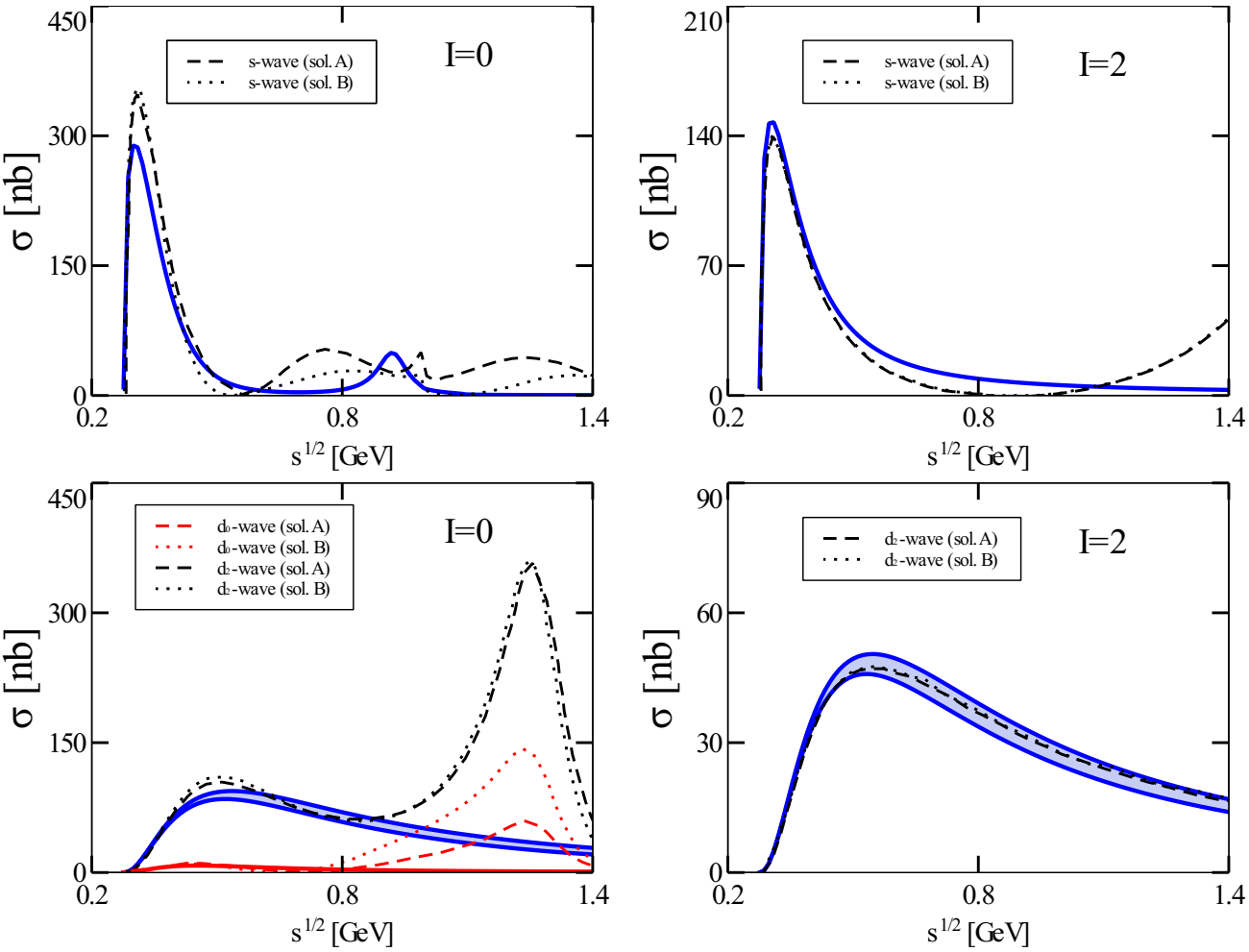

Figure 2.22.: Comparison of our results (solid lines) with the results of [PMUW08] for s-wave (top panels) and d-waves (bottom panels) and for different isospin (left panels: $I = 0$; right panels: $I = 2$). The subscript for the d-waves denotes the helicity. A variation of $g_5 \in [-5, 5]$ is indicated by the bands. According to [PMUW08] two solutions have been obtained: solution A (dashed) is favored by a χ^2 fit, while solution B (dotted) is at the edge of acceptability.

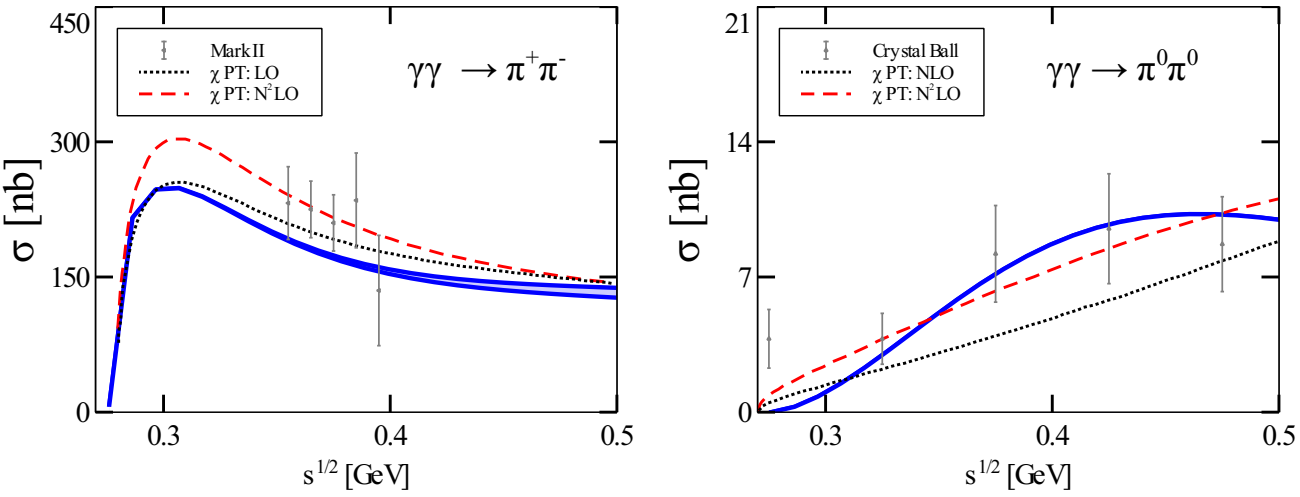

Figure 2.23.: Comparison of our results (full lines) to the calculations from chiral perturbation theory (χPT) and to data. The dashed lines denote the next-to-next-to-leading-order calculations. The dotted lines denote the respective lowest-order non-trivial χPT result, which is leading order for the charged case and next-to-leading order for the neutral case. A variation of $g_5 \in [-5, 5]$ is indicated by the band. See also the figure caption of Fig. 2.18 for more details.

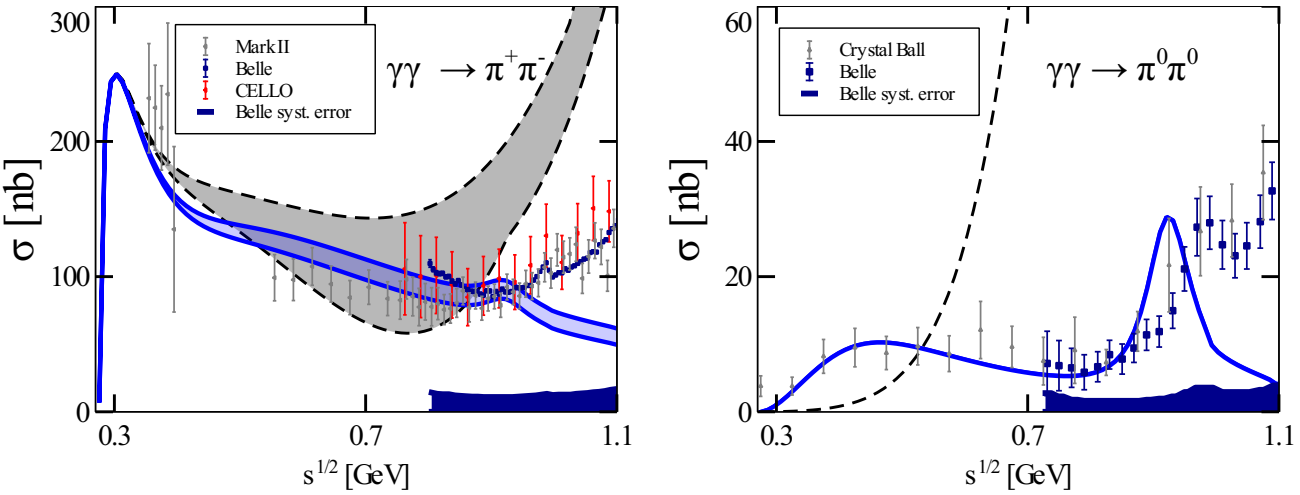

Figure 2.24.: Comparison of tree-level calculations to the full results and to data. Tree-level calculations are depicted by dashed lines. A variation of $g_5 \in [-5, 5]$ is indicated by the bands. See also the figure caption of Fig. 2.18 for more details.

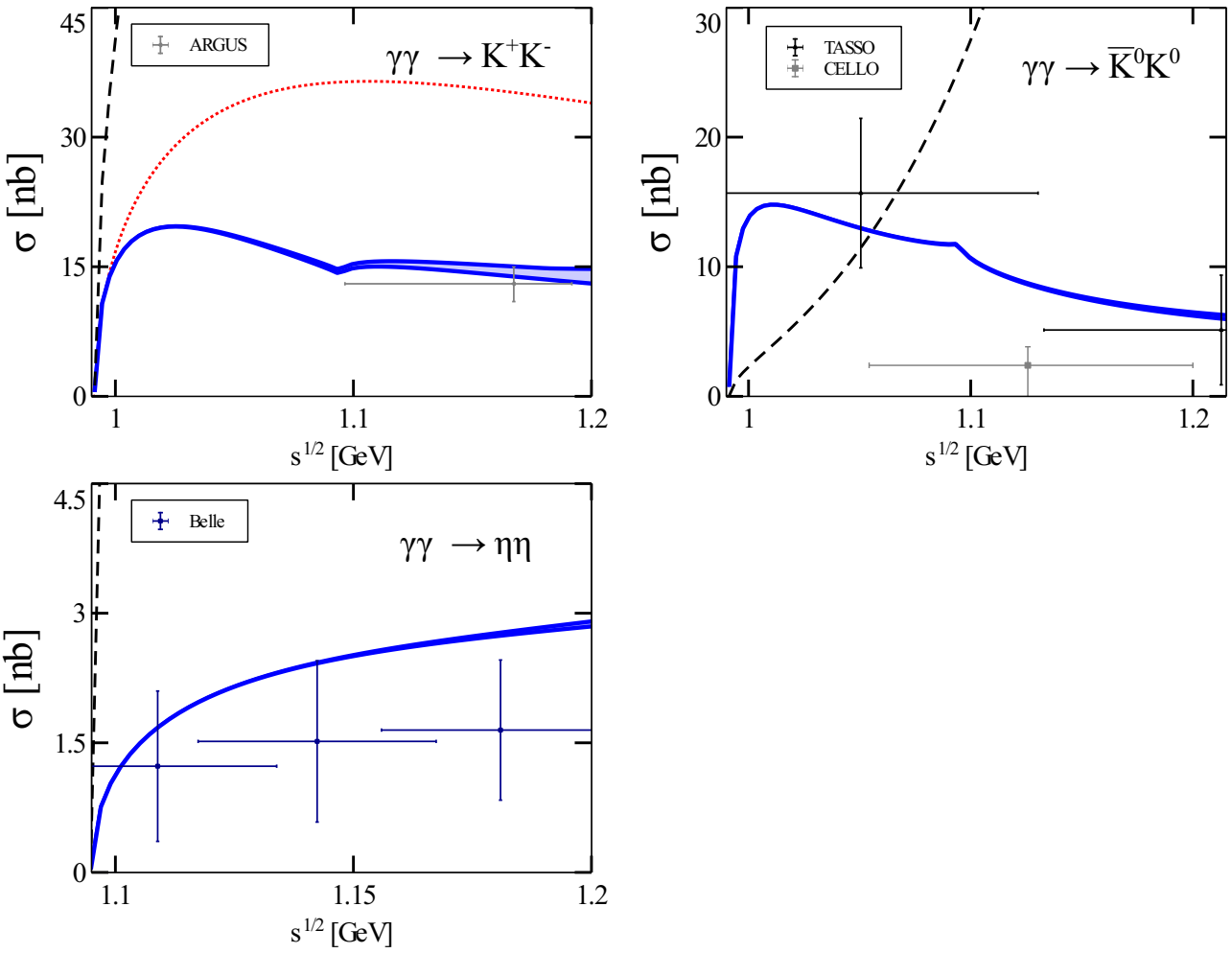

Figure 2.25.: Theoretical predictions for $\gamma\gamma \to K^+K^-$, $K^0\bar{K}^0$ and $\eta\eta$ total cross sections. A variation of $g_5 \in [-5,5]$ is indicated by the bands. Tree-level calculations are depicted by dashed lines. For the charged-kaon case a pure Born-term calculation (one-kaon exchange) is shown by the dotted curve. The data are taken from [A$^+$90, B$^+$89, A$^+$85, U$^+$10].

rectly for the amplitude and not for the potential of the full coupled-channel calculation. An alternative tree-level approach is to use just the kaon-exchange Born diagrams. We recall that the corresponding pion-exchange Born diagrams are very significant for the low-energy part of the reaction $\gamma\gamma \to \pi^+\pi^-$ (the χPT-LO curve of Fig. 2.23). For the kaon case the situation is obviously different. While tree-level calculations fail to reproduce even the close-to-threshold data, our full coupled-channel approach leads to a significant reduction of the Born amplitude and matches the available data point very nicely. Hence, the final-state interactions are strong in this channel. A similar finding has been reported in [OO98]. Finally we note that our approach shows a visible cusp at the two-eta threshold. It is even more pronounced in the neutral-kaon channel to which we turn next.

The reaction $\gamma\gamma \to K^0\bar{K}^0$ is shown in the top right panel of Fig. 2.25. The data, albeit with large error bars, point to an initial steep increase of the cross section with energy, followed by a not so rapid fall. This behavior is qualitatively reproduced by our full calculation, though we do not fully match the second data point quantitatively. Tree-level calculations cannot reproduce

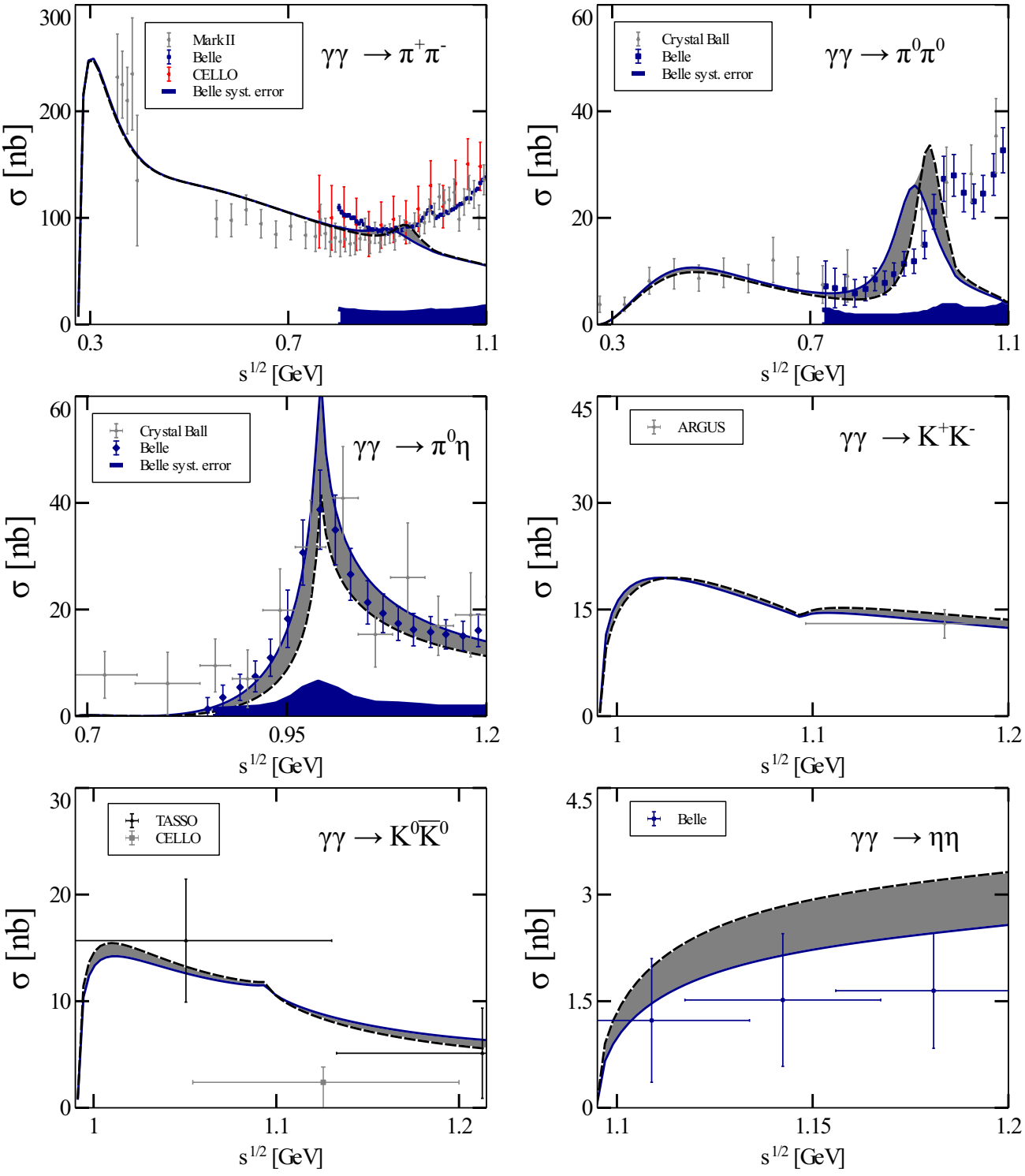

Figure 2.26.: Total cross sections for the reactions $\gamma\gamma \to \pi^+\pi^-$, $\pi^0\pi^0$, $\pi^0\eta$, K^+K^-, $K^0\bar{K}^0$ and $\eta\eta$, using (2.89) and (2.90). For definiteness, we fix $g_5 = 0$. The various bands are implied by a variation of the parameter Λ_s with 1.4 GeV (dashed line) $< \Lambda_s <$ 1.8 GeV (solid line).

at all this rise-and-fall behavior. Indeed, it is natural to expect that final-state interactions are strong because the photons couple stronger to the intermediate charged states than to the final neutral ones.

The bottom panel of Fig. 2.25 shows the cross section for the reaction $\gamma\gamma \to \eta\eta$ (see also [LYZ99]). The data suggest a rather flat energy dependence which cannot be reproduced by a pure tree-level calculation (dashed line). In contrast, our full calculation (solid lines) including rescattering meets this requirement of a comparatively flat cross section.

We stress again that our results for $\gamma\gamma \to K^+K^-$, $K^0\bar{K}^0$ and $\eta\eta$ cross sections are pure predictions. These channels did not enter the determination of free parameters. Note also that the results are basically insensitive to the remaining free parameter g_5. Clearly, better data in these channels would be highly welcome to further check the validity of our coupled-channel approach with dynamical vector mesons.

In Fig. 2.26 we finally show the sensitivity to a variation of Λ_s from 1.4 GeV to 1.8 GeV. As one can see, the impact of this variation on the results is small.

We conclude that the reaction amplitudes which were derived from the chiral Lagrangian with dynamical vector meson fields and then properly constrained by micro-causality and coupled-channel unitarity, allow us to perform a controlled study of the reactions $\gamma\gamma \to \pi^0\pi^0$, $\pi^+\pi^-$, $K^0\bar{K}^0$, K^+K^-, $\eta\,\eta$ and $\pi^0\eta$ up to about 1.2 GeV.

3 Summary and Outlook

In this thesis we have successfully used the chiral Lagrangian formulated with light vector degrees of freedom to describe Goldstone-boson scattering and photon-fusion reactions. Within a recently developed novel unitarization approach we obtained a unified description of $\pi\pi \to \pi\pi$, $\pi\pi \to K\bar{K}$, $\pi K \to \pi K$ and $\gamma\gamma \to \pi\pi$, $K\bar{K}$, $\eta\eta$, $\pi\eta$ reactions in agreement with the experimental data up to about 1.2 GeV.

As a first step we derived from the chiral Lagrangian the two-body partial-wave amplitudes at tree-level with respect to coupled-channel states of definite isospin, G-parity and strangeness. The important s-, t- and u- vector meson exchange processes were taken into account explicitly. In order to extrapolate subthreshold amplitudes into the physical region, we set the constraints from micro-causality and coupled-channel unitarity. By means of partial-wave dispersion relation we decomposed left- and right-hand singularities, where the so-called generalized potential characterized by left-hand cuts only. The latter was evaluated with help of chiral amplitudes and suitably constructed conformal variables, which permit to achieve a correct asymptotic boundary of the potential. This leads to results which comply with analyticity and unitarity conditions. Moreover our analysis preserves the electromagnetic gauge invariance constraint.

After illustrating the usefulness and ability of the novel unitarization approach on Yukawa-type interactions we have considered Goldstone-boson scattering. The resulting s- and p-wave phase shifts for $\pi\pi$ and πK were obtained in a good agreement with the experimental data. In the isoscalar and isovector sectors we dynamically generated the $f_0(980)$ and $a_0(980)$ resonances, respectively, in accordance with the hadrogenesis conjecture. In the p-wave scattering, vector mesons are described as Castillejo-Dalitz-Dyson poles. In particular, ρ and K^* mesons were reproduced accurately. The description was obtained with two relevant and known parameters only, the chiral limit value of the pion decay constant and the coupling constant characterizing the decay of the rho meson into a pair of pions. The success of these results motivated us to extend our analysis to photon-fusion reactions, where recently new data on $\gamma\gamma \to \pi^+\pi^-$, $\pi^0\pi^0$, $\pi^0\eta$ and $\eta\eta$ processes have been reported by the Belle Collaboration. For photon-fusion processes the chiral Lagrangian with dynamical vector fields has five unknown parameters. They have been fixed from the reactions $\gamma\gamma \to \pi^0\pi^0$, $\pi^+\pi^-$, $\pi^0\eta$ and from the differential decay $\eta \to \pi^0\gamma\gamma$. Based on our parameter constraints we predicted the low-energy $\gamma\gamma \to K^+K^-$, $K^0\bar{K}^0$ and $\eta\,\eta$ cross sections. We emphasize that accurate low-energy photon fusion data would further help us to examine the intricate dynamics of the Goldstone bosons and light vector mesons.

There are a few possible extensions of this work. First, a calculation of higher order contributions which include pseudoscalar and vector-meson loops. In practice, however, it will lead to an increasing number of free parameters in addition to a highly non-trivial step of the renormalization of vector-meson loops. Second, another natural extension can be an inclusion of more inelastic channels, like $\rho\rho$, $\pi\rho$, $N\bar{N}$ etc. and the investigation of their importance to coupled-channel dynamics. According to the hadrogenesis conjecture we expect to obtain significant results up to about 2 GeV once such channels are incorporated in a controlled manner.

A Conventions

In this appendix we collect the basis conventions and notations used in this thesis.

1. Metric tensor:

$$g^{\mu\nu} = g_{\mu\nu} = \mathrm{diag}\{1,-1,-1,-1\}\,. \tag{A.1}$$

2. Scalar product:

$$(a\cdot b) = a_\mu b^\mu = g^{\mu\nu}\, a_\mu b_\nu\,. \tag{A.2}$$

3. Levi-Civita tensor:

$$\epsilon^{\mu\nu\alpha\beta} = \begin{cases} 1 & \text{if } (\mu,\nu,\alpha,\beta) \text{ is an even permutation of } (0,1,2,3) \\ -1 & \text{if it is an odd permutation} \\ 0 & \text{otherwise} \end{cases}\,. \tag{A.3}$$

4. Pauli matrices:

$$\sigma_1 = \begin{pmatrix} 0 & 1 \\ 1 & 0 \end{pmatrix}, \quad \sigma_2 = \begin{pmatrix} 0 & -i \\ i & 0 \end{pmatrix}, \quad \sigma_3 = \begin{pmatrix} 1 & 0 \\ 0 & -1 \end{pmatrix}. \tag{A.4}$$

5. Gell-Mann matrices:

$$\begin{aligned} \lambda_1 &= \begin{pmatrix} 0 & 1 & 0 \\ 1 & 0 & 0 \\ 0 & 0 & 0 \end{pmatrix}, \ \lambda_2 = \begin{pmatrix} 0 & -i & 0 \\ i & 0 & 0 \\ 0 & 0 & 0 \end{pmatrix}, \ \lambda_3 = \begin{pmatrix} 1 & 0 & 0 \\ 0 & -1 & 0 \\ 0 & 0 & 0 \end{pmatrix}, \\ \lambda_4 &= \begin{pmatrix} 0 & 0 & 1 \\ 0 & 0 & 0 \\ 1 & 0 & 0 \end{pmatrix}, \ \lambda_5 = \begin{pmatrix} 0 & 0 & -i \\ 0 & 0 & 0 \\ i & 0 & 0 \end{pmatrix}, \ \lambda_6 = \begin{pmatrix} 0 & 0 & 0 \\ 0 & 0 & 1 \\ 0 & 1 & 0 \end{pmatrix}, \\ \lambda_7 &= \begin{pmatrix} 0 & 0 & 0 \\ 0 & 0 & -i \\ 0 & i & 0 \end{pmatrix}, \ \lambda_8 = \frac{1}{\sqrt{3}} \begin{pmatrix} 1 & 0 & 0 \\ 0 & 1 & 0 \\ 0 & 0 & -2 \end{pmatrix} \end{aligned} \tag{A.5}$$

   with standard normalization

$$\mathrm{tr}\{\lambda_i \lambda_j\} = 2\,\delta_{ij}\,. \tag{A.6}$$

   Note that in this normalization the first three Gell-Mann matrices contain three Pauli matrices in the upper-left corner. The matrices $\lambda_{i=1,..,8}$ are the generators of the SU(3) group and together with $\lambda_0 = \sqrt{2/3}\,\mathrm{diag}\{1,1,1\}$ form a complete basis of the $U(3)$ group.

6. Masses and quantum numbers of the light pseudo-scalar and vector mesons.

meson	$I^G(J^P)$	mass [MeV]	meson	$I^G(J^P)$	mass [MeV]
π	$1^-(0^-)$	138,039	ρ	$1^+(1^-)$	770,00
K	$1/2(0^-)$	495,675	K^*	$1/2(1^-)$	893,88
η	$0^+(0^-)$	547,450	ω	$0^-(1^-)$	782,57
			ϕ	$0^-(1^-)$	1019,46

7. Throughout this thesis we use natural system of units, where $\hbar = 1$ and $c = 1$. Furthermore we adopt Heaviside system for electric charges, in which the factor 4π appears in the fine structure constant, $\alpha = \frac{e^2}{4\pi} \simeq \frac{1}{137}$. An electric charge has no dimension in these units and equals to $e \simeq 0.303$.

B Tensor representation for the vector-meson fields

Typically, a massive vector field is described by a Lorenz field V^μ with four indices. However, by the Lorenz condition

$$\partial^\mu V_\mu = 0\,, \tag{B.1}$$

a mixture of the spin-0 component is frozen. This implies that the massive vector field has only three polarization states and the free vector meson Lagrangian has the form

$$\mathcal{L} = -\frac{1}{4} F^{\mu\nu} F_{\mu\nu} + \frac{1}{2} m^2 V_\mu V^\mu \tag{B.2}$$

with the field strength $F_{\mu\nu} = \partial_\mu V_\nu - \partial_\nu V_\mu$.

An alternative description of vector mesons is the antisymmetric tensor field representation [EGPdR89]. The most general free Lagrangian for an antisymmetric tensor field of rank two $W_{\mu\nu} = -W_{\nu\mu}$ has the form

$$\mathcal{L} = a\,\partial^\mu W_{\mu\nu}\,\partial_\rho W^{\rho\nu} + b\,\partial^\rho W_{\mu\nu}\,\partial_\rho W^{\mu\nu} + c\,W_{\mu\nu} W^{\mu\nu} \tag{B.3}$$

with arbitrary constants a, b and c. The field $W^{\mu\nu}$ has six degrees of freedom, but only three of them actually propagate (massive spin-1 fields). Freezing out three fields by the choice of the constants, $a = 1/2$, $b = 0$ and $c = m^2/4$, the free Lagrangian takes the form [EGPdR89]

$$\mathcal{L} = -\frac{1}{2}\,\partial^\mu W_{\mu\nu}\,\partial_\rho W^{\rho\nu} + \frac{1}{4} m^2 W_{\mu\nu} W^{\mu\nu}\,, \tag{B.4}$$

where m is the mass of the vector meson. Note that for simplicity, we consider here real fields corresponding to neutral particles. The generalization to charged particles or, more generally, to $SU(3)$ multiplets of particles is straightforward[1]. The above Lagrangian (B.4) gives the equation of motion

$$\partial^\mu \partial_\sigma W^{\sigma\nu} - \partial^\nu \partial_\sigma W^{\sigma\mu} + m^2 W^{\mu\nu} = 0\,. \tag{B.5}$$

Contracting this equation with $\epsilon_{\alpha\beta\mu\nu}\,\partial^\beta$ one can find that for $m \neq 0$ the following constraint is satisfied

$$\epsilon_{\alpha\beta\mu\nu}\,\partial^\beta W^{\mu\nu} = 0. \tag{B.6}$$

Note, that exactly this combination appears in the h_O term of the Lagrangian (1.40).

[1] In the SU(3) case $m = m_V$ is the light vector meson mass in the chiral limit.

From the Lagrangian one constructs the free propagator

$$\langle 0|T\,W^{\bar{\alpha}\bar{\beta}}(x)\,W^{\alpha\beta}(y)|0\rangle = \int \frac{d^4k}{(2\pi)^4}\,e^{-i\,k\cdot(x-y)}\,iS^{\bar{\alpha}\bar{\beta},\alpha\beta}(k)\,, \tag{B.7}$$

$$S^{\bar{\alpha}\bar{\beta},\alpha\beta}(k) = -\frac{1}{m^2}\,\frac{1}{k^2-m^2+i\epsilon}\left[(m^2-k^2)\,g^{\bar{\alpha}\alpha}\,g^{\bar{\beta}\beta} + g^{\bar{\alpha}\alpha}\,k^{\bar{\beta}}\,k^{\beta} - g^{\bar{\alpha}\beta}\,k^{\bar{\beta}}\,k^{\alpha} - (\bar{\alpha}\leftrightarrow\bar{\beta})\right],$$

with the associated wave function[2]

$$\begin{aligned}\langle 0|W_{\mu\nu}|p,\lambda\rangle &= \epsilon_{\mu\nu}(p,\lambda) = \frac{i}{m}\,(p_\mu\,\epsilon_\nu(p,\lambda) - p_\nu\,\epsilon_\mu(p,\lambda))\,,\\ \sum_{\lambda=1}^{3}\epsilon_\mu^\dagger(p,\lambda)\,\epsilon_\nu(p,\lambda) &= -g_{\mu\nu} + \frac{p_\mu\,p_\nu}{m^2}\,,\end{aligned} \tag{B.8}$$

where $\epsilon_\mu(p,\lambda)$ is the conventional wave function of a vector particle in the vector representation. The free propagator (B.7) can be written in terms of longitudinal (L) and transversal (T) components,

$$\langle 0|T\,W^{\bar{\alpha}\bar{\beta}}(x)\,W^{\alpha\beta}(y)|0\rangle = i\int \frac{d^4k}{(2\pi)^4}\,e^{-i\,k\cdot(x-y)}\left(-\frac{2}{k^2-m^2}\,P_T^{\bar{\alpha}\bar{\beta}\,\alpha\beta} + \frac{2}{m^2}\,P_L^{\bar{\alpha}\bar{\beta}\,\alpha\beta}\right), \tag{B.9}$$

where the tensors

$$\begin{aligned}P_T^{\bar{\alpha}\bar{\beta}\alpha\beta} &= \frac{1}{2\,k^2}\left(g^{\bar{\alpha}\alpha}\,k^{\bar{\beta}}\,k^{\beta} - g^{\alpha\bar{\beta}}\,k^{\bar{\alpha}}\,k^{\beta} - (\alpha\leftrightarrow\beta)\right),\\ P_L^{\bar{\alpha}\bar{\beta}\alpha\beta} &= -\frac{1}{2\,k^2}\left(g^{\bar{\alpha}\alpha}\,k^{\bar{\beta}}\,k^{\beta} - g^{\alpha\bar{\beta}}\,k^{\bar{\alpha}}\,k^{\beta} - k^2\,g^{\bar{\alpha}\alpha}\,g^{\bar{\beta}\beta} - (\alpha\leftrightarrow\beta)\right)\end{aligned} \tag{B.10}$$

are transverse and longitudinal with respect to the four momentum k [Leu07]. From (B.9) it is easy to see that only transverse modes propagate.

Generally, the physical results are independent on the particular choice of representation. However in practice two, three,... point vertices can look different in different representations and can have different orders according to some counting scheme. Moreover for electromagnetic processes, the tensor representation for vector mesons overcomes complications of the mixing between scalar and vector modes and provides gauge invariant amplitudes [LS08].

[2] Note the properties $\epsilon_{\mu\nu} = -\epsilon_{\nu\mu}$ and $q^\mu\,q^\nu\,\epsilon_{\mu\nu} = 0$

C Conformal mapping technique

In the application of dispersion integrals, a conformal mapping technique may be used. This method allows to approximate an analytic function in a cut plane, based on the knowledge of that function in a small region only. The approximation is achieved by first mapping the cut plane conformally into a unit circle and then expanding into a power series.

Let us consider a typical function

$$f(w) = \log\left[\frac{w-\Lambda_0}{\mu_E-\Lambda_0}\right], \tag{C.1}$$

which is characterized by the left-hand cut structure at $w < \Lambda_0$ in the complex w-plane. Imagine that we know $f(w)$ only in a small region around an expansion point $w = \mu_E$ and we want to reconstruct this function for $w > \Lambda_0$. An extrapolation can be performed by means of a standard Taylor expansion around $w = \mu_E$,

$$f(w) = f(\mu_E) + f'(\mu_E)(w-\mu_E) + \frac{1}{2}f''(\mu_E)(w-\mu_E)^2 + \ldots, \tag{C.2}$$

but the convergence radius, $\Lambda_0 < w < 2\mu_E - \Lambda_0$, is limited by the distance to the closest singularity at $w = \Lambda_0$ (left-hand branch point).

Progress is made by performing the Taylor expansion in power of ξ, where ξ is a suitable conformal variable constructed as to map the left-hand cut onto the unit circle in the complex $\xi-$plane (see Fig.C.1),

$$\xi(w) = \frac{\sqrt{w-\Lambda_0} - \sqrt{\mu_E-\Lambda_0}}{\sqrt{w-\Lambda_0} + \sqrt{\mu_E-\Lambda_0}}. \tag{C.3}$$

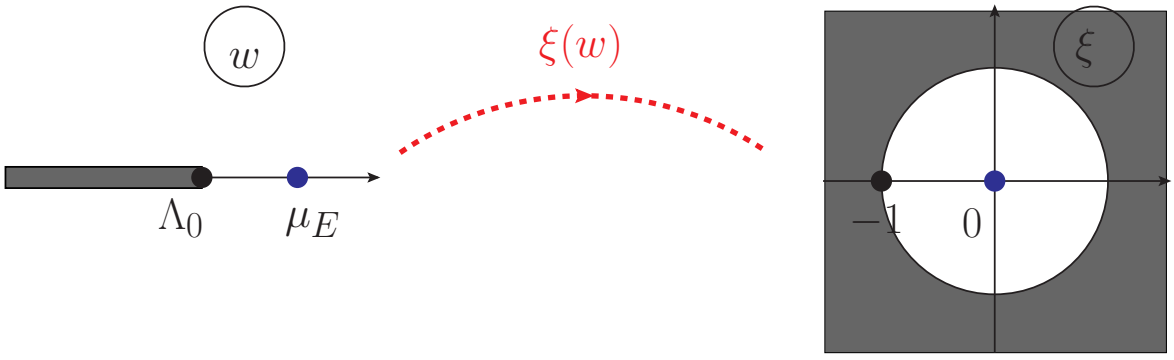

Figure C.1.: The conformal mapping $w \to \xi$ that is given by Eq.(C.3).

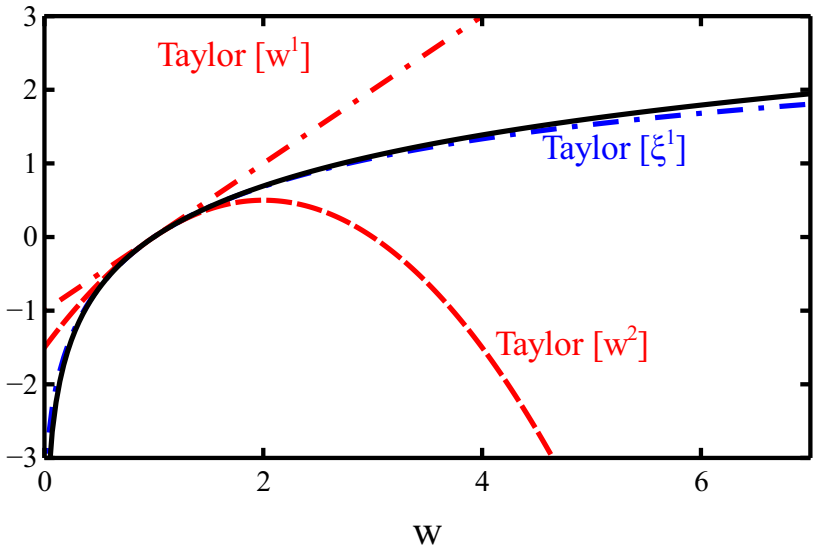

Figure C.2.: The sensitivity of the expansions (C.2) and (C.4) around $\mu_E = 1$ with $\Lambda_0 = 0$ on the truncation order. First and second orders (dotted and dashed lines) of the standard Taylor expansion are displayed in comparison to the first order of the Taylor expansion in power of ξ (dot-dashed line). Solid line is $f(w)$.

The requirements that $w = \mu_E \to 0$ and $w = \Lambda_0 \to -1$ make the mapping unique. The cut now lies along the unit circle in the ξ-plane. As a result, we obtain the following Taylor expansion around $\xi_0 = \xi(\mu_E) = 0$,

$$f(w(\xi)) = f(w(\xi_0)) + \left.\frac{df(w(\xi))}{d\xi}\right|_{\xi=\xi_0} (\xi - \xi_0) + \dots \tag{C.4}$$

$$f(w) = \sum_{n=0}^{\infty} c_n \left[\xi(w)\right]^n = f(\mu_E) + f'(\mu_E)\, w'(\xi(\mu_E))\,(\xi(w) - \xi(\mu_E)) + \dots,$$

which converges at $\Lambda_0 < w < \infty$ and recovers $f(w)$ in its analyticity domain. In Fig.C.2 we present the result for $\mu_E = 1$ and $\Lambda_0 = 0$. One can see that the Taylor expansion around $w = 1$ only converges in the region $0 < w < 2$, while the Taylor expansion around $\xi = 0$ converges for all $w > 0$.

It is important to stress that the coefficients c_n in Eq.(C.4) are all determined by the derivatives of $f(w)$ at an expansion point $w = \mu_E$.

D Kinematics

In this appendix, the basic definitions of kinematics are given. We consider scattering of two particles of four-momenta p and q and masses m_1 and m_2 to particles of four-momenta $\bar{p}$ and $\bar{q}$ and masses $\bar{m}_1$ and $\bar{m}_2$. In the center-of-mass frame the energies of the initial particles are denoted by ω_1, ω_2, and the energies of the final particles by $\bar{\omega}_1$, $\bar{\omega}_2$. It holds

$$\begin{aligned}
p^\mu &= (\omega_1, 0, 0, +p_{cm}) \,, & \bar{p}^\mu &= (\bar{\omega}_1, +\bar{p}_{cm}\sin\theta, 0, +\bar{p}_{cm}\cos\theta) \,, \\
\omega_1 &= \sqrt{p_{cm}^2 + m_1^2}, & \bar{\omega}_1 &= \sqrt{\bar{p}_{cm}^2 + \bar{m}_1^2}, \\
q^\mu &= (\omega_2, 0, 0, -p_{cm}) \,, & \bar{q}^\mu &= (\bar{\omega}_2, -\bar{p}_{cm}\sin\theta, 0, -\bar{p}_{cm}\cos\theta) \,, \\
\omega_2 &= \sqrt{p_{cm}^2 + m_2^2}, & \bar{\omega}_2 &= \sqrt{\bar{p}_{cm}^2 + \bar{m}_2^2},
\end{aligned} \tag{D.1}$$

where θ is the scattering angle in the center-of-mass frame (see Fig.D.1), p_{cm} and $\bar{p}_{cm}$ are the momenta of the initial and final state. The Lorenz-invariant Mandelstam variables are defined by

$$\begin{aligned}
s &= (p+q)^2 = (\bar{p}+\bar{q})^2 \,, \\
t &= (\bar{q}-q)^2 = (\bar{p}-p)^2 \,, \\
u &= (\bar{q}-p)^2 = (\bar{p}-q)^2 \,,
\end{aligned} \tag{D.2}$$

and satisfy the relation

$$s + t + u = m_1^2 + m_2^2 + \bar{m}_1^2 + \bar{m}_2^2 \,.$$

The center-of-mass three momenta p_{cm} and $\bar{p}_{cm}$ of two particle system are expressed in terms of the total energy $\sqrt{s}$ as

$$\begin{aligned}
p_{cm}^2 &= \frac{1}{4s}\left(s - (m_1+m_2)^2\right)\left(s - (m_1-m_2)^2\right) \,, \\
\bar{p}_{cm}^2 &= \frac{1}{4s}\left(s - (\bar{m}_1+\bar{m}_2)^2\right)\left(s - (\bar{m}_1-\bar{m}_2)^2\right) \,.
\end{aligned} \tag{D.3}$$

We define the polarization vectors $\epsilon^\mu(k,\lambda)$ (where k is a momentum and λ is a helicity) for a spin-one particle by

$$\epsilon^\mu(\bar{p},\pm1) = \begin{pmatrix} 0 \\ \frac{\mp\cos\theta}{\sqrt{2}} \\ \frac{-i}{\sqrt{2}} \\ \frac{\pm\sin\theta}{\sqrt{2}} \end{pmatrix} \,, \quad \epsilon^\mu(\bar{p},0) = \begin{pmatrix} \frac{\bar{p}_{cm}}{\bar{m}_1} \\ \frac{\bar{\omega}_1}{\bar{m}_1}\sin\theta \\ 0 \\ \frac{\bar{\omega}_1}{\bar{m}_1}\cos\theta \end{pmatrix} \,,$$

$$\epsilon^\mu(\bar{q},\pm1) = \begin{pmatrix} 0 \\ \frac{\pm\cos\theta}{\sqrt{2}} \\ \frac{-i}{\sqrt{2}} \\ \frac{\mp\sin\theta}{\sqrt{2}} \end{pmatrix} \,, \quad \epsilon^\mu(\bar{q},0) = \begin{pmatrix} \frac{\bar{p}_{cm}}{\bar{m}_2} \\ -\frac{\bar{\omega}_2}{\bar{m}_2}\sin\theta \\ 0 \\ -\frac{\bar{\omega}_2}{\bar{m}_2}\cos\theta \end{pmatrix} \,,$$

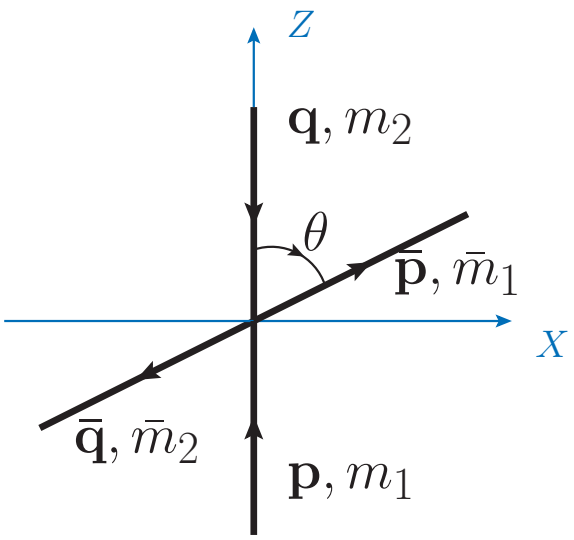

Figure D.1.: Definition of the scattering angle in the center-of-mass frame of $m_1+m_2 \to \bar{m}_1+\bar{m}_2$ scattering. The scattering plane is chosen to be the azimuthal plane ($\phi = 0$).

where the polarizations vectors of the corresponding incoming states are recovered with $\theta = 0$ and removing the bars. The photon, being massless, can only have two helicities $\lambda = \pm 1$.

Bibliography

[A+85] M. Althoff et al. Search for two photon production of resonances decaying into $K\bar{K}$ and $K\bar{K}\pi$. *TASSO Collaboration, Z. Phys.*, C 29:189, 1985.

[A+86] D. Antreasyan et al. Formation of $\delta(980)$ and $a_2(1320)$ in photon-photon collisions. *Crystal Ball Collaboration, Phys. Rev.*, D 33:1847, 1986.

[A+90] H. Albrecht et al. Measurment of K^+K^- production in $\gamma\gamma$ collisions. *ARGUS Collaboration, Z. Phys.*, C 48:183–190, 1990.

[A+09] S. Aoki et al. 2+1 flavor lattice QCD toward the physical point. *Phys. Rev.*, D79:034503, 2009.

[ABBC92] L. Ametller, J. Bijnens, A. Bramon, and F. Cornet. Chiral perturbation theory for $\eta \to \pi^0\gamma\gamma$. *Phys. Lett.*, B 276:185–190, 1992.

[ACGL01] B. Ananthanarayan, G. Colangelo, J. Gasser, and H. Leutwyler. Roy equation analysis of $\pi\pi$ scattering. *Phys.Rept.*, 353:207–279, 2001.

[AS11] N. N. Achasov and G. N. Shestakov. Light scalar mesons in photon-photon collisions. *Phys. Usp.*, 54:799–828, 2011.

[B+89] H. J. Behrend et al. The $K_s^0K_s^0$ final state in $\gamma\gamma$ interactions. *CELLO Collaboration, Z. Phys.*, C 43:91, 1989.

[B+90] J. Boyer et al. Two photon production of pion pairs. *Phys. Rev.*, D 42:1350–1367, 1990.

[B+92] H. J. Behrend et al. An Experimental study of the process $\gamma\gamma \to \pi^+\pi^-$. *CELLO Collaboration, Z. Phys.*, C 56:381–390, 1992.

[BBC+75] S. L. Baker, S. Banerjee, J. R. Campbell, G. Hall, A. K. M. A. Islam, et al. A study of $K^+\pi^-$ elastic scattering in the reaction $K^+n \to K^+\pi^-p$ between 2.0-GeV/c and 3.0-GeV/c. *Nucl. Phys.*, B99:211, 1975.

[BC88] Johan Bijnens and Fernando Cornet. Two pion production in photon-photon collisions. *Nucl. Phys.*, B 296:557, 1988.

[BCE+96] J. Bijnens, G. Colangelo, G. Ecker, J. Gasser, and M. E. Sainio. Elastic $\pi\pi$ scattering to two loops. *Phys. Lett.*, B374:210–216, 1996.

[BCE+97] J. Bijnens, G. Colangelo, G. Ecker, J. Gasser, and M. E. Sainio. Pion pion scattering at low-energy. *Nucl. Phys.*, B508:263–310, 1997.

[BCK+08] J. R. Batley, A. J. Culling, G. Kalmus, C. Lazzeroni, D. J. Munday, et al. New high statistics measurement of K_{e4} decay form factors and $\pi\pi$ scattering phase shifts. *Eur. Phys. J.*, C54:411, 2008.

[BDD+72] H. H. Bingham, W. M. Dunwoodie, D. Drijard, D. Linglin, Y. Goldschmidt-Clermont, et al. A new analysis of $K\pi$ scattering as observed in $K^+ p \to K^+ \pi^0 \Delta^{++}$ from 3-GeV/c to 13-GeV/c. *Nucl. Phys.*, B41:1–34, 1972.

[BDGM04] Paul Buettiker, S. Descotes-Genon, and B. Moussallam. A new analysis of πK scattering from Roy and Steiner type equations. *Eur. Phys. J.*, C33:409–432, 2004.

[Bir96] Michael C. Birse. Effective chiral Lagrangians for spin 1 mesons. *Z. Phys.*, A355:231–246, 1996.

[BJ76] G. E. Brown and A. D. Jackson. *The nucleon-nucleon interaction*. North Holland, Amsterdam, 1976.

[BKM91] Veronique Bernard, Norbert Kaiser, and Ulf G. Meissner. Chiral perturbation theory in the presence of resonances: Application to $\pi\pi$ and πK scattering. *Nucl. Phys.*, B364:283–320, 1991.

[BLP82] V. B. Berestetskii, E.M. Lifshitz, and L. P. Pitaevskii. *Quantum Electrodynamics*. Pergamon Press, 1982.

[CAD+80] Daniel H. Cohen, D. S. Ayres, R. Diebold, S. L. Kramer, A. J. Pawlicki, et al. Amplitude analysis of the $K^- K^+$ system produced in the Reactions $\pi^- p \to K^- K^+ n$ and $\pi^+ n \to K^- K^+ p$ at 6-GeV/c. *Phys. Rev.*, D22:2595, 1980.

[CCWZ69] Jr. Callan, Curtis G., Sidney R. Coleman, J. Wess, and Bruno Zumino. Structure of phenomenological Lagrangians. II. *Phys. Rev.*, 177:2247–2250, 1969.

[CDD56] L. Castillejo, R. H. Dalitz, and F. J. Dyson. Low's scattering equation for the charged and neutral scalar theories. *Phys. Rev.*, 101:453–458, 1956.

[CDG76] Jr. Callan, Curtis G., R. F. Dashen, and David J. Gross. The structure of the gauge theory vacuum. *Phys. Lett.*, B63:334–340, 1976.

[CEP09] V. Cirigliano, G. Ecker, and A. Pich. Reanalysis of pion pion phase shifts from $K \to \pi\pi$ decays. *Phys. Lett.*, B679:445–448, 2009.

[CGL01] G. Colangelo, J. Gasser, and H. Leutwyler. $\pi\pi$ scattering. *Nucl. Phys.*, B603:125–179, 2001.

[CJ68] P. D. Collins and R. C. Johnson. Use of Born approximations in N/D calculations. *Phys. Rev.*, 169(5):1222–1231, 1968.

[CK00] Pietro Colangelo and Alexander Khodjamirian. QCD sum rules, a modern perspective. *hep-ph/0010175*, 2000.

[CM60] Geoffrey F. Chew and Stanley Mandelstam. Theory of low-energy pion pion interactions. *Phys. Rev.*, 119:467–477, 1960.

[CWZ69] Sidney R. Coleman, J. Wess, and Bruno Zumino. Structure of phenomenological Lagrangians. I. *Phys. Rev.*, 177:2239–2247, 1969.

[DBG+73] N. B. Durusoy, M. Baubillier, R. George, M. Goldberg, A. M. Touchard, et al. Study of the $I = 2$ $\pi\pi$ scattering from the reaction $\pi^- d \to \pi^- \pi^- p_s p$ at 9.0 gev/c. *Phys. Lett.*, B45:517–520, 1973.

[DGL11a] I. V. Danilkin, A. M. Gasparyan, and M. F. M. Lutz. On causality, unitarity and perturbative expansions. *Phys. Lett.*, B697:147–152, 2011.

[DGL11b] I. V. Danilkin, L. I. R. Gil, and M. F. M. Lutz. Dynamical light vector mesons in low-energy scattering of Goldstone bosons. *Phys. Lett.*, B 703:504–509, 2011.

[DHL88] John F. Donoghue, Barry R. Holstein, and Y. C. Lin. The reaction $\gamma\gamma \to \pi^0\pi^0$ and chiral loops. *Phys. Rev.*, D 37:2423, 1988.

[DL12] I. V. Danilkin and M. F. M. Lutz. Chiral dynamics with vector fields: an application to $\pi\pi$ and πK scattering. *arXiv:1208.2568 [hep-ph]*, 2012.

[DLLT12] I. V. Danilkin, M. F. M. Lutz, S. Leupold, and C. Terschluesen. Photon-fusion reactions from the chiral Lagrangian with dynamical light vector mesons. *arXiv:1211.1503 [hep-ph]*, 2012.

[DMOR11] M. Doring, Ulf-G. Meissner, E. Oset, and A. Rusetsky. Unitarized chiral perturbation theory in a finite volume: Scalar meson sector. *Eur. Phys. J.*, A 47:139, 2011.

[ECM+78] P. Estabrooks, R. K. Carnegie, Alan D. Martin, W. M. Dunwoodie, T. A. Lasinski, et al. Study of $K\pi$ scattering using the reactions $K^{\pm}p \to K^{\pm}\pi^+n$ and $K^{\pm}p \to K^{\pm}\pi^-\Delta^{++}$ at 13-GeV/c. *Nucl. Phys.*, B133:490, 1978.

[EGPdR89] G. Ecker, J. Gasser, A. Pich, and E. de Rafael. The role of resonances in chiral perturbation theory. *Nucl. Phys.*, B321:311, 1989.

[EM74] P. Estabrooks and Alan D. Martin. $\pi\pi$ phase shift analysis below the $K\bar{K}$ threshold. *Nucl. Phys.*, B79:301, 1974.

[EW88] Torleif Ericson and Wolfram Weise. *Pions and nuclei*. Oxford, UK: Clarendon (The international series of monographs on physics, 74), 1988.

[FK60] Daniel I. Fivel and Abraham Klein. On the analytic properties of partial-wave amplitudes in Yukawa potential scattering. *J. Math. Phys.*, 1(4):274–279, Jul-Aug 1960.

[FW63] Graham Frye and Robert Lee Warnock. Analysis of partial-wave dispersion relations. *Phys. Rev.*, 130(1):478–494, Apr 1963.

[Gas83] Stephen Gasiorowicz. *Elementary particle physics*. New York, Wiley, 1983.

[GHJ+74] G. Grayer, B. Hyams, C. Jones, P. Schlein, P. Weilhammer, et al. High statistics study of the reaction $\pi^-p \to \pi^-\pi^+n$ apparatus, method of analysis, and general features of results at 17-GeV/c. *Nucl. Phys.*, B75:189, 1974.

[GIS05] Juerg Gasser, Mikhail A. Ivanov, and Mikko E. Sainio. Low-energy photon-photon collisions to two loops revisited. *Nucl. Phys.*, B 728:31–54, 2005.

[GIS06] Juerg Gasser, Mikhail A. Ivanov, and Mikko E. Sainio. Revisiting $\gamma\gamma \to \pi^+\pi^-$ at low energies. *Nucl. Phys.*, B 745:84–108, 2006.

[GL84] J. Gasser and H. Leutwyler. Chiral perturbation theory to one loop. *Annals Phys.*, 158:142, 1984.

[GL85] J. Gasser and H. Leutwyler. Chiral perturbation theory: Expansions in the mass of the strange quark. *Nucl. Phys.*, B250:465, 1985.

[GL10] A. Gasparyan and M. F. M. Lutz. Photon- and pion-nucleon interactions in a unitary and causal effective field theory based on the chiral Lagrangian. *Nucl. Phys.*, A848:126–182, 2010.

[GLP11] A. M. Gasparyan, M. F. M. Lutz, and B. Pasquini. Compton scattering from chiral dynamics with unitarity and causality. *Nucl. Phys.*, A866:79–92, 2011.

[GMKP$^+$11] R. Garcia-Martin, R. Kaminski, J. R. Pelaez, J. Ruiz de Elvira, and F. J. Yndurain. The pion-pion scattering amplitude. IV: Improved analysis with once subtracted Roy-like equations up to 1100 MeV. *Phys. Rev.*, D83:074004, 2011.

[GMM10] R. Garcia-Martin and B. Moussallam. MO analysis of the high statistics Belle results on $\gamma\gamma \to \pi^+\pi^-$, $\pi^0\pi^0$ with chiral constraints. *Eur. Phys. J.*, C 70:155–175, 2010.

[GNP02] A. Gomez Nicola and J. R. Pelaez. Meson-meson scattering within one loop chiral perturbation theory and its unitarization. *Phys. Rev.*, D65:054009, 2002.

[Gol61] J. Goldstone. Field theories with superconductor solutions. *Nuovo Cim.*, 19:154–164, 1961.

[GSW62] Jeffrey Goldstone, Abdus Salam, and Steven Weinberg. Broken Symmetries. *Phys. Rev.*, 127:965–970, 1962.

[GW73] D. J. Gross and Frank Wilczek. Ultraviolet behavior of nonabelian gauge theories. *Phys. Rev. Lett.*, 30:1343–1346, 1973.

[HJW$^+$73] B. Hyams, C. Jones, P. Weilhammer, W. Blum, H. Dietl, et al. $\pi\pi$ phase shift analysis from 600-MeV to 1900-MeV. *Nucl. Phys.*, B64:134–162, 1973.

[HPG$^+$77] W. Hoogland, S. Peters, G. Grayer, B. Hyams, P. Weilhammer, et al. Measurement and analysis of the $\pi^+\pi^+$ system produced at small momentum transfer in the reaction $\pi^+p \to \pi^+\pi^+n$ at 12.5-GeV. *Nucl. Phys.*, B126:109, 1977.

[HPS11] Martin Hoferichter, Daniel R. Phillips, and Carlos Schat. Roy-Steiner equations for $\gamma\gamma \to \pi\pi$. *Eur. Phys. J.*, C 71:1743, 2011.

[JOP00] Matthias Jamin, Jose Antonio Oller, and Antonio Pich. S-wave $K\pi$ scattering in chiral perturbation theory with resonances. *Nucl. Phys.*, B587:331–362, 2000.

[JPHS95] G. Janssen, B. C. Pearce, K. Holinde, and J. Speth. On the structure of the scalar mesons $f_0(975)$ and $a_0(980)$. *Phys. Rev.*, D52:2690–2700, 1995.

[Kap05] David B. Kaplan. Five lectures on effective field theory. *arXiv:0510023 [hep-th]*, 2005.

[Kle11] Christoph Klein. Calculation of hadronic transition amplitudes in charm physics. *PhD thesis*, 2011.

[KLR97] R. Kaminski, L. Lesniak, and K. Rybicki. Separation of S-wave pseudoscalar and pseudovector amplitudes in $\pi^- p$ (polarized) $\to \pi^+\pi^- n$ reaction on polarized target. *Z. Phys.*, C74:79–91, 1997.

[KLR02] R. Kaminski, L. Lesniak, and K. Rybicki. A joint analysis of the S-wave in the $\pi^+\pi^-$ and $\pi^0\pi^0$ data. *Eur. Phys. J. direct*, C4:4, 2002.

[KM01] Bastian Kubis and Ulf-G. Meissner. Low-energy analysis of the nucleon electromagnetic form-factors. *Nucl. Phys.*, A679:698–734, 2001.

[KMSF95] M. Knecht, B. Moussallam, J. Stern, and N.H. Fuchs. The low-energy $\pi\pi$ amplitude to one and two loops. *Nucl. Phys.*, B457:513–576, 1995.

[Kog83] John B. Kogut. The lattice gauge theory approach to quantum chromodynamics. *Rev. Mod. Phys.*, 55:775, 1983.

[Kra90] A. Krause. Baryon matrix elements of the vector current in chiral perturbation theory. *Helv. Phys. Acta*, 63:3–70, 1990.

[Lal10] Kavita Lalwani. *Measurement of the branching ratio of a rare decay $\eta \to \pi^0\gamma\gamma$ with WASA-at-COSY*. PhD thesis, Department of Physics, Indian Institute of Technology Bombay, 2010.

[LCD+73] D. Linglin, B. Chaurand, B. Drevillon, G. Labrosse, R. Lestienne, et al. $K^-\pi^-$ elastic scattering cross-section measured in 14.3 Gev/c $K^- p$ interactions. *Nucl. Phys.*, B57:64–76, 1973.

[LCF+74] M. J. Losty, V. Chaloupka, A. Ferrando, L. Montanet, E. Paul, et al. A study of $\pi^-\pi^-$ scattering from $\pi^- p$ interactions at 3.93-GeV/c. *Nucl. Phys.*, B69:185–204, 1974.

[Leu07] Stefan Leupold. Selfconsistent approximations, symmetries and choice of representation. *Phys. Lett.*, B646:155–164, 2007.

[LK01] M. F. M. Lutz and E. E. Kolomeitsev. Covariant meson baryon scattering with chiral and large N_c constraints. *Found. Phys.*, 31:1671–1702, 2001.

[LK02] M. F. M. Lutz and E. E. Kolomeitsev. Relativistic chiral SU(3) symmetry, large N_c sum rules and meson-baryon scattering. *Nucl. Phys.*, A700:193–308, 2002.

[LK04] M. F. M. Lutz and E. E. Kolomeitsev. On meson resonances and chiral symmetry. *Nucl. Phys.*, A730:392–416, 2004.

[LK05] M. F. M. Lutz and E. E. Kolomeitsev. Baryon resonances from chiral coupled-channel dynamics. *Nucl. Phys.*, A755:29–39, 2005.

[LKK04] M. F. M. Lutz, E. E. Kolomeitsev, and C. L. Korpa. Chiral symmetry, strangeness and resonances. *Prog. Theor. Phys. Suppl.*, 156:51–71, 2004.

[LL08] M. F. M. Lutz and S. Leupold. On the radiative decays of light vector and axial-vector mesons. *Nucl. Phys.*, A813:96–170, 2008.

[LL09] S. Leupold and M. F. M. Lutz. Hadronic three-body decays of light vector mesons. *Eur. Phys. J.*, A39:205–212, 2009.

[LS08] Matthias F. M. Lutz and Madeleine Soyeur. Radiative and isospin-violating decays of D_s-mesons in the hadrogenesis conjecture. *Nucl. Phys.*, A813:14–95, 2008.

[Lum64] Max Luming. Application of N/D and determinantal methods to Yukawa potential scattering. *Phys. Rev.*, 136(4B):B1120–B1133, Nov 1964.

[Lut00] Matthias Lutz. Effective chiral theory of nucleon nucleon scattering. *Nucl. Phys.*, A677:241–312, 2000.

[LV12] M. F. M. Lutz and I. Vidana. On kinematical constraints in boson-boson systems. *Eur. Phys. J.*, A 48:124, 2012.

[LYZ99] C. H. Lee, H. Yamagishi, and I. Zahed. Master formulae approach to photon fusion reactions. *Nucl. Phys.*, A 653:185–208, 1999.

[M$^+$90] H. Marsiske et al. A measurement of $\pi^0\pi^0$ production in two photon collisions. *Crystal Ball Collaboration, Phys. Rev.*, D 41:3324, 1990.

[M$^+$07] T. Mori et al. High statistics measurement of the cross-sections of $\gamma\gamma \to \pi^+\pi^-$ production. *Belle Collaboration, J. Phys. Soc. Jap.*, 76:074102, 2007.

[MAC$^+$71] R. Mercer, P. Antich, A. Callahan, C.-Y. Chien, B. Cox, et al. $K\pi$ scattering phase shifts determined from the reactions $K^+p \to K^+\pi^-\Delta^{++}$ and $K^+p \to K^0\pi^0\Delta^{++}$. *Nucl. Phys.*, B32:381, 1971.

[Man63] S. Mandelstam. Regge poles as consequences of analyticity and unitarity. *Annals Phys.*, 21:302–343, 1963.

[Man96] Aneesh V. Manohar. Effective field theories. *arXiv:9606222 [hep-ph]*, 1996.

[MO79] Alan D. Martin and E. N. Ozmutlu. Analyses of $K\bar{K}$ production and scalar mesons. *Nucl. Phys.*, B158:520, 1979.

[MWZ$^+$09] Yu Mao, Xuan-Gong Wang, Ou Zhang, H.Q. Zheng, and Z. Y. Zhou. A dispersive analysis on the $f_0(600)$ and $f_0(980)$ resonances in $\gamma\gamma \to \pi^+\pi^-$, $\pi^0\pi^0$ processes. *Phys. Rev.*, D 79:116008, 2009.

[N$^+$10] K. Nakamura et al. Review of particle physics. *J. Phys. G*, G37:075021, 2010.

[OO97] J. A. Oller and E. Oset. Chiral symmetry amplitudes in the S-wave isoscalar and isovector channels and the σ, $f_0(980)$, $a_0(980)$ scalar mesons. *Nucl. Phys.*, A620:438–456, 1997.

[OO98] J. A. Oller and E. Oset. Theoretical study of the $\gamma\gamma$ meson - meson reaction. *Nucl. Phys.*, A 629:739–760, 1998.

[OO99] J. A. Oller and E. Oset. N/D description of two meson amplitudes and chiral symmetry. *Phys. Rev.*, D60:074023, 1999.

[OPR03] E. Oset, J. R. Pelaez, and L. Roca. $\eta \to \pi^0\gamma\gamma$ decay within a chiral unitary approach. *Phys. Rev.*, D 67:073013, 2003.

[OPR08] E. Oset, J. R. Pelaez, and L. Roca. $\eta \to \pi^0\gamma\gamma$ decay within a chiral unitary approach revisited. *Phys. Rev.*, D 77:073001, 2008.

[OR08] J. A. Oller and L. Roca. Two photons into $\pi^0\pi^0$. *Eur. Phys. J.*, A 37:15–32, 2008.

[P$^+$08] S. Prakhov et al. Measurement of the invariant-mass spectrum for the two photons from the $\eta \to \pi^0\gamma\gamma$ decay. *Phys. Rev.*, C 78:015206, 2008.

[PAGBG$^+$73] S. D. Protopopescu, M. Alston-Garnjost, A. Barbaro-Galtieri, Stanley M. Flatte, J.H. Friedman, et al. $\pi\pi$ partial wave analysis from reactions $\pi^+p \to \pi^+\pi^-\Delta^{++}$ and $\pi^+p \to K^+K^-\Delta^{++}$ at 7.1-GeV/c. *Phys. Rev.*, D7:1279, 1973.

[PMUW08] M. R. Pennington, T. Mori, S. Uehara, and Y. Watanabe. Amplitude analysis of high statistics results on $\gamma\gamma \to \pi^+\pi^-$ and the two photon width of isoscalar states. *Eur. Phys. J.*, C 56:1–16, 2008.

[Pol73] H. David Politzer. Reliable perturbative results for strong interactions? *Phys. Rev. Lett.*, 30:1346–1349, 1973.

[Pra07] S. Prakhov. New results on the rare decay $\eta \to \pi^0\gamma\gamma$. *eConf*, C070910:159, 2007.

[Roy71] S. M. Roy. Exact integral equation for pion pion scattering involving only physical region partial waves. *Phys. Lett.*, B36:353, 1971.

[Sch03] Stefan Scherer. Introduction to chiral perturbation theory. *Adv. Nucl. Phys.*, 27:277, 2003.

[SGBDV10] Adam P. Szczepaniak, Peng Guo, M. Battaglieri, and R. De Vita. P-wave $\pi\pi$ amplitude from dispersion relations. *Phys. Rev.*, D82:036006, 2010.

[SVZ79] Mikhail A. Shifman, A. I. Vainshtein, and Valentin I. Zakharov. QCD and resonance physics. theoretical foundations. *Nucl. Phys.*, B147:385–447, 1979.

[Tay83] John R. Taylor. *Scattering theory: the quantum theory of nonrelativistic collisions*. Robert E. Krieger Publishing Company Malabar, 1983.

[tH76] Gerard 't Hooft. Symmetry breaking through Bell-Jackiw anomalies. *Phys. Rev. Lett.*, 37:8–11, 1976.

[TL10] Carla Terschluesen and Stefan Leupold. Electromagnetic transition form factors of light vector mesons. *Phys. Lett.*, B 691:191–201, 2010.

[TLL12] C. Terschluesen, S. Leupold, and M. F. M. Lutz. Electromagnetic transitions in an effective chiral Lagrangian with the eta-prime and light vector mesons. *arXiv:1204.4125 [hep-ph]*, 2012.

[U$^+$09a] S. Uehara et al. High-statistics study of $\eta\pi^0$ production in two-photon collisions. *Belle Collaboration, Phys. Rev.*, D 80:032001, 2009.

[U$^+$09b] S. Uehara et al. High-statistics study of neutral-pion pair production in two-photon collisions. *Belle Collaboration, Phys. Rev.*, D 79:052009, 2009.

[U+10] S. Uehara et al. Measurement of $\eta\eta$ production in two-photon collisions. *Belle Collaboration, Phys. Rev.*, D 82:114031, 2010.

[Unv10] Marc Unverzagt. η and η-prime physics at MAMI. *Crystal Ball at MAMI Collaboration, Nucl. Phys. Proc. Suppl.*, 198:174–181, 2010.

[vBRM+86] E. van Beveren, T. A. Rijken, K. Metzger, C. Dullemond, G. Rupp, et al. A low lying scalar meson nonet in a unitarized meson model. *Z. Phys.*, C30:615–620, 1986.

[VMK88] D.D. Varshalovich, A.N. Moskaev, and V.K. Khersonskii. *Quantum theory of angular momentum*. World Scientific, Singapore, 1988.

[Wei63] Steven Weinberg. Quasiparticles and the Born Series. *Phys. Rev.*, 131:440–460, 1963.

[Wei67] Steven Weinberg. A model of leptons. *Phys. Rev. Lett.*, 19:1264–1266, 1967.

[Wei79] Steven Weinberg. Phenomenological Lagrangians. *Physica*, A96:327, 1979. Festschrift honoring Julian Schwinger on his 60th birthday.

[WI90] John D. Weinstein and Nathan Isgur. $K\bar{K}$ molecules. *Phys. Rev.*, D41:2236, 1990.

[Ynd06] Francisco J. Yndurain. *The Theory of Quark and Gluon Interactions*. Springer, 2006.

Acknowledgements

I would like to express my sincere gratitude to my supervisor Priv. Doz. Dr. Matthias F. M. Lutz. First of all, thanks a lot for the opportunity to be part of your group at GSI and for the interesting topic of my Ph.D. I am also grateful for your help and support in the work, as well as for willingness to answer any of my questions. This allowed me to understand better many issues raised in my project. During this collaboration I have learned a lot and I am convinced, that our numerous discussions helped me to significantly improve the efficiency level of my work and develop my own style in theoretical physics.

Above all, I acknowledge the organization of my participation and scholarship program in HGS-HIRe for FAIR.

I am grateful to Dr. Ashot Gasparyan, Dr. Evgeni Kolomeitsev and Prof. Dr. Stefan Leupold for many interesting discussions. Many thanks to Prof. Dr. Bengt Friman for useful PhD committee meetings and fruitful discussions.

My special thanks go to Prof. Dr. Hans Feldmeier, Dr. Christoph Klein and Hans-Friedrich Fuhrmann for a careful reading and remarks of my thesis. I also acknowledge the help of Dennis Weber for explaining me the basic rules of PhD defence at TU Darmstadt.

I express my appreciation to all the members of the GSI theory group for the pleasant atmosphere. Special thanks are for my roommates Dr. Alexander Semke, Yonggoo Heo and Dr. Julian Hofmann.

Finally, I want to cordially thank my family and friends for their support.

Lebenslauf

Igor Danilkin
geboren am 9. Juni 1987
in Moskau (Russland)
verheiratet

Sep. 1992 - Mai 1999	Grundschule Nr. 708 in Moskau
Sep. 1999 - Juni 2003	Lyzeum Nr. 1523 in Moskau, Schwerpunkt Mathematik und Physik
Sep. 2003 - Aug. 2009	Studium der Physik am Moscow Engineering Physics Institute (Technische Hochschule)
Aug. 2007	Abschluss: Bachelor of Science in Physics Titel der Bachelorarbeit: "*Charmonium Spectroscopy*"
Juni 2009	Abschluss: Master of Science in Physics Titel der Masterarbeit: "*Precision study of heavy quarkonium*"
seit Aug. 2009	Promotionsstudium an der Technischen Universität Darmstadt Doktorand in der Theorie-Abteilung des GSI Helmholtzzentrums für Schwerionenforschung und Anfertigung der Dissertation